UC Irvine

UC Irvine Electronic Theses and Dissertations

Title

Mechanistic Role of Mitochondrial AKT1 in Acute Kidney Injury

Permalink

https://escholarship.org/uc/item/2xr3c1c1

Author

Lin, You-Hsien

Publication Date

2019

Peer reviewed|Thesis/dissertation

UNIVERSITY OF CALIFORNIA,
IRVINE

Mechanistic Role of Mitochondrial AKT1 in Acute Kidney Injury

DISSERTATION

submitted in partial satisfaction of the requirements
for the degree of

DOCTOR OF PHILOSOPHY

in Biomedical Sciences

by

Hugo You-Hsien Lin

Dissertation Committee:
Professor Ping H. Wang, Chair
Professor Nosratola D. Vaziri
Professor Hamid M. Said
Professor Jefferson Y. Chan
Associate Professor Qin Yang

2019

DEDICATION

To

my lovely wife, Kai-Ting Chang and four kids, Daniel, Sophia, Olivia and Noah.

My wonderful parents, Dr. Sheng-Fung Lin and Man-Mei Yeh.
And Dr. Chang-Jung Liang, Dr. Tzongshi Lu, Dr. Ben Shih, Dr. Yaw-Syan Fu, and Sheng-I Lue.

in recognition of their worth

TABLE OF CONTENTS

Page

LIST OF FIGURES

Page

ACKNOWLEDGMENTS

Foremost, I would like to express the deepest appreciation to my advisor Dr. Ping H. Wang for the continuous support of my PhD study and research, for his patience, motivation, enthusiasm, and immense knowledge. His guidance helped me in all the time of research and writing of this thesis. I could not have imagined having a better advisor and mentor for my PhD study.

Besides my advisor, I would like to thank the rest of my thesis committee: Dr. Nick Vaziri, Dr. Hamid Said, Dr. Jefferson Chan and Dr. Qin Yang, for their encouragement, perceptive comments, and constructive questions.

I would like to express my sincere thanks to Dr. Yumay Chen, who is knowledgeable and always be eager to investigate new things in research. This inspired me to pursuit a new page of scientific career.

I would like to express my special thanks to Dr. Yu-Han (Hank) Chen, who is another mentor to me in the laboratory. He is always reachable, knowledgeable, logical and patient. I appreciate his passion and attitude towards science. His logical thinking and enthusiasm for learning new things have inspired my motivation to become a scientist like him.

I thank my labmates in UC Irvine group, Dr. Hsiao-Chen Lee and Albert Ta, for the stimulating discussions, for the sleepless nights we were working together before deadlines, and for all the fun we have had in the last four years.

A special thank goes to those who have accompanied me during my 4 years at UC Irvine and reached such far. Thank you for the Kaohsiung Medical University group, Dr. Theresa Tseng, and Dr. Mendel Chen being such a nice supporting group during my stay in America. I want to thank the UC Irvine Stem Cell group and Christina Tu for providing supportive knowledge and technique platforms. The UC Irvine doctorate friends, Dr. Laura, thank you for providing supportive energies during every stressful event.

Last but not least, I would like to thank my parents, Man-Mei Yeh and Dr. Sheng-Fung Lin, for birth to me at the first place and supporting me spiritually throughout my life. Also, I want to thank all my families and friends in the United States of America and Taiwan, Kai-Ting Chang and four beautiful kids, my cousins, Jonathan Chang and his families, Richard Yeh, Chien lin Shermatz and her families, and high school classmate, Wei-Chung Hsu.

CURRICULUM VITAE

Hugo You-Hsien Lin

2004   M.D. Kaohsiung Medical University, Taiwan

2009   M.S. in Medical Science, Kaohsiung Medical University, Taiwan

2019   Ph.D. in Biomedical Sciences, University of California, Irvine

HONORS AND SCHOLARSHIPS

2018   Poster Presentation at American Diabetes Association's 78th Scientific Sessions, Orlando

2018   Poster Presentation at American Society of Nephrology Kidney Week 2018 in San Diego

2018   American Society of Nephrology Kidney STARS award

2019   Poster Presentation at American Diabetes Association's 78th Scientific Sessions, San Francisco

2019   American Society of Nephrology Kidney STARS award

FIELD OF STUDY

Mitochondria, Cellular Metabolism, Cell Signaling Transduction, and Nephrology

PUBLICATIONS

Lin HY, Lin SF. Drug Effects on the Thyroid. N Engl J Med. 2019 Nov 14;381(20):1979.

Chang KT, **Lin HY**. Chronic Kidney Disease of Unknown Cause in Agricultural Communities. N Engl J Med. 2019 Aug 15;381(7):688. **(corresponding author)**

Niu SW, He JS, **Lin HY**. Pioglitazone and nephrolithiasis. Kidney Int. 2019 Aug;96(2):518-519. **(corresponding author)**

Kuo IC, Wu PH, **Lin HY**, Niu SW, Huang JC, Hung CC, Chiu YW, Chen HC. The association of adiponectin with metabolic syndrome and clinical outcome in patients with non-diabetic chronic kidney disease. PLoS One. 2019 Jul 19;14(7):e0220158.

Niu SW, Liang PI, Lin MY, Yeh SM, Zhen YY, Chang YH, Huang PC, Hung CC, Kuo IC, **Lin HY**, Kuo MC, Li WM, Huang CN, Wu WJ, Chen LT, Chiu YW, Hwang SJ. Predominant global glomerulosclerosis in patients of upper urinary tract urothelial carcinoma with pre-existing renal function impairment is a predictor of poor renal outcomes. BMC Cancer. 2019 Apr 8;19(1):337.

Lin HY, Niu SW, Kuo IC, Lim LM, Hwang DY, Lee JJ, Hwang SJ, Chen HC, Hung CC. Hematuria and Renal Outcomes in Patients With Diabetic Chronic Kidney Disease. Am J Med Sci. 2018 Sep;356(3):268-276.

Lin HY, Liang CJ, Liu MC, Huang MF, Chang JS, Liang SS. The use of chemical probes to detect the proteomics of renal tubular injury induced by maleic acid. J Chromatogr A. 2018 Aug 31;1565:96-104.

Kuo IC, **Lin HY**, Niu SW, Lee JJ, Chiu YW, Hung CC, Hwang SJ, Chen HC. Anemia modifies the prognostic value of glycated hemoglobin in patients with diabetic chronic kidney disease. PLoS One. 2018 Jun 22;13(6):e0199378. doi: 10.1371/journal.pone.0199378

Niu SW, Chang KT, Ta A, Chang YH, Kuo IC, Hung CC, Chiu YW, Hwang SJ, Lin SF, **Lin HY**. Decreased incidence of diabetes in patients with gout using benzbromarone. Rheumatology (Oxford). 2018 Sep 1;57(9):1574-1582. **(corresponding author)**

Huang SW, **Lin HY**, Yang SF, Su YC. IgM- Kappa type multiple myeloma with simultaneous gastro-esophageal involvement simulating linitis plastica. Kaohsiung J Med Sci. 2018 Jun;34(6):357-359.

Lau WL, **Lin HY**, Wang PH. Urine mitochondrial DNA and diabetic nephropathy-a new frontier. Nephrol Dial Transplant. 2018 May 1;33(5):719-721.

Niu SW, Chang KT, **Lin HY**, Kuo IC, Chang YH, Chen YH, Hung CC, Chiu YW, Hwang SJ. Decreased incidence of gout in diabetic patients using pioglitazone. Rheumatology (Oxford). 2018 Jan 1;57(1):92-99. **(corresponding author)**

Hung CC, **Lin HY**, Hwang DY, Kuo IC, Chiu YW, Lim LM, Hwang SJ, Chen HC. Diabetic Retinopathy and Clinical Parameters Favoring the Presence of Diabetic Nephropathy could Predict Renal Outcome in Patients with Diabetic Kidney Disease. Sci Rep. 2017 Apr 21;7(1):1236.

Lin HY, Lee YL, Lin KD, Chiu YW, Shin SJ, Hwang SJ, Chen HC, Hung CC. Association of Renal Elasticity and Renal Function Progression in Patients with Chronic Kidney Disease Evaluated by Real-Time Ultrasound Elastography. Sci Rep. 2017 Feb 27;7:43303.

Hung CC, **Lin HY**, Lee JJ, Lim LM, Chiu YW, Chiang HP, Hwang SJ, Chen HC. Glycosuria and Renal Outcomes in Patients with Nondiabetic Advanced Chronic Kidney Disease .Sci Rep. 2016 Dec 23;6:39372.

Lim LM, Tsai NC, Lin MY, Hwang DY, **Lin HY**, Lee JJ, Hwang SJ, Hung CC, Chen HC. Hyponatremia is Associated with Fluid Imbalance and Adverse Renal Outcome in Chronic Kidney Disease Patients Treated with Diuretics. Sci Rep. 2016 Nov 14;6:36817.

ABSTRACT OF THE DISSERTATION

Mechanistic Role of Mitochondrial AKT1 in Acute Kidney Injury

By

Hugo You-Hsien Lin

Doctor of Philosophy in Biomedical Sciences

University of California, Irvine, 2019

Professor Ping H. Wang, Chair

Acute kidney injury (AKI) is a significant public health issue with high morbidity and mortality. Recent evidences suggest that renal tubular dysfunction may modulate glomerular function; however, its mechanism remains unknown. We hypothesized that mitochondrial AKT1 signaling could play a protective role in the pathogenesis of AKI and subsequent kidney failure. We have generated novel renal tubular cell-specific transgenic mice harboring an inducible mitochondria-targeting dominant negative AKT1 (KMDAKT) or constitutively active AKT1 (KMCAKT) with Cre-lox strategy. AKI was induced by ischemia-reperfusion injury (IRI). IRI induced greater renal injury with increased Jablonski score (p=0.018), an index of overall renal tubular injuries, in the tamoxifen (TAM)-injected KMDAKT mice. Renal fibrosis areas (%) by Masson's trichrome stain was significantly larger in the KMDAKT mice as compared to the control mice (p<0.001). Marker for renal tubule injury (kidney injury molecule-1, KIM-1) was significantly increased in the KMDAKT mice (p=0.002). Grades of Periodic acid Schiff (PAS) stain of glomerulosclerosis were significantly higher on day 45 post AKI in the TAM-KMDAKT (p<0.001). Creatinine (Cr.) was significantly higher in the TAM-KMDAKT group 45 days post AKI (p<0.001). Survival rate was significantly lower in the TAM-MDAKT mice 7 days post

ischemia (46.67%) as compared to the controls (85.71%) (p=0.0013). To study whether enhancing tubule mitochondrial AKT1 signaling can further protect kidney injury, we used KMCAKT mice as our experimental model. Histology analysis confirmed lesser renal injury with decreased Jablonski score after AKI (p=0.038). Renal fibrosis areas (%) was significantly smaller when compared to the control mice (p=0.002). KIM-1 were decreased in the KMCAKT mice (p<0.001). PAS stain of glomerulosclerosis were significantly lower in the TAM injected KMCAKT mice45 days post AKI (p<0.001). Survival rate in the TAM-KMCAKT mice after AKI was improved (p<0.001). Mitochondria respiration was investigated and the results showed increased basal respiration (p<0.001), spare respiration (p<0.001), adenosine triphosphate (ATP) dependent respiration (p<0.001), and proton leak in the KMDAKT tubule cells. Activation of mitochondrial AKT1 signaling protected kidney injury from glomerulosclerosis after IRI through attenuating renal tubular damage, therefore, mitochondrial AKT1 is a novel target for therapeutic intervention to prevent AKI and subsequent development of CKD.

CHAPTER 1

Introduction

I. PI3K/AKT Signaling and Cell Metabolism

Phosphoinositide 3-kinase (PI3K) is an intracellular phosphatidyl inositol kinase, which has serine/threonine (Ser/Thr) kinase activity. PI3K is composed of a catalytic subunit (p110) and a regulatory subunit (p85) [1]. There are four classes of PI3K with different structures and functions. Among these classes, the most widely studied is class I PI3K. PI3K can be activated via various stimuli, such as receptor tyrosine kinases, cytokine receptors, B and T cell receptors, and G-protein-coupled receptors [2]. PI3Ks bind to these receptors via p85 or adapter proteins such as insulin receptor substrate (IRS) proteins. The activated receptors trigger the launch of class I PI3K and lead to the production of phosphatidylinositol (3,4,5)-trisphosphate (PIP3) from phosphatidylinositol (3,4)-bisphosphate (PIP2). Protein Kinase B (AKT), which possess a pleckstrin homology (PH) domain, is a downstream signal of PI3K. AKT is partial activated through T308 phosphorylation by phosphoinositide dependent kinase 1 (PDK1) [2]. Further phosphorylation of AKT at S473 in the carboxy-terminal hydrophobic domain, either by the mammalian target of rapamycin (mTOR) [3] or by DNA-dependent protein kinase (DNA-PK) [4], leads to full activation of AKT.

There are three isoforms of AKT, which include AKT1, AKT2 and AKT3, each has characteristic function. AKT1 is the major isoform expressed in renal tubular epithelial (RTE) cells [5]. AKT1 plays a major role in growth signaling [6], and the disruptions of AKT2 could result in severe insulin resistance and diabetes, and AKT3 modulates neuronal function and

neuron cell size in the brain [7, 8].

Activation of AKT1 mediates numerous cellular functions including angiogenesis, cell metabolism, growth/proliferation, cell survival/anti-apoptosis, protein synthesis, and gene transcription [9]. AKT1 signaling may interact with a variety of downstream singling molecules. AKT1 is not fixed in the cytoplasm. AKT1 signaling is a dynamic process, it can move around in the cytosol and translocate into mitochondria and nucleus to exert specific biological actions. Coa et al. reported that, when translocated into nucleus, AKT1 interacted with several nuclear proteins, including heterogeneous nuclear ribonucleoprotein (hnRNP), cytoskeleton proteins β-actin, γ-actin, β-actin-like 2 and vimentin [10]. In our previous studies, insulin stimulated AKT1 translocating into mitochondria and modulated oxidative phosphorylation complex V in cardiac muscle [11]. Activation of mitochondrial AKT1 could improve bioenergetics and reduced oxidative stress in cardiomyocytes [12].

II. Mitochondria in Metabolism

Mitochondrion is an organelle encapsulated with outer and inner membranes, the core constituents of the mitochondrial respiratory complexes I–V are embedded in the inner membrane. Tricarboxylic acid (TCA) cycle is located in the matrix and the respiratory chain creates an electrochemical gradient through the coupled transfer of electrons to oxygen and the transport of protons from the matrix across the inner membrane into the intermembrane space. Mitochondrion is the major site of energy production through oxidative phosphorylation [13]. It is not only a powerhouse, but also a specialized organelle that regulates cellular metabolism, reactive oxygen species (ROS), apoptosis, and calcium flux [14]. Mitochondrial malfunction has been implicated in a wide variety of pathophysiological changes and human diseases. Since ATP

propels most biochemical reactions in the cells, defective mitochondrial bioenergetics may disrupt important biological processes. Moreover, tipping the homeostasis of enzymatic reactions within mitochondria could re-direct carbohydrates, amino-acids and lipids into cellular pathways for macromolecule biosynthesis [15]. Altered mitochondrial enzymatic activities and accumulation of mitochondrial metabolic intermediates may induce carcinogenic transformation [16]. Certain mitochondrial metabolites, such as succinate, could serve as signaling molecule and trigger hypoxia-responsive element (HIF-1α) expression and lead to nuclear factor kappa-light-chain-enhancer of activated B cells (NFKB) activation [17].

III. Mitochondrial AKT1

The vast majority of mitochondrial proteins are synthesized and imported from cytosol. Protein import into mitochondria had been recognized for more than twenty years, but its mechanisms are not completely understood. Some mitochondria proteins contain a mitochondria targeting presequence at the amino-terminus of the precursor protein and the presequences are intimately involved in the protein transport process [18]. However, there is a significant fraction of mitochondrial proteins (about 30%) that do not contain typical N-terminal presequences. These proteins can be found at the outer membrane, intermembrane space and the inner membrane. Their importing mechanisms are not quite understood, but could be associated with an internal peptide segment rather than an amino-terminal presequence.

AKT1 had been found to be accumulated in the mitochondrial matrix upon stimulation [19] and known AKT1 substrates are being reported in the mitochondrion, such as glycogen synthesis kinase β [20, 21], hexokinase II [22], and β-subunit of complex V [23], pyruvate dehydrogenase complex [24], suggesting that AKT1 plays a regulatory role in mitochondrion. Several studies

have investigated the physiological functions of mitochondrial AKT1. Impaired mitochondrial AKT1 translocation and activation had been implicated in the development of diabetic cardiomyopathy [25]. Activation of mitochondrial AKT1 mediated anti-apoptosis effect in cardiac muscle cells [26]. The activation of mitochondrial ATP-dependent K+ (mitoK$_{ATP}$) channels elicited strong cardioprotection against Ca2$^+$ overload and ischemic injury and was associated with phosphorylated AKT1 translocating into mitochondria [27]. AKT1 intra-mitochondrial-cycling was central for redox modulation of cell cycle progression [28]. Although AKT1 was associated with heat shock protein 90 (HSP 90) and thus may partially explain AKT1 processing in mitochondria, the detailed mechanisms of AKT translocation into mitochondria remain largely unknown [29].

IV. Mitochondria and Kidney

The kidney is one of the most energy-demanding organs in the human body [30]. Nutrient-sensing pathways can directly affect mitochondrial energy production in response to external stimuli, such as oxidative stress, hypoxia, and energy depletion. Two signaling pathways have been extensively explored in the kidney, including the mTOR and adenosine monophosphate (AMP)-activated protein kinase (AMPK) signaling pathways [31, 32]. Both signaling pathways have a role in regulating mitochondrial biogenesis to help maintain healthy mitochondria.

Besides nutrient-sensing pathways, perturbation in ATP generation and mitochondria dysfunction can be associated with higher levels of ROS, leading to impairment of renal cell homeostasis. In vitro study showed that mitochondrial electron transport inhibitor treatment in renal cell could not compensate ATP deficit [33]. In podocyte model, ROS decreased expression of nephrin and podocin, which are required to maintain glomerular filtration [34]. Renal

4

proximal and distal tubular cells activate glucogenesis during starvation, metabolic acidosis, glucocorticoid treatment, and increased circulating catecholamines [35]. In animal models of renal tubular injuries (diabetic nephropathy, sepsis, cisplatin induced AKI, and IRI), mitochondrial biogenesis restored by peroxisome proliferator-activated receptor gamma coactivator 1-alpha (PGC1α) could ameliorate the disease course [36-38]. These data suggest renal mitochondria plays a critical role in the regulation of protection against AKI.

V. The Role of Mitochondria in Ischemia and Reperfusion Injury

Mitochondrion is a unique organelle that plays a critical protective role against IRI [39-41]. During ischemia, the depletion of oxygen inhibits the electron transport in the mitochondrial respiratory chain and decreases the production of ATP. Anaerobic metabolism lowers pH and activates Na+/H+ exchanger, leading to sodium ions influx to reduce the uptake of Ca2+ by endoplasmic reticulum (ER).

Some cells may die in the ischemia stage, and those cells that survive from ischemia can be further damaged during reperfusion. During reperfusion, reestablishment of blood flow is associated with increased ROS and Ca2+. After IRI, mitochondrial respiration is disrupted, accompanied by Na+/K+ pump failure and mitochondria membrane depolarization. This respiratory perturbation is associated with concurrent lactic acidosis due to anaerobic metabolism. Activation of proteases, phospholipases, lipases, and ATPase further precipitates secondary cellular injuries [42]. With the intracellular influx of $Ca2^{+}$ into mitochondria, loss of the membrane impermeability electrochemical gradient may trigger apoptotic pathways [43]. Concomitant inflammatory response can be activated, with increased tumor necrosis factor, interleukins, and nitride oxide, which can contribute to the production of superoxide anion,

hydrogen peroxideand peroxynitrite [44].

Mitochondria are the major source of intracellular ROS; 3% to 5% of the O2 available for the respiratory chain undergo incomplete reduction, and create oxidative stress [45]. Beclin-1/class III PI3K,AMPK/(mTOR), and PI3K/AKT/mTOR pathways are known defense mechanisms against tissue damage and cell death [46]. Our lab had demonstrated that the anti-apoptosis action of AKT was mediated through translocation and activation of AKT in mitochondria during IRI in cardiac muscle [12]. However, the role of mitochondria AKT signaling during AKI has not yet been study in the past.

CHAPTER 2

Mitochondrial AKT1 Signaling in Acute Kidney Injury

Preliminary Study

I.   Introduction

AKI is a major clinical problem. The prevalence of AKI is estimated to affect 2–3 people per 1,000 individuals in the United States [47]. The total number of AKI hospitalizations has been increasing and reached approximately 4 million per year. The mortality associated with AKI is alarmingly high, ranges from 35 to 45% of all patients with the diagnosis of AKI within 90 days after discharge from hospital. There is an upward trend in the incidences of AKI worldwide over last decade [48-51]. Although some AKI might be reversible, current evidence indicated that AKI may predispose the kidney to subsequent development of chronic kidney disease (CKD), end-stage renal disease (ESRD) with renal replacement therapy (RRT),or even mortality [50-52]. The risk factors for AKI include old age, sepsis, hypovolemia, preexisting CKD, cardiovascular (CV) disease, hypertension, type 2 diabetes (DM), dementia and cancer [48, 53]. Currently, other than supportive therapy, there is no specific treatment that can be used to effectively prevent or reverse AKI [54]. Better understanding on the molecular mechanisms of AKT will allow us to develop specific therapies to correct its mechanistic defects. IRI is a major cause of AKI [55]. During IRI, RTE cells are the major site of renal damage and have been implicated in renal injury and recovery [56]. In healthy kidney, appropriate oxygen (O_2) supply is necessary for ATP production, nitiric oxide (NO) maintenance, and ROS homeostasis [57]. Mitochondria dysfunction has been noted during IRI, accompanied by reduced ATP

production and increased oxidative stress [58]. Therefore, mitochondria and the signaling pathways modulating mitochondria function may become potential target for therapeutic intervention during IRI in AKI. The majority of kidney mitochondria reside in the proximal renal tubules. We designed the experiments to characterize renal tubule mitochondrial AKT1 signaling during IRI.

II. Materials and Methods

1. Experimental Animals

Eight-week-old male C57BL/6Jmice (Jackson Laboratory, Bar Harbor, ME) were used for these studies. Mice were kept in humidity-controlled environment within a thermoneutral zone. Mice were fed with standard laboratory chow (2020X, EnvigoTeklad, UK) and water until the start of the experiment. All mice were kept under identical condition. The experimental protocol was approved by the Institutional Animal Care and Use Committee at the University of California at Irvine and complied with the National Institutes of Health guidelines.

2. Mice Model of IRI AKI

Mice were anesthetized with 2.5% tribromoethanol (avertin). Unilateral renal ischemia was induced by ligating the left renal pedicles for 30 minutes under anesthesia with concurrent contralateral total nephrectomy (Nx). During the surgery, the core body temperature was maintained at 34°C–36°C. Reperfusion was induced by releasing the ligation. Mice were kept at ambient temperature (30°C–32°C) after ischemia and reperfusion at indicated time intervals. Control mice were subjected to the same procedure (sham), but the renal pedicles were not ligated and no Nx was performed.

3. Serum BUN and Cr.

At the end of experiment, blood was collected from the retro-orbital plexus under anesthesia with avertin. Serum was obtained by centrifugation at 10,000 relative centrifuge force (RCF) for 30 min at room temperature. Serum BUN and Cr. was determined with a colorimetric assay kit (BioAssay Systems, Hayward, CA), and analyzed with a Biotek Synergy HT plate reader.

4. Renal Histology

a. Hematoxylin and Eosin (HE) Staining

Kidney samples were fixed in 10% formalin for 24 hours, dehydrated, and embedded in paraffin. Paraffin-embedded kidney blocks were sectioned at 4μm thick.

HE staining was performed to evaluate renal structure injury. After deparaffinization, the tissue sections were stained in Mayer's hematoxylin solution (Sigma-Aldrich, MO) for 15 minutes, rinsed with running tap water for 2 minutes, and stained with bluing solution (0.1% sodium bicarbonate) for 5 minutes. The slides were counterstained with eosin-phloxine solution for 20 seconds, mounted and dehydrated with ethanol (70, 90, and 100%). Images were captured with Keyence BZ-X810 Inverted Microscope (Keyence, Osaka, Japan) and analyzed with Keyence BZ-X800 Analyzer software. Cross-sectional glomerular area (in μm) was determined from at least 20 randomly images from each sample. The investigators who analyzed the histology were blinded to the samples. Renal damage in proximal tubules from cortex area, outer stripe of outer medulla (OSOM), inner stripe of outer medulla (ISOM) and inner medulla (IM) of the kidney were evaluated with a semi-quantitative analysis of histological damage areas as

previously described [59]. The Jablonski grading scale (0–4) was used for the assessment of IRI

induced necrosis of the overall proximal tubules [60]. In both analysis, about one hundred

tubules were scored in each section and the total scores divided by the number of tubules

analyzed, and according to the following criteria:0, normal; 1, areas of tubular epithelial cell

swelling, vacuolar degeneration, necrosis and desquamation involving<25% of the tubular

profile; 2, similar changes involving>25% but<50% of the tubular profile; 3, similar changes

involving>50% but<75% of the tubular profile; 4, similar changes involving>75% of the tubular

profile [59].

b. Masson's Trichrome Staining

Paraffin-embedded tissues were de-paraffinized in xylene (2washes for 3 min each) and

hydrated in graded ethanol to distilled water. Masson's trichrome staining was performed to

evaluate collagen fibrils in renal tissues by using the reagents from Sigma-Aldrich (MO, USA)

[61]. The slides were mordant in Bouin's solution (picric acid, formaldehyde, and glacial acetic

acid) overnight. After washing with water, and the slides were stained with Weigert's Iron

Hematoxyline Solution for 30 minutes, Biebrich Scarlet-Acid Fucshin for 15 minutes,

phosphomolybdic-phosphotungstic acid solution for 10 minutes, and then aniline blue for 20

minutes. After briefly submerged in 0.5% acetic acid solutions, the slides were dehydrated

through 95% alcohol, 100% alcohol, and xylene. Blue coloration, indicative of collagen in the

extracellular matrix (ECM), was digitally calculated with ImageJ [62], ECM content was

quantified as mean blue intensity per tissue area.

c. Immunohistochemistry (IHC) Staining of Phospho-AKT1(Ser473)

Paraffin-embedded kidney sections were deparaffinized and incubated with 0.05%saponin at room temperature for 30 minutes for antigen unmasking. Then the slides were sequentially incubated with 4% bovine serum albumin (BSA) for background blocking, anti-phosphor-AKT antibody at 4 °C overnight, and biotinylated α-rabbit secondary antibody (Vector Lab) for 45 minutes at room temperature. After several rinses in phosphate-buffered saline (PBS), they were incubated with VECTASTAIN ABC kit (Vector Lab) to recognize biotinylated secondary antibody and conjugate with horseradish Peroxidase (HRP).After several rinses in PBS, the bound peroxidase was visualized by incubating the sections with a solution containing DAB (3, 3 –diaminobenzidine) (Sigma-Aldrich, MO) following the manufacturer's instructions. Finally, the slides were counterstained with 1% Methyl Green. 20 microscopic fields were randomly selected from each tissue section and the percentage of positive staining tubules was evaluated by ImageJ.

d. Immunofluorescence (IF) Staining

Paraffin-embedded kidney sections were deparaffinized and immersed with 0.1M Tris (pH 10) antigen retrieval buffer and they were heated in an 1100 W GE microwave oven for three sequential 5-min cycles at power levels 5, 4 and then 3 in microwave oven. After washing with PBS, slides were incubated with specific primary antibodies overnight at 4°C, washed with PBS, conjugated secondary antibodies with 3 minutes heating cycle and 2 minutes incubation, counterstained with4',6-diamidino-2-phenylindole(DAPI, 1ug/ml) and Mitotracker (10nM), and analyzed with Keyence BZ-X810 Inverted Microscope (Keyence, Osaka, Japan).

5. Mitochondria Preparation

Renal cortical and outer medulla tissues were isolated from the kidney, minced, washed

with ice-cold PBS 3 times, and suspended in mitochondria isolation buffer (20 mM HEPES-

KOH, pH 7.2, 10mMKCl, 1.5 mM $MgCl_2$, 1.0 mM sodium EDTA, 1.0 mM sodium EGTA, 1.0

mMdithiothreitol,2 mM phenylmethylsulfonyl fluoride, 20 mM NaF, 2 mM Na3VO4, and

250mM sucrose). After centrifugation at 2500 revolutions per minute (RPM) for 10 min at 4°C,

the samples were incubated on ice for 30 min and homogenized with 20 strokes of loose pestle

and 50 strokes of tight pestle in a Dounce homogenizer. The nuclei and cell debris were removed

by centrifugation at 1,000g for 15 min at 4°C. The supernatants were centrifuged at 10,000g for

30 min at 4°C, and the resulting mitochondrial fractions were re-suspended with mitochondria

isolation buffer. The supernatants were further centrifuged at 100,000g for 1 hour at 4°C. The

supernatants and mitochondrial fractions were stored at -80°C if not immediately used for

biochemical analysis.

6. **Western Blots**

The mitochondrial frations were dissolved in 2% lauryl maltoside solution supplemented

with 10% SigmaFAST[TM]protease inhibitor (Sigma-Aldrich, S8820). Protein contents were

determined with an Eppendorf BioPhotometer by BCA method [63]. Equal amounts of proteins

from each sample were resolved with10% SDS-polyacrylamide gel and then transferred onto

polyvinylidene difluoride membranes. The membranes were blocked with 5% fat-free milk or 5%

bovine serum albumin (BSA) for one hour before incubation with primary antibodies overnight

at 4℃, washed three times with Tris-buffered saline (TBS-T, 20mM Trisered, pH7.5, 0.5 mM

NaCl, and 0.1% Tween 20), incubated with anti-rabbit IgG, horseradish peroxidase -linked

antibody (#7074) (1:2000 dilution in5% fat-free milk or 5% BSA), washed three times with

TBS-T, and then incubated with West Pico Chemiluminescent Substrate to visualize the proteins

(Thermo Scientific, Pittsburgh, PA). The images were acquired with a Syngene G:BOX and

analyzed with ImageJ.

7. Materials

Phospho-Akt (Ser473) Antibodies (＃9271) were purchased from Cell Signaling

Technology (Danvers, MA).AKT1 antibodies (E45) (ab32038) were purchased from Abcam

(Cambridge, UK). voltage-dependent anion-selective channel (VDAC) Antibodies were from

MiliporeSigma (Burlington, MA). MitoTracker®Green FM (M7514) was purchased from

Invitrogen (Carlsbad, CA).Secondary antibody Alexa Fluor® 555 (A31572) was purchased from

Thermo Fisher Scientific (Waltham, MA). The QuantiChrom^{TM} Urea Assay Kit and

QuantiChrom^{TM} Creatinine Assay Kit were purchased from BioAssay Systems (Hayward, CA).

Other chemicals and reagents were from Sigma Aldrich (St Louis, MO).

8. Statistical Analysis

Data are presented as mean ± SD, unless noted otherwise. Statistical data were analyzed

with GraphPd Prism 5 software, with Student's t test or ANOVA when indicated. The region of

interest (ROI) of western blot were quantified by ImageJ, normalized with the ROI value of

loading control and analyzed with Student's t test. The statistical significance level was set at $p<0.05$.

III. Results

1. Establish a Murine Model of AKI with Subsequent CKD

The first goal of my project was to establish a murine model of AKI that may turn into CKD after the initial recovery from acute IRI. To this end, IRI was induced by temporary ligation of left renal artery for 30 minutes, followed by contralateral Nx. The baseline characteristics were identical in the shame control and IRI groups (Fig 2.1). In the IRI-AKI group, serum Cr. began to rise in 2 hours ($p=0.005$), and continued to increase 1 day post procedure ($p<0.001$) and 1 week ($p=0.0025$). BUN also increased accordingly after the procedure (1 hour, $p=0.0019$; 2 hours, $p<0.001$; 1 day, $p<0.001$; 2 days, $p<0.001$; 1 week, $p=0.001$) (Fig 2.2). Significant renal injuries were found with severe tubular lysis, loss of tubular brush border, and sloughed debris in tubular lumen space on the renal tissue sections with HE stain (Figure 2.3). Jablonski Scores were used to assess tubular injuries, the scores were significantly higher in the IRI-AKI mice in 1-2 days ($p=0.0004$) and 1 week ($p=0.038$) as compared to the sham control (Figure 2.3). These results indicated that our IRI procedure successful induced AKI with renal tubular injuries in this mice model.

2. IRI Induced Translocation of Phosphorylated AKT1 (pAKT1) into Mitochondria

Next I sought to characterize whether AKT could be activated and translocated into mitochondria upon IRI. The kidney was quickly harvested after IRI, and we used two complimentary approaches to characterize AKT translocation into mitochondria. First,

mitochondria were isolated from the cortical region of kidney, which is enriched with renal

tubular cells, and the mitochondria preps were solubilized for immunoblotting. Fig 2.4A showed

translocation of pAKT1 into mitochondria can be detected as early as 10 min after reperfusion.

The content of AKT protein also increased in the mitochondria after reperfusion (p=0.0468),

however it lagged behind phosphorylation of AKT1 in mitochondria, which suggests IRI

modulated mitochondrial AKT1 signaling by both phosphorylating mitochondria AKT1 and

translocating AKT1 proteins into mitochondria. Activation of AKT1 in renal tubules after IRI

was confirmed with IHC staining. There was minimal p-AKT1 staining in the sham control renal

tubule, whereas pAKT1 was clearly increased in the renal tubules after IRI (Fig 2.5). To confirm

pAKT1 localized to mitochondria in renal tubules after IRI, subcellular localization of pAKT1

was analyzed by IF. Upon IRI, there was distinct co-localization of p-AKT1 and mitochondria in

the renal tubular cells (Figure 2.6).These results indicated that IRI induced mitochondrial AKT1

signaling by phosphorylation and translocation of AKT1 into mitochondria in the renal tubules.

3. Development of CKD after IRI

To further determine whether IRI may induce permanent structural damage to the kidney,

we examined renal sections with Masson's trichrome stain. The results showed prominent renal

damage and severe loss of structure, with necrotic cells, casts or intraluminal debris,

inflammatory infiltration and fibrosis in the kidneys from the IRI group, renal fibrosis area (%)

was significantly higher 7 days post IRI (Figure 2.7), which suggests AKI induced by IRI can

sustain permanent kidney damages and potentially lead to development of CKD.

IV. Discussions

Our results indicate that I have successfully established a mice model of AKI with unilateral IRI and contralateral Nx. In this AKI model, serum BUN and Cr. became significantly elevated. After the AKI episode, serum BUN and Cr. improved, but remained higher than baseline, indicating the development of CKD, thus this model can be used to study the transition of AKI to CKD. Histological studies showed tubular damages and development of fibrosis, which corroborate the changes of serum BUN and Cr after IRI AKI. The majority of renal mitochondria reside in the proximal tubules. IRI induced rapid accumulation of pAKT1 in the mitochondria by phosphorylation and translocation of AKT1 into mitochondria.

AKT1 is a protein kinase, it can be phosphorylated and translocated into mitochondria in response to growth factor stimulation or stress [64]. AKT family has three members AKT1, AKT2 and AKT3, but only AKT1 can be translocated into mitochondria [65]. AKT1 may interact with different proteins at different subcellular localizations to exert different cellular functions. Activated AKT1 translocation into mitochondria involved interaction with HSP 90 [66]. Our group and other laboratories have identified AKT1 translocation to mitochondria as a key component of AKT1 signaling in cells [11, 64, 67, 68]. Mitochondrial AKT1 regulation of oxidative phosphorylation, ROS, and cell survival were independent of cytosolic AKT1 and nuclear AKT1 [69]. Activating mitochondrial AKT1 signaling could protect cardiac muscle against cell injuries and preserve mitochondrial function, which minimized myocardial injury and improved myocardial function [19]. Our lab has shown that activation of AKT1 in mitochondria suppressed apoptosis in cardiomyotes by stabilizing mitochondria cross-membrane electrochemical gradient, inhibiting cytochrome *c* efflux, and suppressing caspase 3 activation [68, 69].

The role of mitochondrial AKT1 signaling in renal function has not yet been investigated in the past. Based on the results of my preliminary study, it is possible that activation of mitochondrial AKT1 during IRI may play an important role in the regulation of renal protection and subsequent development of CKD. Understanding the mechanisms underlying the mitochondrial signaling in renal tubular epithelial cell metabolism may help develop new strategy to improve the outcome of IRI-AKI.

V. Hypothesis

Activation of mitochondrial AKT1during ischemia-reperfusion in renal tubules protects kidney against AKI and subsequent development of CKD.
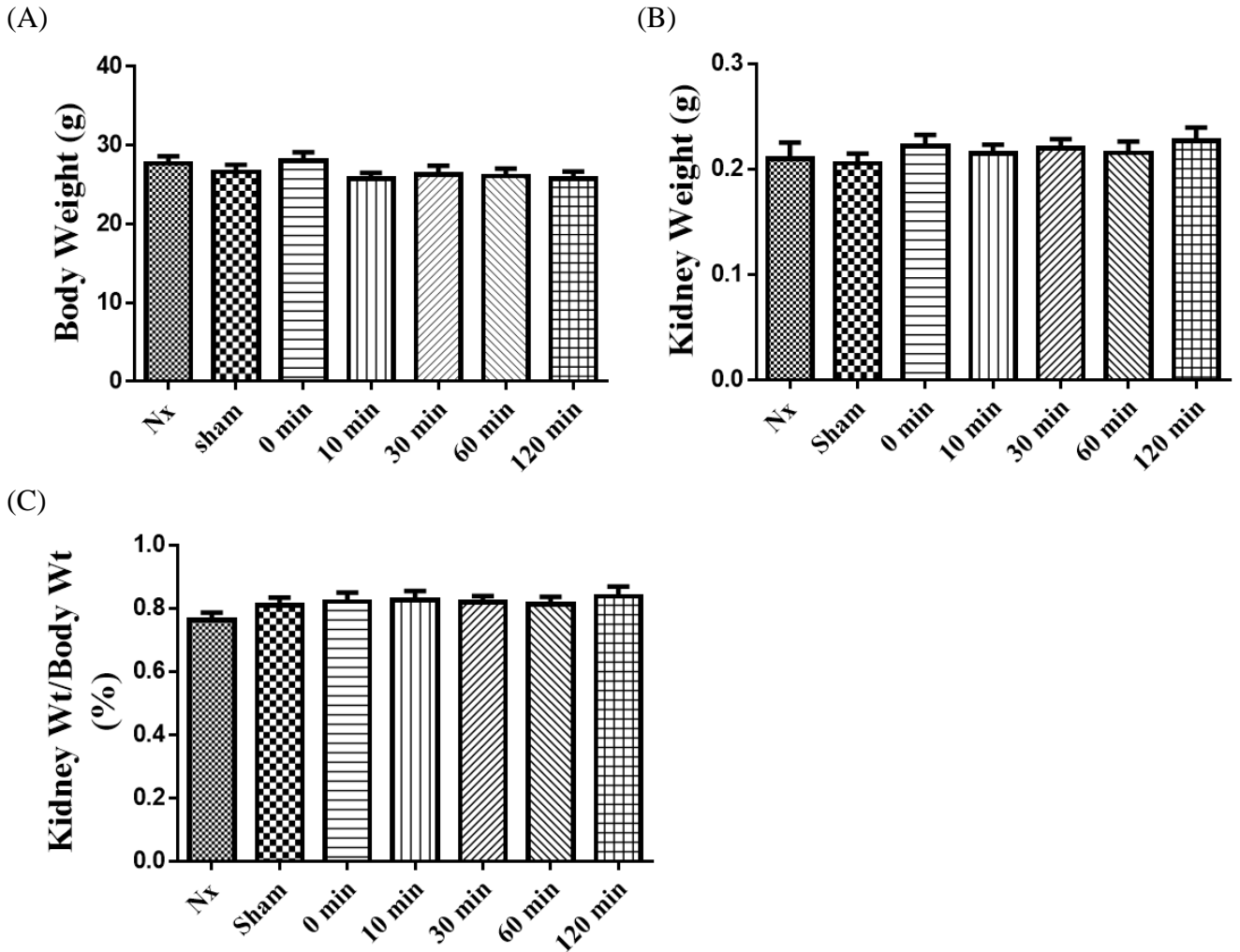
Figures

Figure 2.1

(A)

(B)

(C)

Figure 2.1 **Baseline Characteristics of Mice Model**. There was no significant difference in body weight (BW), kidney weight (KW) and KW to BW ratio in all three groups of mice: Nx only mice, sham control mice and renal IRI mice. (**A**) BW of mice (one way ANOVA $p=0.48$). (**b**) KW of mice ($p=0.86$). (**c**) KW to BW ratio ($p=0.59$) (Nx: nephrectomy; R: reperfusion)) (n=11-15).
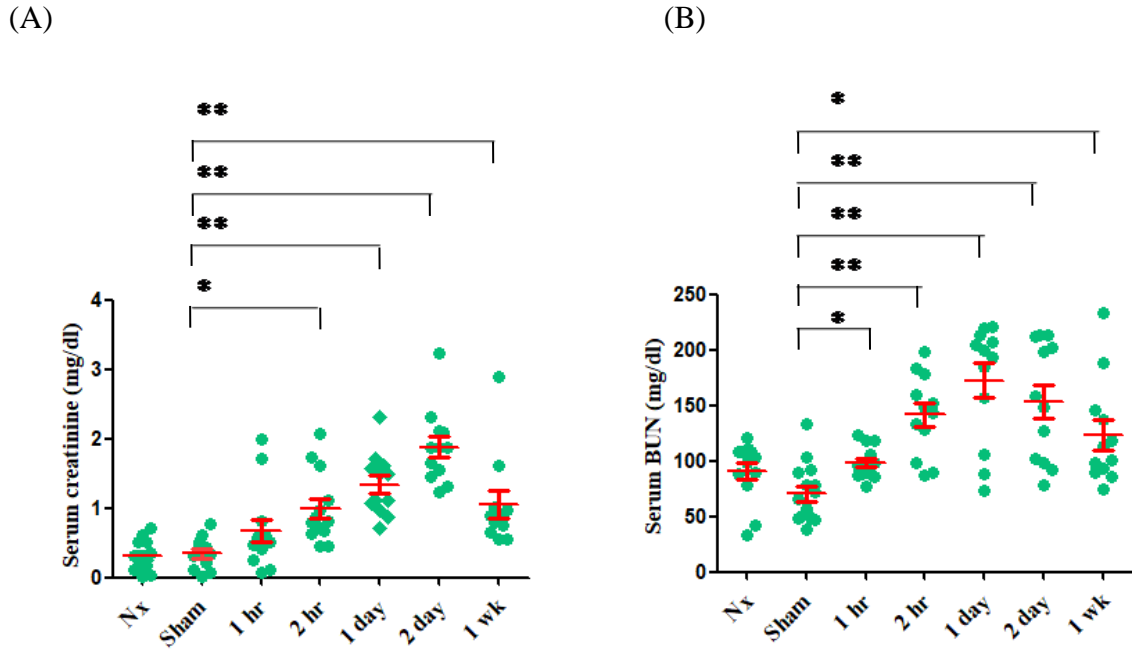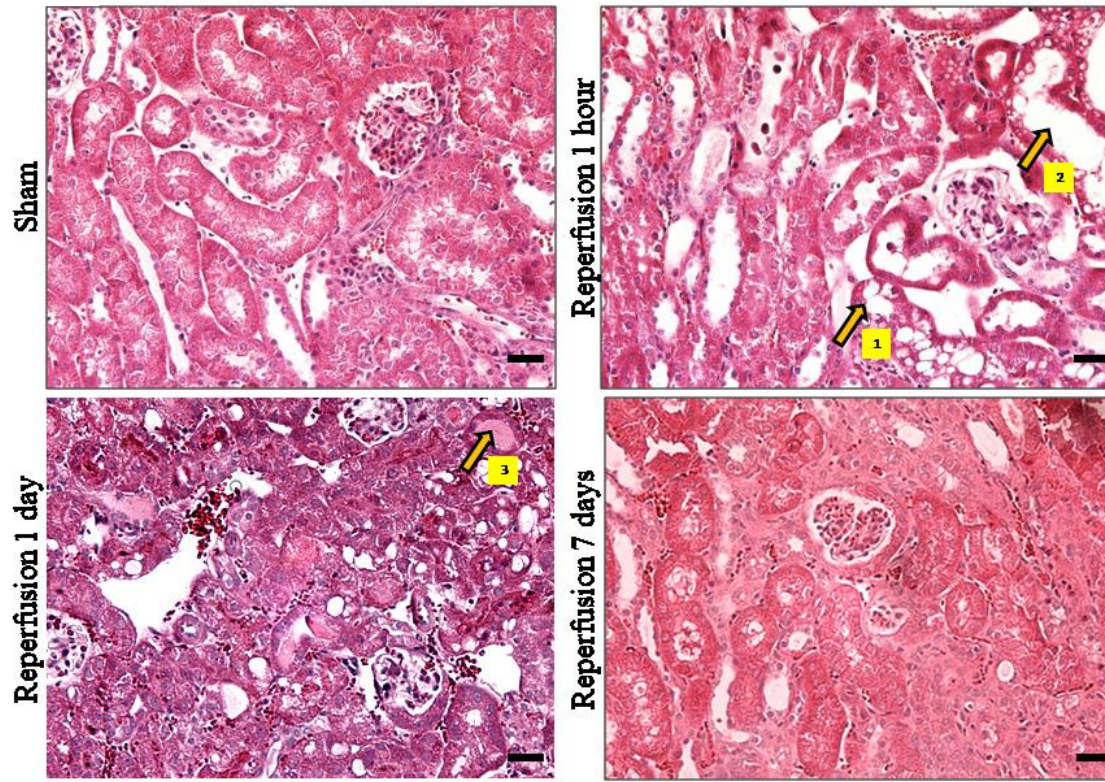
Figure 2.2

(A)

(B)

Figure 2.2 **Renal Function Analysis in Mice upon IRI.** Both serum Cr. (A) and serum BUN

(B) were elevated in mice with IRI injury. (A) Elevated serum Cr. after IRI. There was

significant elevation of serum Cr. 2 hours (p=0.005), 1 day (p<0.001), 2 days (p<0.001), and 1

week (p=0.0025) after IRI compared to the sham control group. (B) Elevated serum BUN after

IRI. There was significant elevation of serum BUN 1 hours (p=0.0019), 2 hours (p<0.001), 1 day

(p<0.001), 2 days (p<0.001), and 1 week (p=0.001) after IRI compared to the sham control

group. (Nx: nephrectomy) (n=11-13)
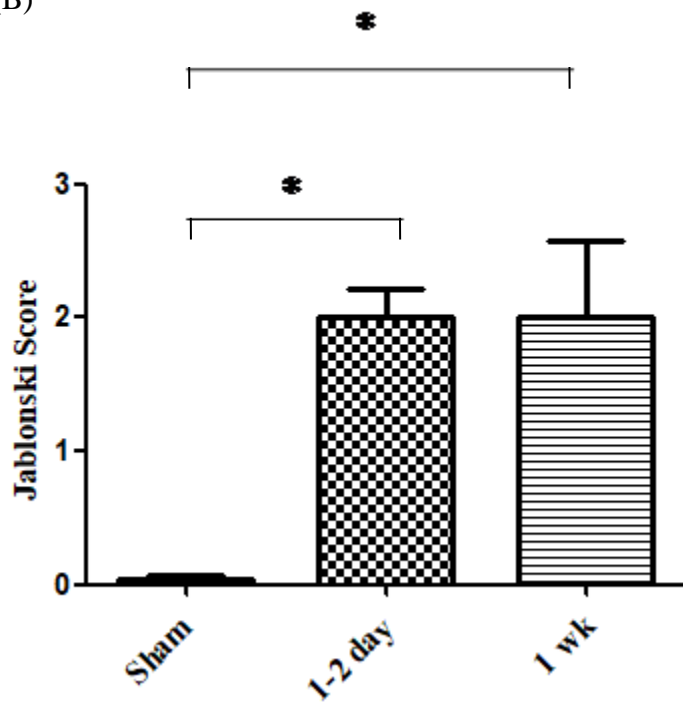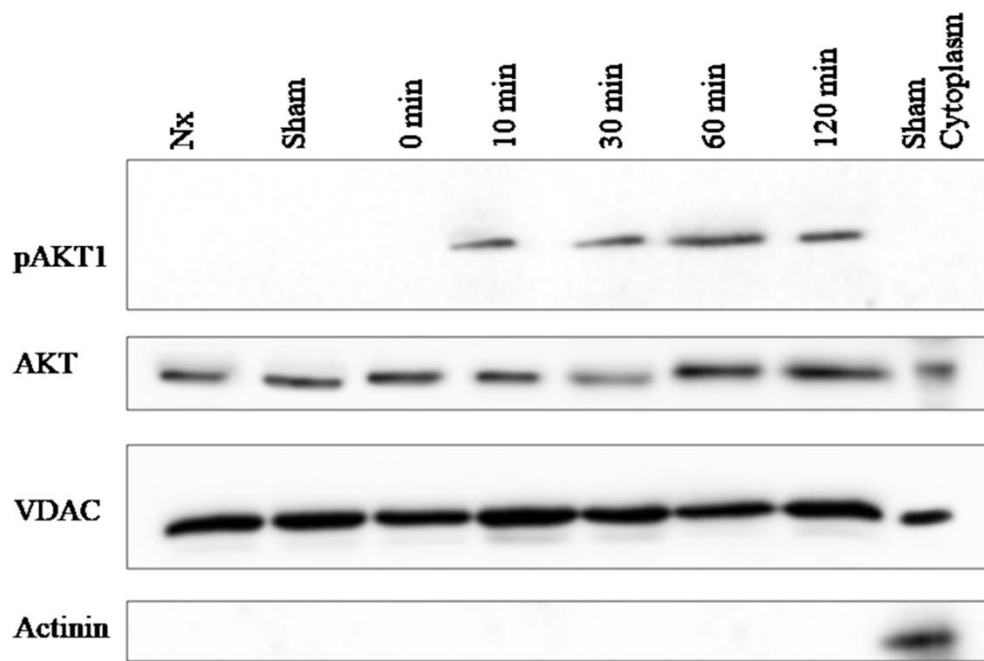
Figure 2.3

(A)

(B)

Figure 2.3 **Renal Tubular Injury after IRI AKI.** (A) Representative histology images of renal sections with HE staining from the sham control, IRI 1 hour, IRI 1 day and IRI 7 days. Scale bar: 50μm. The examples of tubular cellular injury (arrow): renal tubular cell necrosis with dissolving nuclei (1), tubular dilation (2), and cast formation (3). (B) Renal injury after AKI by IRI injury as analyzed by Jablonski Score. There was significant renal injury in 1-2 days (p=0.0004) and 1 week (p=0.038) as compared to the sham control (n=11-13). Jablonski Score (grade 0: normal; grade 1: necrosis of individual cell; grade 2: necrosis of proximal convoluted tubule with survival of surrounding tubules; grade 3: necrosis of distal third of proximal convoluted tubule with a band necrosis extending across the inner cortex; grade 4: necrosis of all three segments of proximal convoluted tubule [70].

Figure 2.4
(A)

(B)
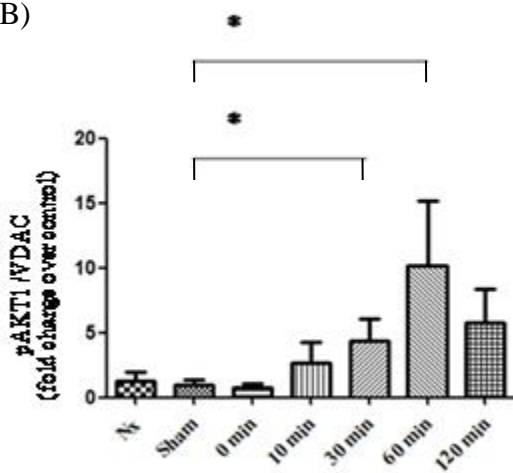
(C)
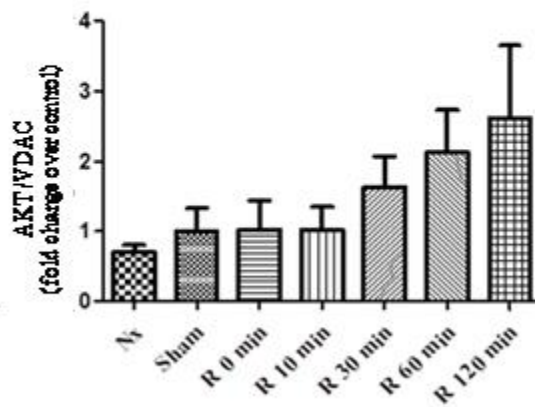
Figure 2.4 **AKT1 is Phosphorylated and Translocated into Mitochndria in Kidney upon**

IRI. Mitochondrial fraction was isolated from kidneys with reperfusion time of 0, 10, 30, 60 or

120 minutes. Protein lysate were analyzed by Western Blotting with antibodies for total AKT1,

pAKT1, VDAC and actinin (A). The ratio between pAKT1 and VDAC was expressed as

histogram in (B). There were significant increases of mitochondrial pAKT1 after 30 minutes of

reperfusion (Mann-Whitney test, p=0.0303) and 60 minutes (Mann-Whitney test, p=0.0173) of

reperfusion compared to sham control group (n=11-15). The content of AKT1 protein in

mitochondria was also increased (Kruskall-Wallis test, p=0.0468) (C).

Figure 2.5

(A)   (B)
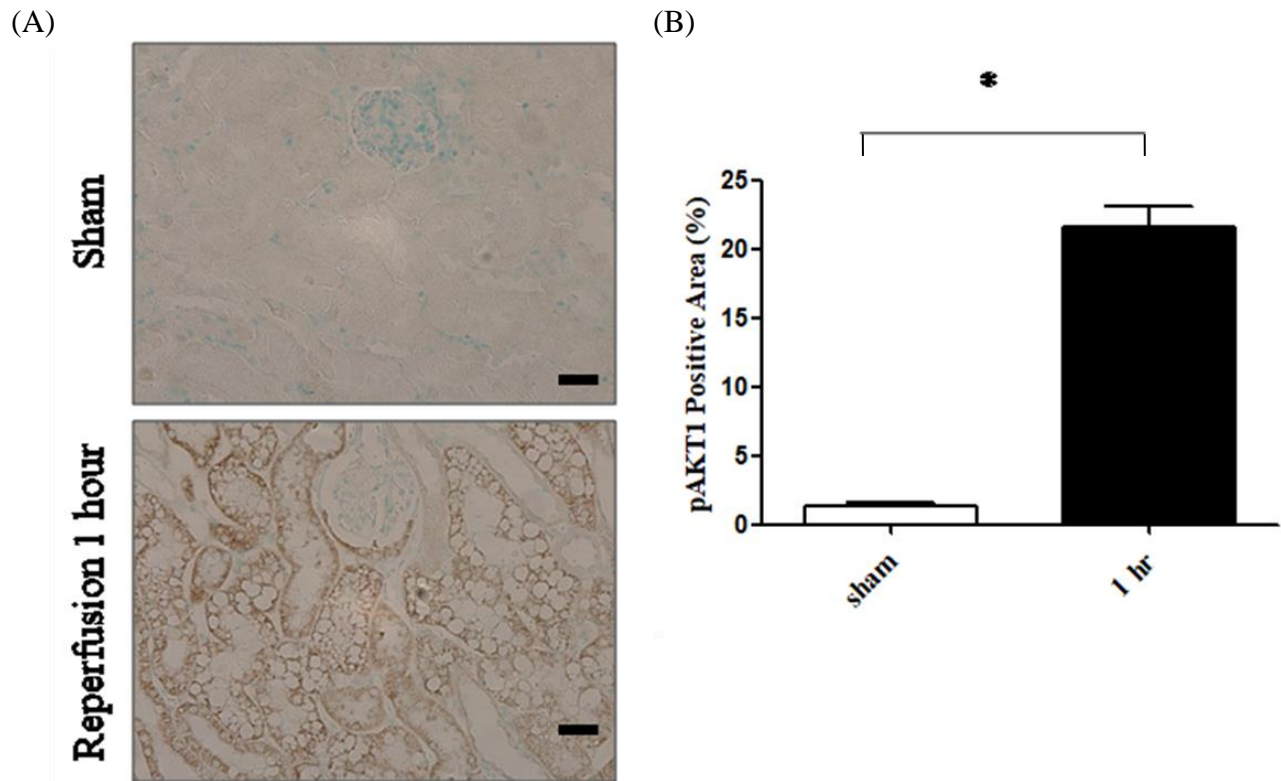
Figure 2.5. **AKT1 Phosphorylation in Renal Tubule by Immunohistochemistry Analysis.**

Renal sections were from sham control or 1 hour after AKI by IRI. (A) Representative pAKT1

IHC stain of renal sections. Scale bar: 50μm. (B) Histogram of renal pAKT positive areas (%) in

sham and 1 hour after AKI by IRI. The area of pAKT1 positive area is significantly higher 1

hour after AKI by IRI compared to sham control group ($p<0.001$) (n=13).

Figure 2.6
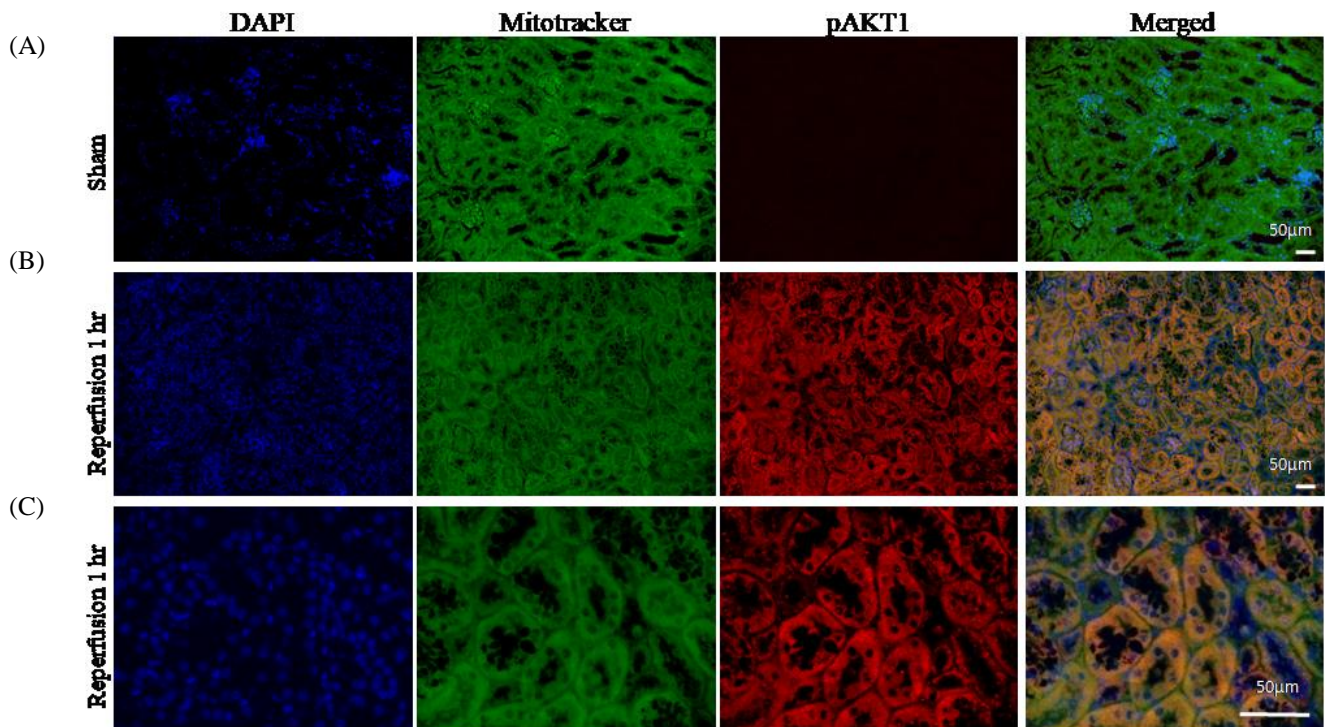
Figure 2.6. **Immunofluorescent Staining of Phosphorylation of AKT1 and its Translocation into Mitochondria in Kidney after AKI by IRI.** Renal sections were immunostained with pAKT1 (S473) antibodies and with Mitotracker Green. Representative images were shown for sham control (A) and 60 minutes after IRI (B). Scale bar: 50μm. The Co-localization of pAKT1 and mitochondria in the renal sections 60 minutes after IRI were shown in (C). Scale bar: 20μm.

Figure 2.7

(A)　　　　　　　　　　　　　　　　　　　　　　(B)
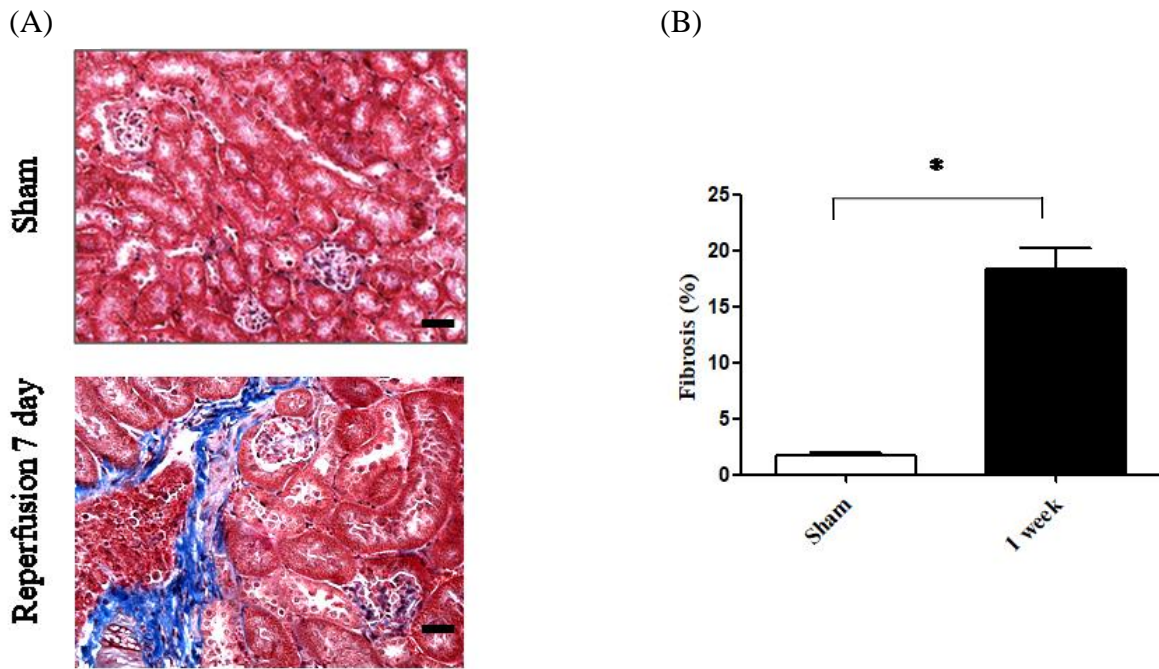
Figure 2.7 **Renal Fibrosis after AKI by IRI.** Renal fibrosis was analyzed by staining the renal

sections from sham control and 7 days after IRI. Representative Masson's trichrome-stained

images of renal tissue sections (A). Scale bar: 50μm. The fibrosis area was expressed as

histogram (B). There are significant renal fibrosis areas (%) in 7days after IRI injured mice

compared to sham control mice group (n=11, $p<0.001$).

CHAPTER 3

Inhibition of Tubular Mitochondrial AKT1 Aggravated the Outcomes of AKI

I. Introduction

Mitochondrial AKT1 plays a key role in the regulation of mitochondria function. In the last chapter, I have observed that IRI induced AKT1 phosphorylation and translocation into mitochondria in renal tubules. However, the role of mitochondria AKT1 during IRI AKI has not yet been investigated in the past. The experiments described in the chapter were designed to test the hypothesis that activation of mitochondrial AKT1 during ischemia-reperfusion in renal tubules protects kidney against AKI and subsequent development of CKD. To this end, we have generated transgenic mice that can be used to specifically manipulate mitochondrial AKT activities in the renal proximal tubules in vivo.

II. Materials and Methods

1. Renal Tubule-specific Mitochondria-targeting Dominant Negative AKT1 Bi-transgenic Mice

To study mitochondrial AKT1 signaling, mutant AKT constructs were used in this project. We mutated K179 to M179 in murine AKT1 to generate a dominant negative murine AKT1 [71]. A constitutive active AKT1 was also constructed with similar strategy as we previously reported [12]. To achieve mitochondria targeting, we inserted a mitochondrial targeting sequence (MSVLTPLLLRGLTGSARRLPVPRAKIHSL) to the N terminus. A His-tagged dominant-negative AKT (substitutions at K179→Methonine), kinase cannot bind ATP, can bind substrate with mitochondria-targeting sequence at the N terminus in a Tet-on inducible lentiviral vector with and without red fluorescent protein (RFP) was used (Figure 3.1). We had used the

same strategy and successfully constructed dominant negative and constitutively active AKT with viral vector to manipulate mitochondrial AKT signaling in cardiac muscle cells and in embryonic stem cells [12, 72]. A transgenic mouse line was generated by knocking in a tamoxifen (TAM)-inducible mdnAKT with CAG promoter into the Rosa26 locus. Bi-transgenic mice (KMDAKT) were obtained by crossing the TAM-inducible mdnAKT mouse with a KSP/CreER^{T2} mouse driven by renal tubular cell specific cadherin promoter (obtained from O'Brien Kidney Research Core, UT Southwestern Medical School) (Figure 3.2) [73].

2. Experimental Animals

KMDAKT mice were kept in humidity-controlled environment within a thermoneutral zone. Mice were fed with standard laboratory chow (2020X, EnvigoTeklad, UK) and water until the start of the experiment. All mice were kept under identical condition. The experimental protocol was approved by the Institutional Animal Care and Use Committee at the University of California at Irvine and complied with the National Institutes of Health guidelines.

a. TAM Treatment

KMDAKT mice were injected with TAM (25 mg/ml, in corn oil) for Cre/loxP recombination. TAM (100 mg/Kg body weight, i.p,) was administered daily for five consecutive days. The control bi-transgenic mice received an equal volume of vehicle alone (corn oil). Expression of transgene was verified 4 weeks after the first day of injection.

b. Western Blots

The mitochondrial fractions were dissolved in 2% lauryl maltoside solution supplemented with 10% SigmaFAST™ protease inhibitor (Sigma-Aldrich, S8820). Protein contents were determined with an Eppendorf BioPhotometer by BCA method [63]. Equal amounts of proteins from each sample were resolved with 10% SDS-polyacrylamide gel and then transferred onto polyvinylidene difluoride membranes. The membranes were blocked with 5% fat-free milk or 5% BSA for one hour before incubation with primary antibodies overnight at 4°C, washed three times with TBS-T (20mM Tris–HCl,pH7.5, 0.5 mM NaCl, and 0.1% Tween 20), incubated with anti-rabbit IgG, horseradish peroxidase -linked antibody (#7074) (1:2000 dilution in 5% fat-free milk or 5% BSA), washed three times with TBS-T (define what this is), and then incubated with West Pico Chemiluminescent Substrate to visualize the proteins (Thermo Scientific, Pittsburgh, PA). The images were acquired with a Syngene G:BOX and analyzed with ImageJ.

c. Mice Model of IRI AKI

Mice were anesthetized with 2.5% tribromoethanol (avertin). Unilateral renal ischemia was induced by ligating the left renal pedicles for 30 minutes under anesthesia with concurrent contralateral total Nx. During the surgery, the core body temperature was maintained at 34°C–36°C. Reperfusion was induced by releasing the ligation. Mice were kept at ambient temperature (30°C–32°C) after ischemia and reperfusion at indicated time intervals. Control mice were subjected to the same procedure (sham), but the renal pedicles were not ligated and no Nx was performed. Due to low survival rate (mention later) and to observe the consequent renal failure post IRI AKI, we executed unilateral IRI AKI only without contralateral total Nx in KMDAKT mice.

d. AKT Activity Assay

To confirm the activity of AKT after the transgene induction, AKT enzymatic activity was analyzed with an AKT Assay Kit (#ab65786) (Abcam, Cambridge, UK) according to the manufacturer's instructions [74]. To analyze the mdnAKT effect on mitochondrial AKT activity, IP-kinase assay was performed using GSK3alpha, downstream target of AKT, as substrate and mitochondrial lysate as kinase source.

e. Serum BUN and Cr.

At the end of experiment, blood was collected from the retro-orbital plexus under anesthesia with avertin. Serum was obtained by centrifugation at 10,000 relative centrifuge force (RCF) for 30 min at room temperature. Serum BUN and Cr. was determined with a colorimetric assay kit (BioAssay Systems, Hayward, CA), and analyzed with a Biotek Synergy HT plate reader.

f. Renal Histology

i. HE staining

Kidney samples were fixed in 10% formalin for 24 hours, dehydrated, and embedded in paraffin. Paraffin-embedded kidney blocks were sectioned at 4μm thick.

HE staining was performed to evaluate renal structure injury. After deparaffinization, the tissue sections were stained in Mayer's hematoxylin solution (Sigma-Aldrich, MO) for 15 minutes, rinsed with running tap water for 2 minutes, and stained with bluing solution (0.1% sodium bicarbonate) for 5 minutes. The slides were counterstained with eosin-phloxine solution for 20 seconds, mounted and dehydrated with ethanol (70, 90, and 100%). Images were captured with Keyence BZ-X810 Inverted Microscope (Keyence, Osaka, Japan) and analyzed with

Keyence BZ-X800 Analyzer software. Cross-sectional glomerular area (in μm) was determined from at least 20 randomly images from each sample. The investigators who analyzed the histology were blinded to the samples. Renal damage in proximal tubules from cortex area, OSOM, ISOM, and IM of the kidney were evaluated with a semi-quantitative analysis of histological damage areas as previously described [59]. The Jablonski grading scale (0–4) was used for the assessment of IRI induced necrosis of the overall proximal tubules [60]. In both analysis, about one hundred tubules were scored in each section and the total scores divided by the number of tubules analyzed, and according to the following criteria: 0, normal; 1, areas of tubular epithelial cell swelling, vacuolar degeneration, necrosis and desquamation involving< 25% of the tubular profile; 2, similar changes involving>25% but<50% of the tubular profile; 3, similar changes involving>50% but<75% of the tubular profile; 4, similar changes involving>75% of the tubular profile [59].

ii. Masson's Trichrome Staining

Paraffin-embedded tissues were de-paraffinized in xylene (2 washes for 3 min each) and hydrated in graded ethanol to distilled water. Masson's trichrome staining was performed to evaluate collagen fibrils in renal tissues by using the reagents from Sigma-Aldrich (MO, USA) [61]. The slides were mordant in Bouin's solution (picric acid, formaldehyde, and glacial acetic acid) overnight. After washing with water, the slides were stained with Working Weigert's Iron Hematoxyline Solution for 30 minutes, Biebrich Scarlet-Acid Fucshin for 15 minutes, phosphomolybdic-phosphotungstic acid solution for 10 minutes, and then aniline blue for 20 minutes. After briefly submerged in 0.5% acetic acid solutions, the slides were dehydrated through 95% alcohol, 100% alcohol, and xylene. Blue coloration, indicative of collagen in the

ECM, was digitally calculated with ImageJ [62], ECM content was quantified as mean blue intensity per tissue area.

iii. KIM-1 Staining

Paraffin-embedded kidney sections were de-paraffinized and incubated with 0.05% saponin at room temperature for 30 minutes for antigen unmasking. Then the slides were sequentially incubated with 4% BSA for background blocking, anti-KIM-1 antibody at 4 °C overnight, and biotinylated α-rabbit secondary antibody (Vector Lab) for 45 minutes at room temperature. After washing with PBS, the slides were incubated with VECTASTAIN ABC kit (Vector Lab) to interact with biotinylated secondary antibody conjugated with HRP. After washing with PBS, the peroxidase was visualized by incubating the sections with a solution containing DAB (Sigma-Aldrich, MO) following the manufacturer's instructions. Finally, the slides were counterstained with1% Methyl Green. 20 microscopic fields were randomly selected from each tissue section and the percentage of positive staining tubules was evaluated by ImageJ.

iv. TUNEL Staining

To detect apoptosis of renal cells, renal sections were stained with the In Situ Cell Death Detection Kit according to the manufacturer's instructions (Roche, Basel, Switzerland) [75]. Paraffin-embedded kidney sections were de-paraffinized and incubated with 0.05% saponin at room temperature for antigen unmasking. The slides were counterstained in 1% Methyl Green. For quantitative analysis, 20 microscopic fields were randomly selected from each tissue section and TUNEL-positive nuclei were analyzed with ImageJ.

v. IF Staining

Paraffin-embedded kidney sections were deparaffinized and immersed with 0.1M Tris (pH 10) antigen retrieval buffer and they were heated in an 1100 W GE microwave oven for three sequential 5-min cycles at power levels 5, 4 and then 3 in microwave oven. After washing with PBS, slides were incubated with specific primary antibodies overnight at 4°C, washed with PBS, conjugated secondary antibodies with 3 minutes heating cycle and 2 minutes incubation, counterstained with4',6-diamidino-2-phenylindole(DAPI, 1ug/ml) and mitotracker (10nM), and analyzed with Keyence BZ-X810 Inverted Microscope (Keyence, Osaka, Japan).

g. Mitochondria Preparation

Renal cortical and outer medulla tissues were isolated from the kidney, minced, washed with ice-cold PBS 3 times, and suspended in mitochondria isolation buffer (20 mM HEPES-KOH, pH 7.2, 10 mM KCl, 1.5 mM $MgCl_2$, 1.0 mM sodium EDTA, 1.0 mM sodium EGTA, 1.0 mMdithiothreitol, 2 mM phenylmethyl sulfonyl fluoride, 20 mM NaF, 2 mM Na3VO4, and 250 mM sucrose). After centrifugation at 2500 RPM for 10 min at 4°C, the samples were incubated on ice for 30 min and homogenized with 20 strokes of loose pestle and 50 strokes of tight pestle in a Dounce homogenizer. The nuclei and cell debris were removed by centrifugation at 1,000g for 15 min at 4°C. The supernatants were centrifuged at 10,000g for 30 min at 4°C, and the resulting mitochondrial fractions were re-suspended with mitochondria isolation buffer. The supernatants were further centrifuged at 100,000g for 1 hour at 4°C. The supernatants and mitochondrial fractions were stored at -80°C if not immediately used for biochemical analysis.

3. Primary Renal Tubular Epithelial Cell

I harvested the kidneys from KMDAKT. After removing renal capsules and medulla, I minced kidney into small pieces. I incubated kidney tissue in sterile PBS. After passed the buffer through a 70-μm filter (VWR® Cell Strainers, #10199-656), the primary RTE cells were incubated in DMEM/F12 supplemented with 25mM HEPES, 0.1 mM nonessential amino acids, 2mM Glutamic acid, 0.1 mM 2-mercaptoethanol (Figure 3.5).

a. 4 Hydroxy-tamoxifen (4-OH TAM) Treatment

Primary RTE cells were administered 4-OH TAM to induce mitochondrial AKT1 expression by Cre/loxP recombination. 4-OH TAM (Sigma), was dissolved in DMSO as 10 μg/ml stock. The final concentration of successfully induction was 10 ng/ml. Control primary RTE received an equal volume of DMSO alone. The transgene expression was confirmed on 24 hours after 4-OH TAM addition.

b. IF Staining of Primary Renal Tubular Epithelial Cell

Cells were fixed with 3.7% formaldehyde in 1X PBS with 0.1% Triton X 100 for 30 minutes at room temperature. After three wash with 1XPBS, cells were permeabilized with 0.05% saponin in ddH2O for 20 minutes. After three washing with 1XPBS, cells were blocking with 10% goat serum in 1XPBS for 30 minutes before incubated with indicated primary antibodies overnight at 4°C. Following three washes with 1X PBS wash, the cells were incubated with Alexa Fluor®488conjugated secondary antibodies for 30 minutes before additional of DAPI or DAPI withmitotracker (10nM). After extended wash with 1XPBS, the immunostained cells

were mounted before imaged and analyzed with Keyence BZ-X810 Inverted Microscope (Keyence, Osaka, Japan).

c. Analysis of Mitochondrial O2 Respiration by Extracellular Flux Measurement

To measure mitochondrial function in cells, we used a Seahorse Bioscience XF24 Extracellular Flux Analyzer (Seahorse Bioscience, North Billerica, MA) and followed the manufacturer's protocol [76]. Briefly, cells were plated in a 24-well Seahorse XF-24 assay plate with $10x10^4$ cells/well, and grown for 16 hours before analysis. On the day of metabolic flux analysis, cells were washed once with freshly prepared KHB buffer (111 mM NaCl, 4.7 mM KCl, 2 mM MgSO4, 1.2 mM Na2HPO4, 2.5 mM glucose and 0.5 mM carnitine; pH 7.4) and incubated in KHB buffer at 37°C in a non-CO2 incubator for 1 hr. Three baseline measurements of oxygen consumption rate (OCR) were taken before sequential injection of following mitochondrial inhibitors and final concentration: oligomycin (1 µg/ml), carbonilcyanide p-triflouromethoxyphenylhydrazone (FCCP) (3 µM) and rotenone (0.1 µM). Three measurements were taken after addition of each inhibitor. OCR values were automatically calculated and recorded by the Seahorse XF-24 software. The basal respiration was calculated by averaging the three measurements of OCR before injection of inhibitors. The basal respiration was calculated by averaging the 3 measurements of OCR before injecting the inhibitors. The spare respiration capacity was calculated by using the OCR measurement after FCCP and subtracting the basal respiration. The proton leak was calculated by using the OCR measurement after oligomycin injection and subtracting the OCR measurement after rotenone injection (Figure 3.7).

d. ATP Assay

To examine the production of ATP, I used ATP Detection Assay Kit (#700410) (Cayman Chemical, Ann Arbor) following the protocol provided by the manufacturer [77]. Cells were trypsinized and counted before use. For each assay, 1×10^6 cells were used. Cells were homogenized 1X ATP Detection Buffer. The luminescence was measured after adding D-Luciferin Solution and Luciferase by a Synergy HT multidetection microplate reader. The ATP was compared between 4-Hydroxytaoxifen (4OH) treated primary RTE cells and vehicle (DMSO) treated primary RTE cells of KMDAKT (Figure 3.7).

4. Materials

Primary antibody: His-Tag(D3I1O) XP® (＃12698) antibodies were purchased from Cell Signaling Technology (Danvers, MA). KIM-1 (＃AF1817) antibodies were purchased from R&D Systems(Minneapolis, MN).VDAC was from MiliporeSigma (Burlington, MA). MitoTracker®Green FM (M7514) was from Invitrogen (Carlsbad, CA, USA). Secondary antibody Alexa Fluor® 555 (A31572) was purchased from Thermo Fisher Scientific (Waltham, MA). The QuantiChrom^{TM} Urea Assay Kit and QuantiChrom^{TM} Creatinine Assay Kit were from BioAssay Systems (Hayward, CA). Anti-Aquaporin 1(AB2219) antibodies were purchased from Millipore Sigma (Burlington, MA). MitoTracker®Red 580 FM (M22425) was purchased from Invitrogen (Carlsbad, CA, USA). Secondary antibody Alexa Fluor®488(A11013) was purchased from Invitrogen (Carlsbad, CA).

5. Statistical Analysis

Data are presented as mean ± SD, unless noted otherwise. Statistical data were analyzed with GraphPd Prism 5 software, with Student's t test or ANOVA when indicated. The analysis

of survival rate was executed with the Kaplan-Meier method. The region of interest (ROI) of western blot was quantified by ImageJ, normalized with the ROI value of loading control and analyzed with Student's t test. The statistical significance level was set at $p < 0.05$.

III. Results

1. Renal Tubule-specific Expression of mdnAKT in TAM-treated KMDAKT mice

The first goal of this chapter was to establish a transgenic mice model with renal tubular specific mitochondria-targeting dominant negative AKT1. To this end, I crossed the TAM-inducible mdnAKT mouse with the KSP/CreER^{T2} mice to produce a bi-transgenic KMDAKT mouse. To confirm transgene expression, mitochondria prep was isolated by gradient centrifugation and mitochondrial proteins were resolved with SDS-PAGE. Western blot showed that TAM successfully induced the expression of mutant AKT1 in renal mitochondria. The mutant protein could not be detected in the vehicle injected KMDAKT mice, KSP/CreER^{T2} mice or wild type (WT) mice (Figure 3.3A). Therefore the transgene was successfully induced as expected. To verify organ specific expression, mitochondrial proteins were extracted from various organs of KMDAKT after TAM injection. The His-tagged mutant AKT could only be found in the kidney (Figure 3.3B). To verify the mutant AKT was localized to the mitochondria in renal tubule, renal sections were used to visualize co-localization of mutant AKT and mitochondria with IF staining (Figure 3.3C). The results showed all mutant AKT stained with His-tag localized to mitochondria. No mutant AKT was seen in the glomerulus. Enzymatic activities of mitochondria AKT were also analyzed to confirm the dominant negative effect. Since renal tubular mitochondrial AKT was activated after IRI, we compared the enzymatic activities of AKT in the mitochondria isolated from the TAM-treated and corn-oil-treated mice

after IRI, the results showed renal mitochondrial AKT activities were significantly reduced in the TAM-treated KMDAKT mice (Figure 3.4). These data indicated that this transgenic model can be used to study the role of renal tubular mitochondria AKT.

2. **Establish and Characterization of the Isolated Primary Renal Tubular Epithelial (RTE) Cells**

Since the KMDAKT mice will only express Cre-recombinase in RTE cells, in order to characterize mdnAKT effect on mitochondria function, RTE cells were isolated and cultured for mitochondria analysis. At the passage 3 or 4, RTE cells were immunostained with proximal tubular epithelial cells marker, aquaporin 1 (AQP 1). As shown in Figure 3.5, more than 97% of cells were positive for AQP 1 (Figure 3.5). Therefore these cells can be used for the following studies.

3. **Renal Tubule-specific Expression of mdnAKT after 4OH-TAM Treatment**

After the RTE cells were established and characterized, the inducible expression of mitochondrial dominant negative AKT1 were confirmed. At passage 3, isolated RTE cells were treated with DMSO or 10 ng/ml of 4-OH TAM. 72 hours after 4-OH TAM or DMSO treatment, cells were labeled with Mitotracker Red before fixed for immunostaining with anti-His-Tag antibodies. As shown in figure 3.6, there was no His-Tag positive signal in the DMSO treated cells, which suggests there was no leakage in the expression of mdnAKT. In contrast, His-Tag antibodies (Green) was induced in 4-OH TAM treated cells and was colocalized with Mitotracker Red.

4. Dominant Negative Mitochondrial AKT1 Modulated Cellular Respiration in the Primary RTE Cells

The cellular bioenergetics was evaluated with a XF extracellular analyzer (known as Seahorse analyzer). The OCR represents measurements of oxidative respiration and extracellular acidification rate (ECAR) represents magnitudes of glycolysis. Overall basal respiration (OCR) of the 4-OH TAM treated KMDAKT RTE cells was significantly higher than the control ($p<0.001$) (Figure 3.7A). The spare respiration profile of the 4-OH TAM incubated KMDAKT RTE cells was also higher than the control ($p=0.00076$) (Figure 3.7B). The ATP dependent respiration profile of the 4-OH TAM incubated KMDAKT RTE cells was significantly higher than control ($p<0.001$) (Figure 3.7C). The higher proton leak in the 4-OH TAM treated KMDAKT RTE cells was indicated uncoupled respiration with oxidative stress ($p<0.001$) (Figure 3.7D). These findings suggest inhibition of mitochondrial AKT1 signaling caused mitochondria dysfunction and loss of mitochondria electrochemical gradient and corroborated with the increased renal apoptosis.

5. Renal histology, BUN, and Cr. was not Altered in the Unstressed KMDAKT Mice

To determine whether renal tubular structure is altered after inhibiting mitochondrial AKT1, renal histology of KMDAKT mice was analyzed with HE stain. Microscopic structure of kidney did not change in the TAM-treated KMDAKT mice, and was indistinguishable from the corn oil-treated KMDAKT mice or TAM-treated KSP/CreERT2 mice (Figure 3.8A to D). To study whether renal function was altered, serum BUN and Cr. were measured and the results again showed that BUN and Cr. were not changed in the TAM-treated KMDAKT mice (Figure 3.8 E-F).

6. Unilateral IRI AKI with Contralateral Nx in KMDAKT

My preliminary data had shown acute activation and translocation of AKT to mitochondria upon IRI in renal tubules. To investigate whether mitochondrial AKT played a protective role during IRI AKI, I studied the effect of mdnAKT in AKI with KMDAKT mice. For this aim, AKI was induced with the unilateral IRI and contralateral Nx as described in the last chapter. Unfortunately, no TAM-KMDAKT mice survived after 3 day post surgery (Figure 3.9 B). I concluded that this model of AKI is too harsh and not feasible for this aim. Therefore, I changed the surgical protocol to unilateral IRI without concurrent contralateral Nx for the KMDAKT mice. The modified protocol yielded much better survival after surgery and thus was chosen for the rest of this project in KMDAKT mice (Figure 3.9).

7. Aggravation of Renal Failure and Renal Fibrosis in KMDAKT Mice after IRI AKI

To study whether activation of tubular mitochondria AKT played a role in the outcome of IRI AKT, I compared the changes of serum renal function of TAM-KMDAKT and control post IRI AKI (Figure 3.10). There was no difference in BUN or Cr. immediately after AKI, however, both BUN and Cr were significantly higher 45 days after AKI ($p=0.021$, $p<0.001$, respectively) in TAM-KMDAKT mice. These results indicated that blocking activation of mitochondrial AKT in renal tubules during IRI led to development of CKD. To gain insight into changes of renal structure, kidney histology was analyzed. HE staining of renal sections from these mice showed aggravated renal injuries in the TAM-KMDAKT mice. Jablonski scores of renal tubular injury were higher with more tubular brush border loss, tubular lysis, and debris in tubular lumen space ($p=0.018$) (Figure 3.11A and B). A marker for renal tubule injury (KIM-1) was

also significantly increased in the TAM-KMDAKT mice. These data indicated more kidney injury in the TAM-KMDAKT group ($p=0.002$) (Figure 3.12A and B). Besides renal injuries, the Masson's trichrome stain showed higher fibrosis area (%) in the TAM-KMDAKT mice after IRI ($p<0.001$), accompanied by intensified structure loss with casts and intraluminal debris (Figure 3.13A and B).

To evaluate apoptosis of renal cells, TUNEL staining was carried out in renal tissue sections. Apoptosis were not only significantly increased in the renal tubules ($p=0.0054$), but also in glomeruli ($p<0.001$) of TAM-KMDAKT mice when compared to the controls (Figure 3.14A and B). These results suggest that inhibiting the tubular mitochondrial AKT1 during IRI could aggravate tubular cell death and amplify glomerular injury.

To further explore glomerular changes, renal sections were stained with PAS. The results are rather interesting, although there was no significant of glomerulosclerosis 7 days after IRI ($p=0.2634$) (Figure 3.15), more glomerulosclerosis was found 45 days after IRI in the TAM-KMDAKT mice ($p<0.001$). These data further demonstrated the impact of renal tubular mitochondria AKT signaling on long-term health of renal glmeruli.

To study whether activation of tubular mitochondria AKT played a role in the outcome of IRI AKT, I compared the survival rates of KMDAKT post IRI AKI and control. Compared to the corn oil injected mice, TAM-KMDAKT mice showed significantly worse survival after IRI ($p=0.0013$) (Figure 3.16) and negatively affected long-term survival.

8. Exclusion of Cre Recombinse Effect in KMDAKT Mice

To exclude the possibility that the experimental results in KMDAKT mice might have been confounded by effect of TAM or Cre recombinase, I analyzed renal tissue sections (Figure 3.17).

Tubular necrosis, tubular lysis, tubular dilation, and cast were found in kidney of KMDAKT mice injected with TAM, but not in corn-oil injected group or TAM-injected KSP/Cre ERT2 group. There was significant higher Jablonski scores between TAM injected KMDAKT group compared with TAM injected KMDAKT group on day 7 after IRI AKI (p=0.0072). But there was no significant differences of Jablonski scores between corn oil injected KMDAKT group compared with TAM injected KSP/Cre ERT2 group on day 7 after IRI AKI (Figure 3.17) (p=0.7613). Therefore, my finding is the renal injury of KMDAKT was not confounded by TAM or Cre recombinase.

IV. Discussion

We demonstrated the inhibition of mitochondrial AKT1signaling aggravated renal injury after IRI. Moreover, inhibition of the mitochondrial AKT1 in renal tubules exaggerated subsequent renal fibrosis and glomerulosclerosis after IRI. We also demonstrated that inhibition of mitochondrial AKT1 led to mitochondrial dysfunction with uncoupled respiration, higher proton leak, and reduced ATP production. Mitochondria dysfunction likely contributed to the development of AKI in this model.

Mitochondria provide energy to sustain the function of kidney. In the kidney, the proximal tubule, the loop of Henle, the distal tubule and the collecting duct all require active transport to reabsorb ions [78]. Proximal tubules require more active transport support than other renal cell types because they reabsorb 80% of the filtrate passing through the glomerulus. Proximal tubules contain more mitochondria than any other structure in the kidney. Mitochondrion serves as a major cellular organelle to metabolize nutrients and metabolites for ATP production. Mitochondrial AKT1 regulates cellular oxidative phosphorylation, ROS, and cell survival.

Impaired mitochondrial AKT1 signaling caused uncoupled respiration and lowered ATP

production. The wasteful energy production or impaired metabolic flow may be the cause of

different diseases [79]. Our lab previously identified pyruvate dehydrogenase (PDH) as a target

of AKT1 signaling in mitochondria, which anchors the production of NADH and succinate.

NADH and succinate are respectively used as substrate by complex I and complex II to pump

protons (H^+) into intermembrane space. The electron flow from complex I and II then transports

to complex III then complex IV and finally to oxygen molecules and leads to the production of

ROS. The process establishes a proton (H^+) gradient across inner membrane space and allows

complex V to generate ATP.

The renal tubules are the major component of the kidney and are vulnerable to a variety of

injuries including ischemia, proteinuria, toxins, and metabolic disorders. Tubular injury is an

early and decisive step in many cases of AKI [55, 80]. Renal proximal tubules are especially

susceptible to ischemic and toxic injury, probably because of their lower capacity for anaerobic

respiration and a lack of antioxidants and anti-apoptotic protection [81, 82]. In addition, the

proximal tubule is associated with higher production of reactive oxygen species [83]. In

unilateral ureteral obstruction AKI model, proximal tubule mitochondria became swollen and

vacuolated, and renal ATP production was decreased by 50% [84]. Ischemic renal injury is

associated with reduced ATP production and increased tubular cell death, which ultimately led to

disintegration of tubule structure and function [85].

The results of our study provide novel insight into how mitochondria participated in the

defense against kidney injury upon IRI. The data in this chapter demonstrated a new mechanism

of renal protection against IRI by translocation and activation of AKT1 in tubular mitochondria.

Inhibiting mitochondrial AKT during IRI eventually led to tubular cell death, retrograde

glomerular apoptosis, glomerulosclerosis, and renal fibrosis. Activation of mitochondrial AKT1 also played an important role during the transition from AKI to CKD, and inhibiting mitochondrial AKT1 during acute IRI significantly reduced long-term survival after transition into CKD.

Little is still known about the sequence of events following AKI and the relationship between glomerular filtration rate (GFR) and tubular alterations. In a clinical study, in patients with severe renal artery stenosis, there were widespread formation of atubular glomeruli [86], suggested chronic ischemia might have induced tubule damage and disintegration of renal tubule structure. On the other hand, there are ample evidence indicated that renal tubular dysfunction could led to loss of tubular cell polarity, loss of gap junction, tubular cell death, subsequent tubular obstruction, and retrograde glomerular damage [87-89]. Our results indicated mitochondrial AKT1 indirectly protected against the development of glomerulosclerosis by maintaining the integrity of renal tubular structure and function. In molecular level, modulation of mitochondrial AKT1 may regulate mitochondrial metabolism. And the interference of mitochondrial AKT1 results in alteration of oxygen consumption.
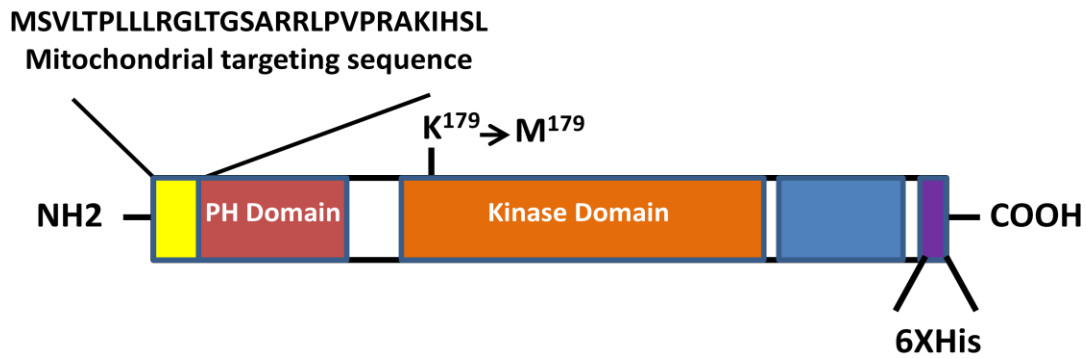
Figure 3.1

Figure 3.1 **The Mitochondria-targeting Dominant Negative AKT1 Construct.** Mitochondria targeting sequence was in frame fused to AKT1 cDNA at the N terminus. A 6X His was in frame fused to the C terminus of AKT1 cDNA. To generate the dominant negative AKT1, the ATP binding site of AKT1, lysine 179 was mutated into methionine.
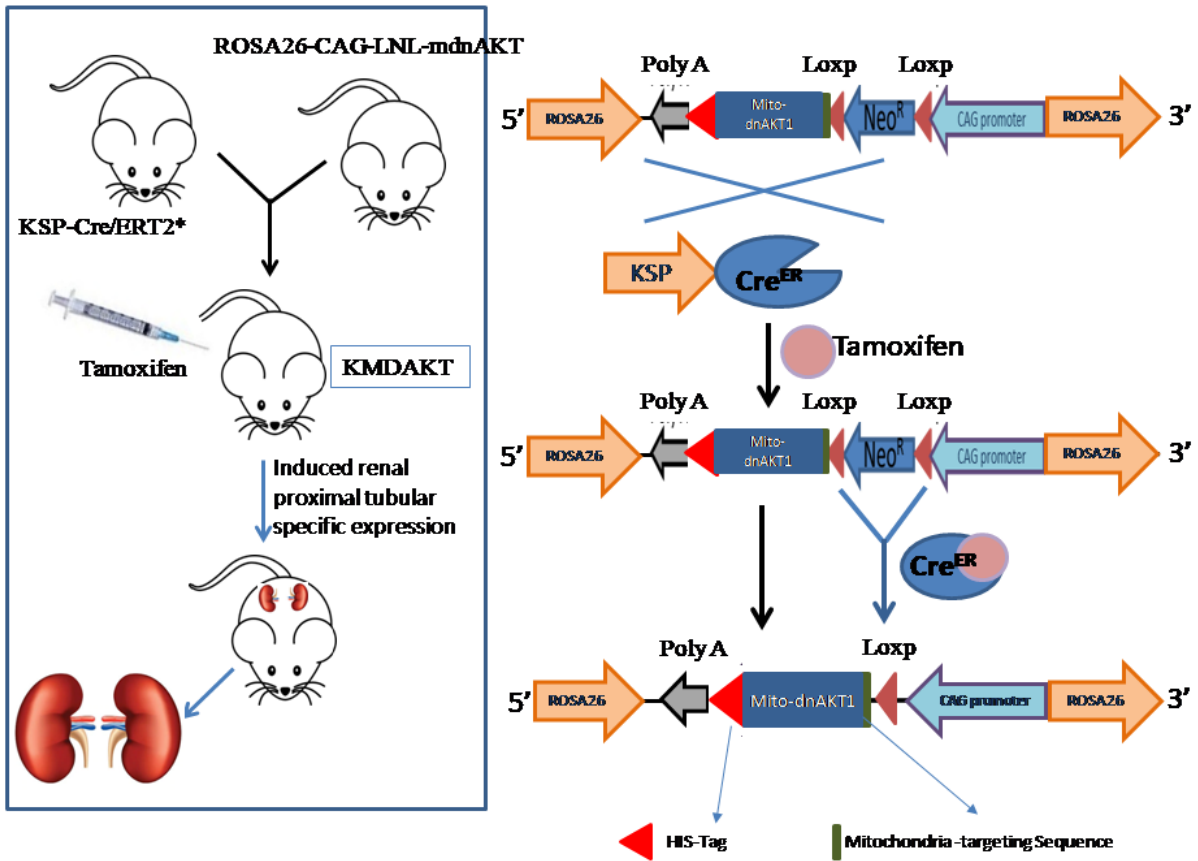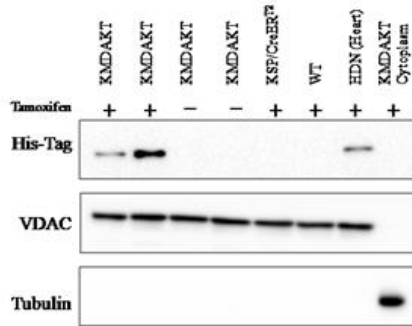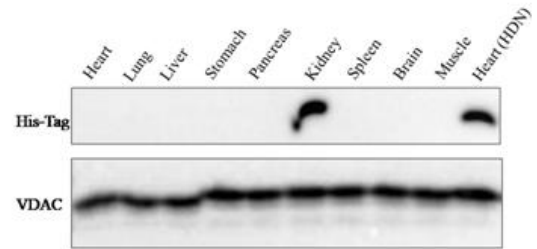
Figure3.2

Figure 3.2 **Design of Bi-transgenic Mice (KMDAKT) for Renal Tubular-specific Mitochondria-targeting Dominant Negative AKT1 (mdnAKT1) Expression.** This is the scheme of the strategy to generate renal-specific overexpression of mitochondria-targeting dominant negative AKT1. A mitochondria-targeting sequence was inserted at the 5' end of the AKT1 cDNA with K179 mutated into Methionine. A mouse with Cre recombinase expressed in kidney renal tubular epithelial cells (KSP/CreER^{T2}) was used to cross with mdnAKT1 mice to generate bi-transgenic mice which mdnAKT expression can be induced by tamoxifen [73].
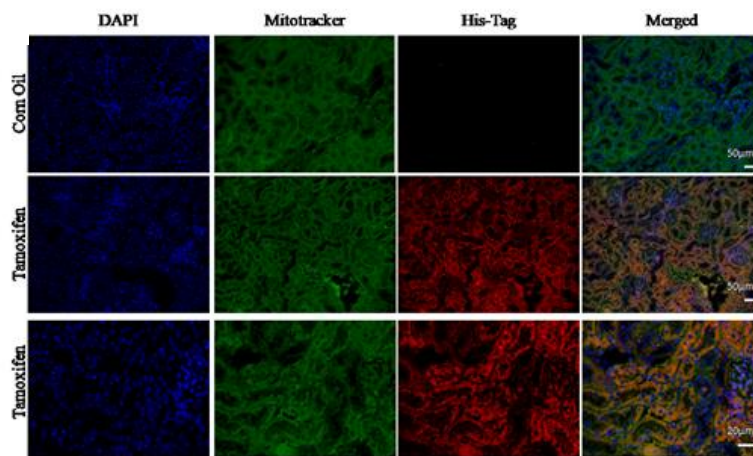
Figure 3.3

(A)

(B)

(C)

Figure 3.3 **Inducible Mitochondria-targeting Dominant Negative AKT1 in Renal Tubular Cells.** Eight weeks old KMDAKT mice were injected with tamoxifen (TAM) or corn oil. The mitochondrial fraction was isolated and expression of mdnAKT was analyzed by Western Blotting using antibodies against His-tag. (A)Western blot with mitochondria proteins showed mdnAKT only expressed in the renal mitochondria isolated from KMDAKT injected with TAM but not in KMDAKT injected with corn oil injected. There was no mdnAKT expression in renal mitochondria of TAM injected KSP/Cre ER^{T2} mice or TAM injected WT mice. There was mdnAKT expression in the heart mitochondria of TAM injected bi-transgenic cardio-specific mdnAKT mice (HDN) as positive control. (B) Renal tubular specific expression of mdnAKT in the KMDAKT mice. After TAM injection, mitochondrial fraction was isolated from different organs. The expression of mdnAKT was analyzed with antibodies against His-tag. VDAC was used as loading control was used. mdnAKT expression in the heart mitochondria of TAM-injected HDN mice was as positive control. The expression of mdnAKT was only detected in the mitochondria isolated from kidney. (C) Mitochondrial localization of mdnAKT1. Co-localization of mdnAKT and mitochondria in the renal tubules was demonstrated with IF staining with anti-His-Tag antibody (His-Tag (D3I1O)XP® and MitoTracker® Green FM (ThermoFisher Scientific) WT: wild type mice, HDN: bi-transgenic heart-specific mdnAKT mice
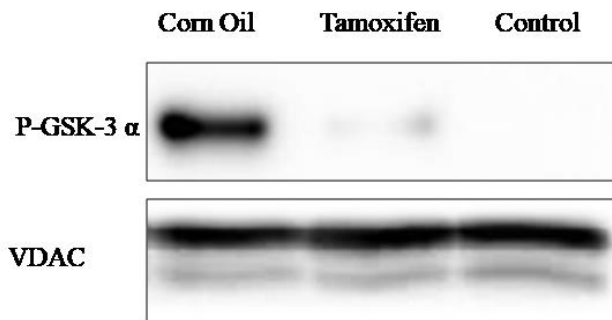
Figure 3.4

Figure 3.4 **Decreased Renal Mitochondrial AKT1 Activity in TAM-injected KMDAKT**

kidney after IRI. To analyze the mdnAKT effect on mitochondrial AKT activity, IP-kinase

assay was performed using recombinant GSK3alpha, downstream target of AKT, as a substrate

and mitochondrial lysate as kinase source. Renal mitochondrial AKT1 activity decreased in

TAM injected KMDAKT mice when compared to corn oil injected KMDAKT mice after IRI

(one hour). Mitochondrial lysate from KMDAKT kidney without AKT antibody incubation was

used for IP-kinase assay (lane 3). P-GSK-3α: phosphorylated GSK-3-α. GSK-3α is the
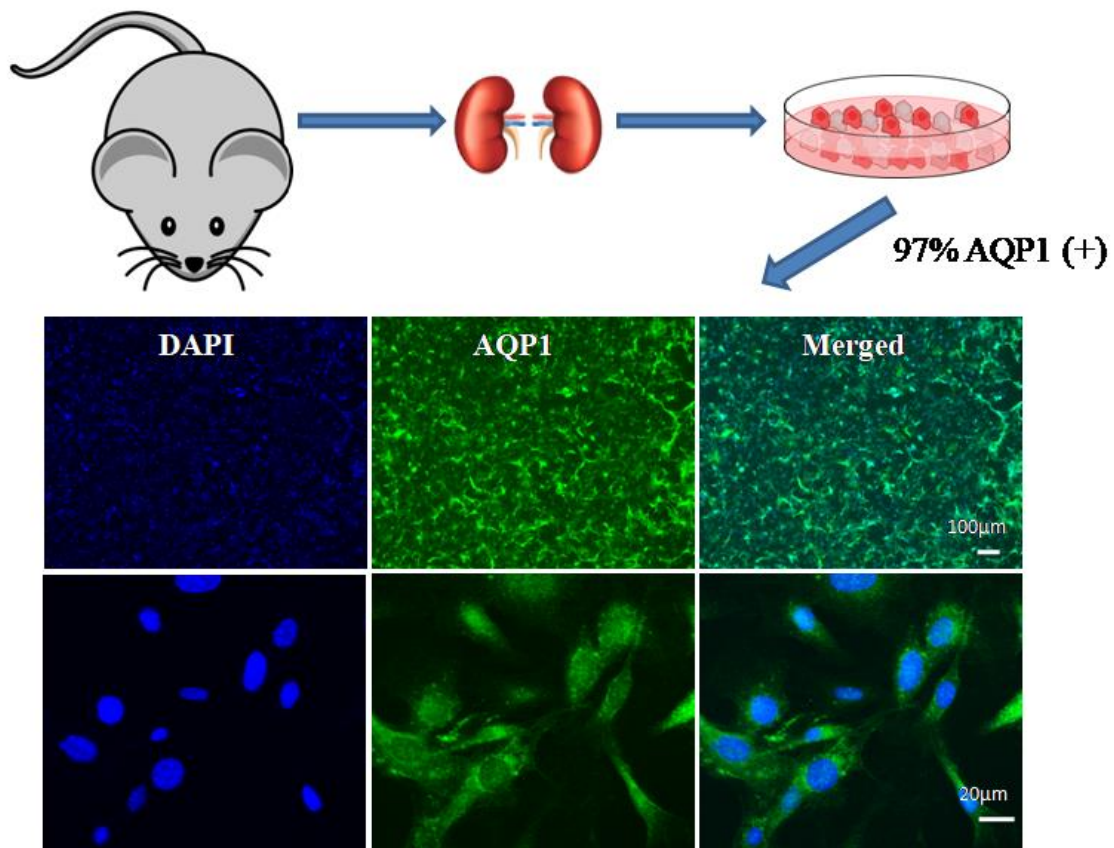
downstream substrate of AKT.

Figure 3.5

Figure 3.5 **Isolation and Characterization of Primary RTE Cells.** 3 weeks old KMDAKT

mice were used for primary renal epithelial cells isolation. After removing renal capsules and

medulla, the kidney was miniced into small pieces, plated onto culture dishes and cultured in

DMEM/F12 media. Cells were sub-cultured when the cells reach confluence. At passage 3 or 4,

the cells were plated onto 12mm circular coverglass and fixed for immunostaining with anti-

renal proximal cells marker (aquaporin 1, AQP1) antibody. Near 97% of culture cells isolated

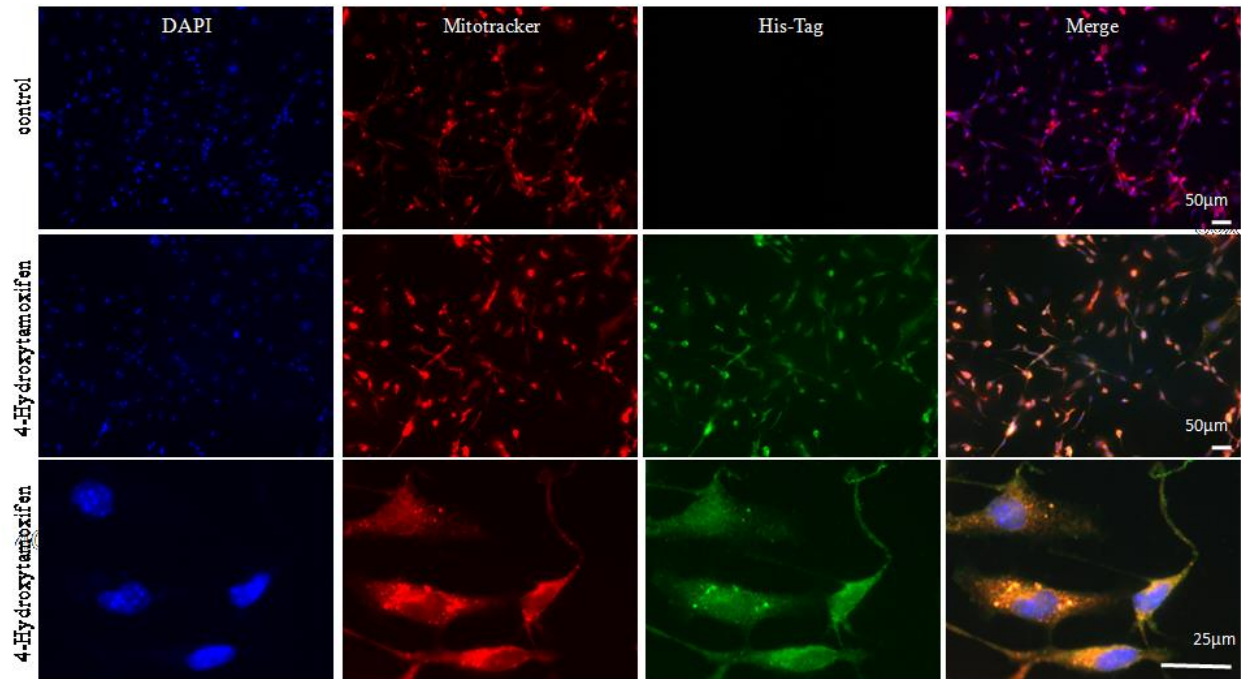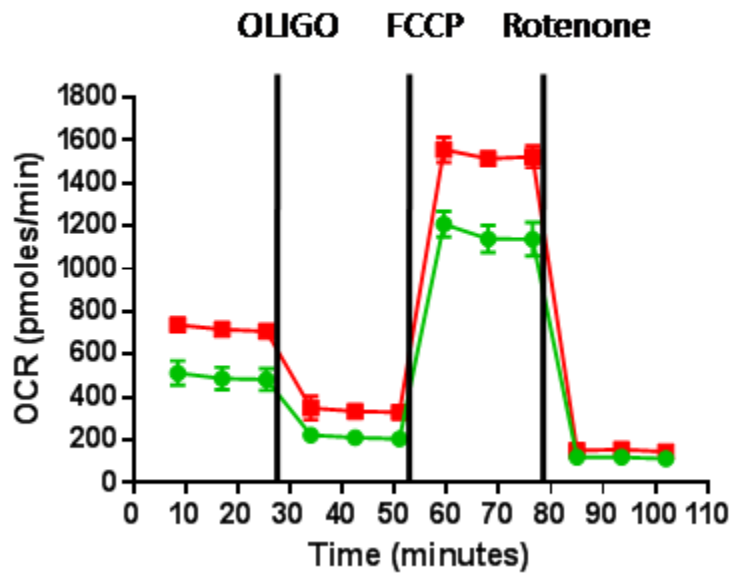using this technique are positive for AQP1 staining.

Figure 3.6

Figure 3.6 **Mitochondrial Localization of mdnAKT1 in the Renal Tubule Epithelial (RTE)**

Cells from KMDAKT Mice. At passage 3, isolated RTE cells were treated with DMSO or

10ng/ml of 4-Hydroxy tamoxifen (4-OH TAM). 72 hours after 4-OH TAM or DMSO treatment,

cells were labeled with Mitotracker Red and immunostained with anti-His-Tag antibodies. There

was no His-positive signal in DMSO treated cells. The positive signal of His-tag (Green) in 4-

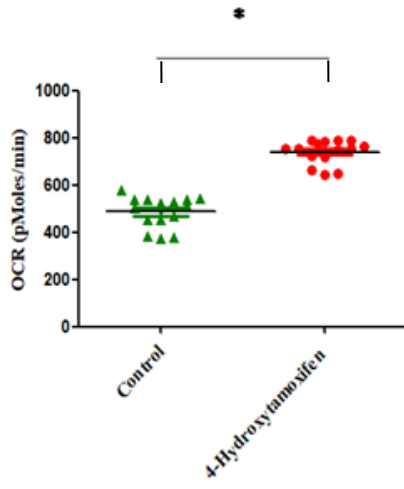OH TAM treated cells colocalized with mitotracker Red.
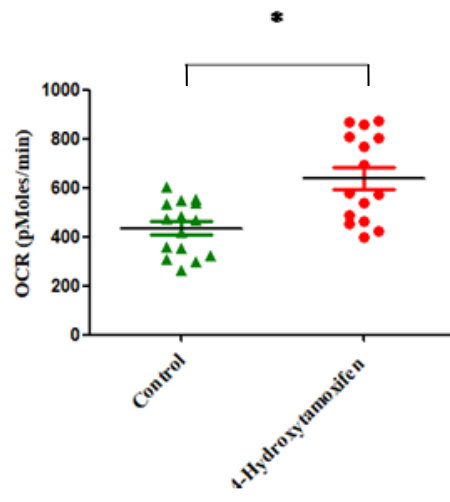
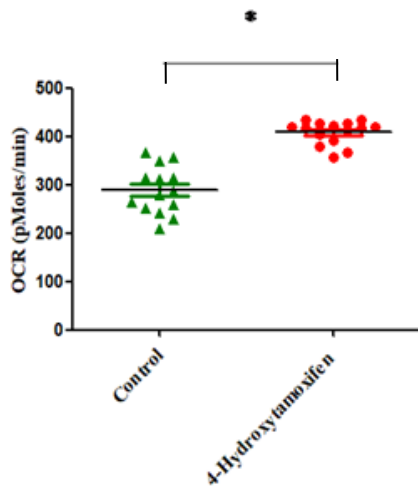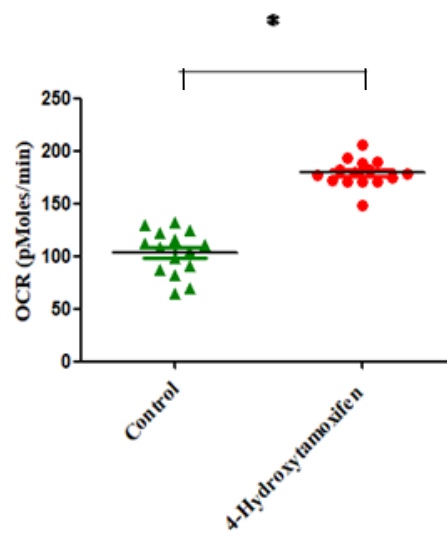Figure 3.7

(A)

(B)

Basal Respiration

OCR (pMoles/min)

(C)

Spare Respiration

OCR (pMoles/min)

(D)

ATP Dependent
Respiration

OCR (pMoles/min)

(E)

Proton Leak

OCR (pMoles/min)
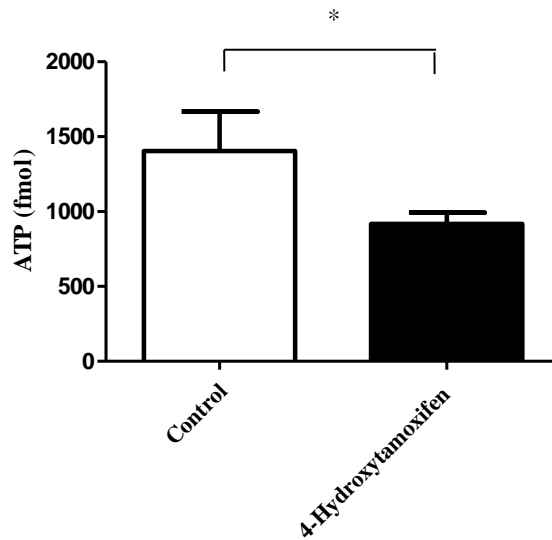
Control 4-Hydroxytamoxifen

53

(F)

Figure 3.7 **Dominant Negative Mitochondrial AKT1 Modulated Cellular Respiration in the Primary RTE Cells.** At passage 3, isolated RTE cells were treated with DMSO or 10ng/ml of 4 hydroxy tamoxifen (4-OH TAM). 60 hours after 4-OH TAM or DMSO treatment, cells were plated onto the Seahorse culture plates at density of 10^5/well. XF extracellular respiration rate was measured at 72 hours after 1st treatment of 4-OH TAM or DMSO. (A) Mitochondrial respiration was measured as oxygen consumption rate. After basal respiration measurements, different inhibitors were injected sequentially to measure different stages of respiration (complex V inhibitor: oligomycin (OLIGO), Uncoupler: FCCP (carbonyl cyanide 4-(trifluoromethoxy) Phenylhydrazone) and complex I inhibitor: Rotenone). The basal respiration (B, ($p<0.001$), spare respiration (C, p=0.00076), ATP dependent respiration (D, $p<0.001$) and proton leak (E, $p<0.001$) were all significantly higher in 4-OH treated cells than in DMSO treated cells. However, the ATP production was significantly lower in 4-OH treated cells than in DMSO treated cells (F, $p=0.0381$).

Figure 3.8

(A)

(D)

(B)

(E)

(C)
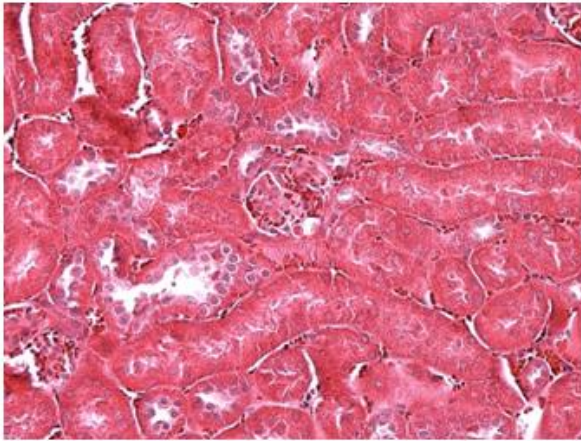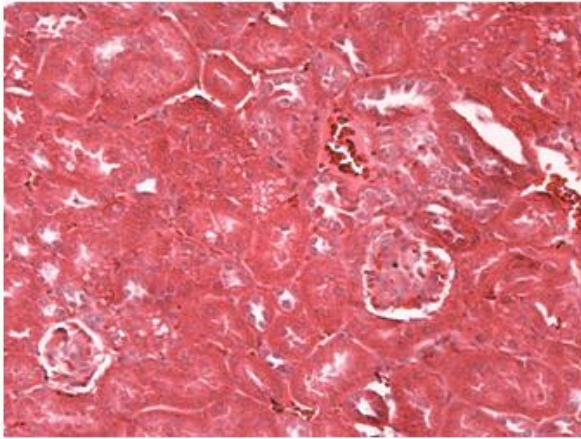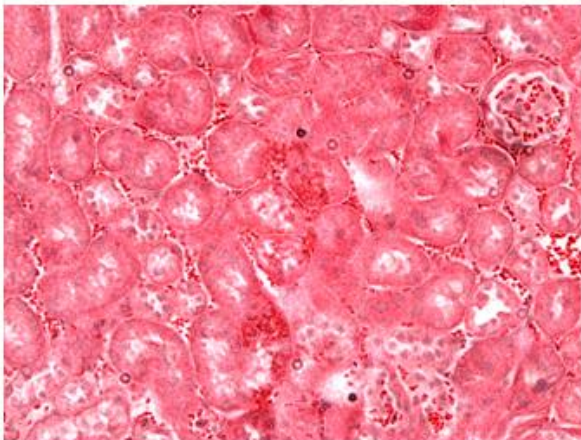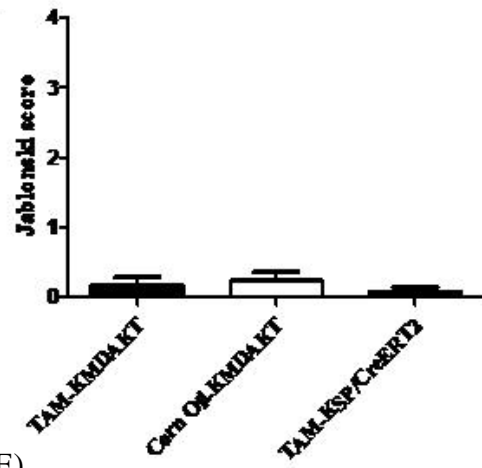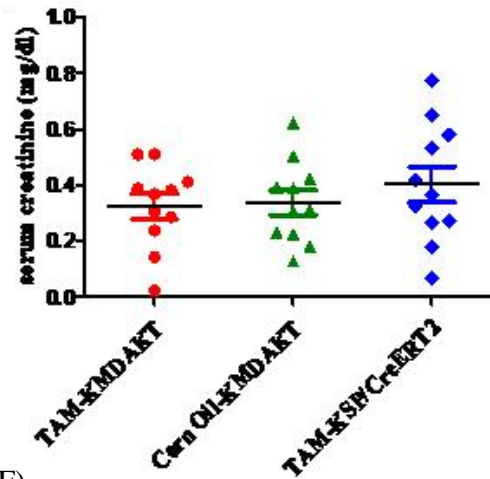
(F)
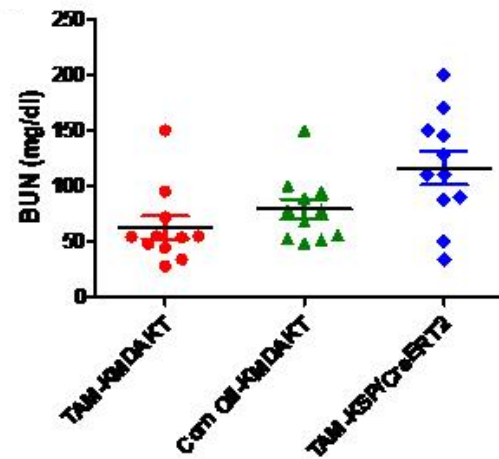
Figure 3.8 **Renal Histology and Serum Renal Function of KMDAKT Mice after TAM**

Injection. One month after TAM injection, kidney was harvested, fixed, and embedded in

paraffin block. After sectioning, the kidney pathology was examined after HE staining. There

was no significant morphological difference among kidney samples from TAM injected

KMDAKT mice (A), corn oil injected KMDAKT mice (B) and TAM injected KSP/Cre ER^{T2}

mice (C). As shown by the Jablonski Score (D), there was no difference among 3 groups of

animals. To examine the renal function, sera were collected at the time of euthanization and

serum creatinine and BUN were measured. There was no significant difference of serum

creatinine (E) or BUN (F) among TAM injected KMDAKT mice, corn oil injected KMDAKT

mice and TAM injected KSP/Cre ER^{T2} mice (n=10-11).

Figure 3.9

(A)   (B)

	Survival (%)	
Days after IRI	Left IRI + Right Nx (n=24)	Left IRI only (n=30)
0	24 (100.00%)	30 (100.00%)
1	9 (37.50%)	30 (100.00%)
2	6 (25%)	30 (100.00%)
3	0 (0.00%)	29 (96.67%)
4		26 (86.67%)
5		18 (60.00%)
6		17 (56.67%)
7		14 (46.67%)
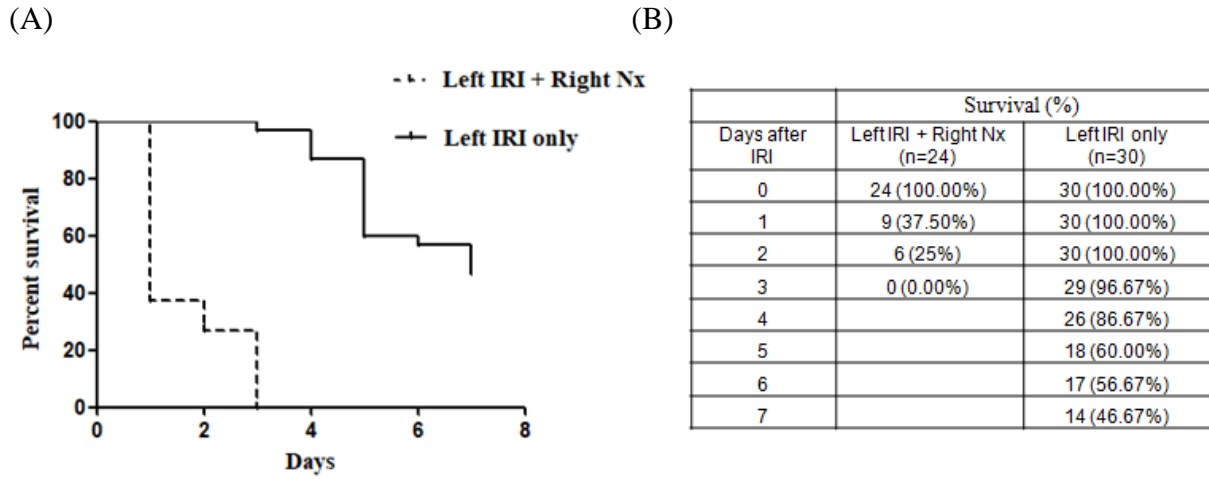
Figure 3.9 **Survival Analysis after Unilateral IRI AKI with/without Contralateral Nx in KMDAKT Mice**. One month after TAM induction, KMDAKT mice were subjected to unilateral IRI AKI and contralateral Nx or unilateral IRI. Survival rates were recorded after surgery. The survival rate was significantly lower with zero survival on day 3 in the group with unilateral IRI AKI and contralateral Nx (A&B). The survival rate was significant higher in the unilateral IRI group ($p<0.001$).

Figure 3.10

(A)

(B)

● Tamoxifen
▲ Corn oil
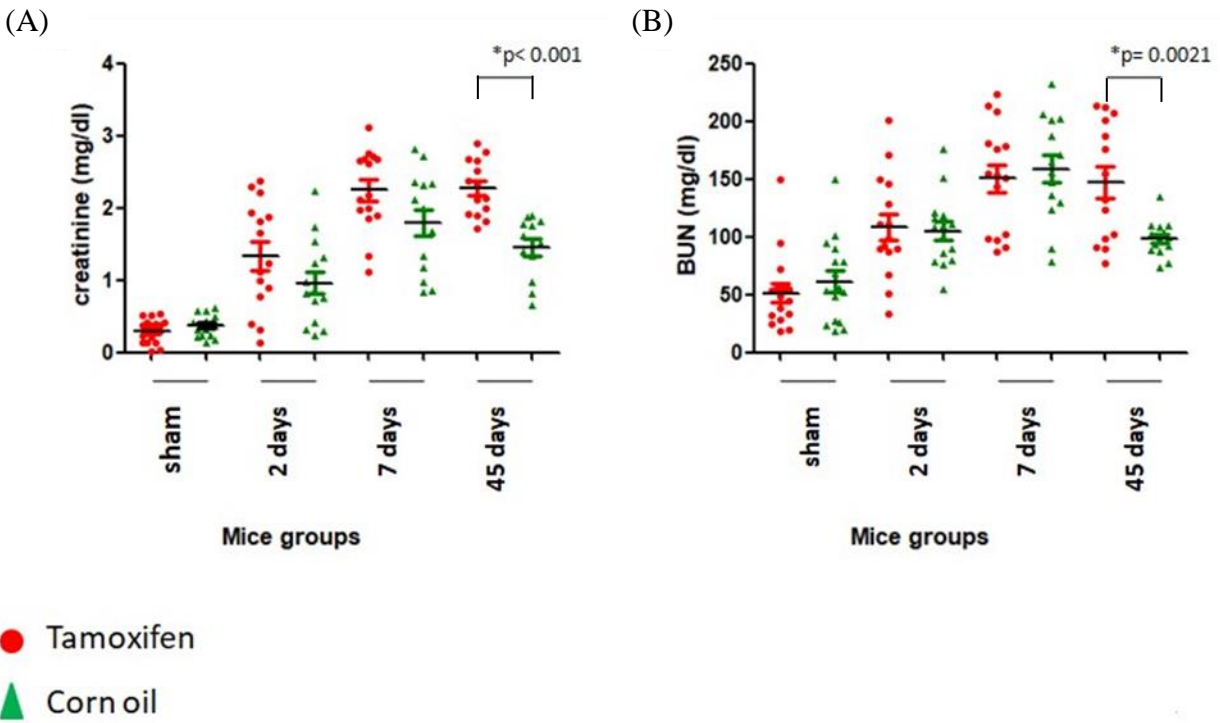
Figure 3.10 **Decreased Renal Function in TAM Treated KMDAKT Mice after IRI.** One month after TAM or corn oil injection, KMDNAKT mice were subjected to IRI AKI. Blood were collected at indicated time after surgery. Serum Cr. (A) and BUN (B) were measured. On day 45 day after IRI, both serum BUN (*p=0.021*) and Cr. (*p<0.001*) are significantly higher in TAM injected KMDAKT mice as compared to control (corn oil injected) KMDAKT mice.

Figure 3.11

(A)   Corn oil   Tamoxifen   (B)

Cortex

OSOM

ISOM

IM

Figure 3.11 **Aggravated Renal Injury in the AKT induced KMDAKT Mice after IRI.** One month after TAM or corn oil injection, unilateral IRI was performed in the mice. Kidney was harvested and fixed for histopathology analysis 7 days after IRI. Tubular necrosis, tubular lysis, tubular dilation, and cast were found in renal cortex, OSOM, ISOM, and IM in KMDAKT mice injected with TAM. The representative images are shown in (A). The tubular injury was scored by Jablonski score and shown in (B). There was significant higher Jablonski score in the TAM injected KMDAKT group when compared with corn oil injected KMDAKT group on day 7 after IRI (p=0.018) (n=12-14).

Figure 3.12

Figure 3.12 **Increased KIM-1 Expression in the KMDAKT Mice after IRI.** One month after

TAM or corn oil injection, unilateral IRI was performed in the mice. Kidney was harvested and

fixed for histopathology analysis 7 days after IRI. KIM-1 expression was examined by

immunohistochemistry to study the tubular injury. The KIM-1 protein (brown staining) was

found in cortex, OSOM, ISOM, and IM in KMDAKT mice injected with TAM, but rarely in

corn-oil injected group. The representative images were shown in (A). The KIM-1 protein

expression was measured by imageJ and shown in (B). There was higher KIM-1 expression (%)

in TAM injected KMDAKT group when compared with corn oil injected KMDAKT group on

day 7 after IRI (p=0.002) (n=12-14).

Figure 3.13
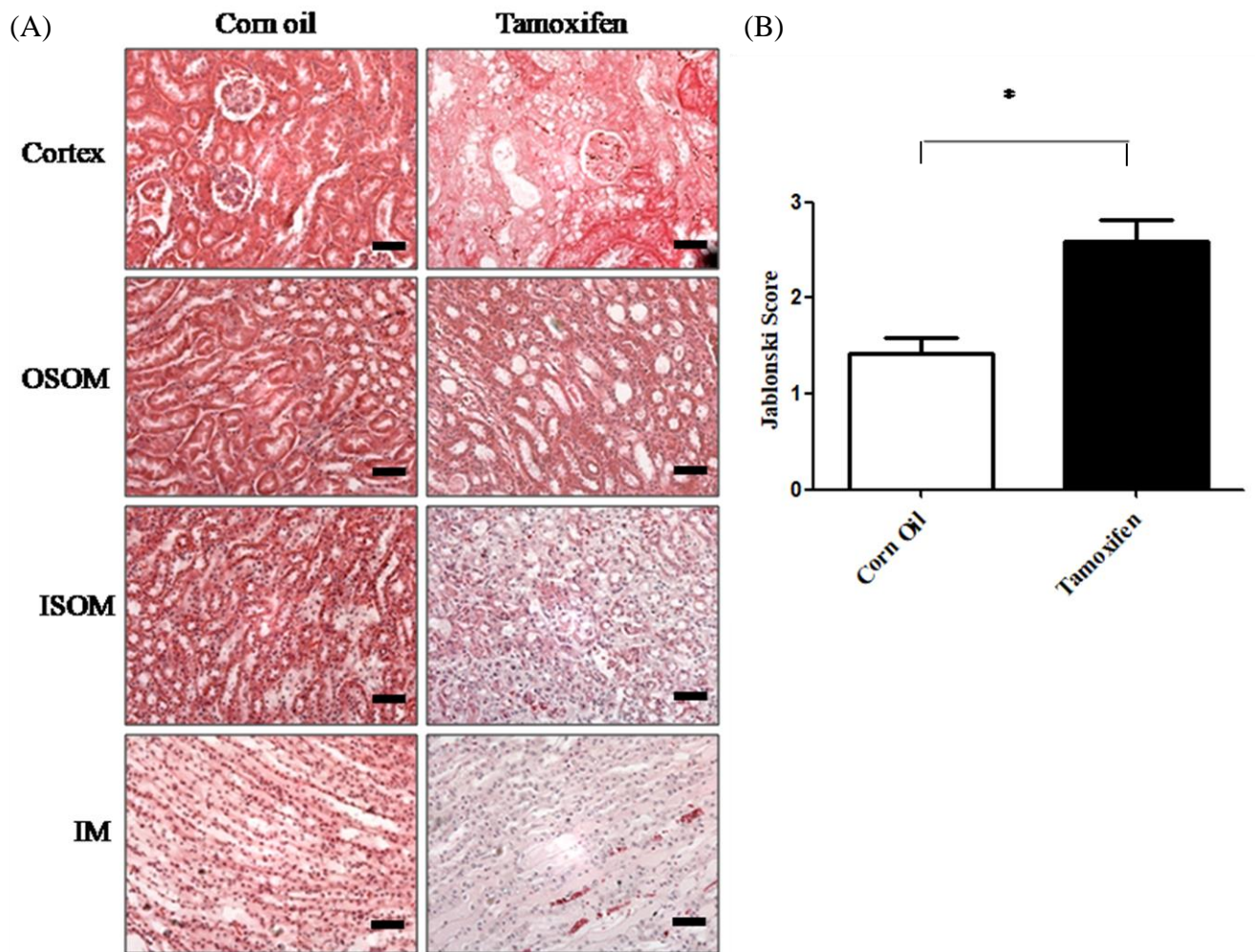
(A)   (B)
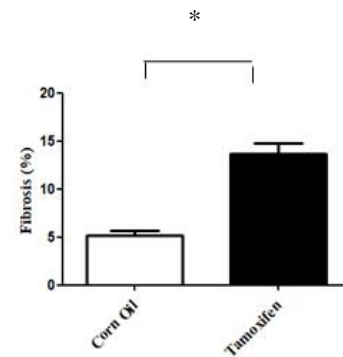
Figure 3.13 **Increased Renal Fibrosis in the KMDAKT Mice after IRI.** One month after TAM

or corn oil injection, unilateral IRI was performed in the mice. Kidney was harvested and fixed

for histopathology analysis 7 days after IRI. Masson's trichrome staining was performed to

examine the fibrosis. The fibrosis (blue staining) was found in kidney of KMDAKT mice

injected with TAM, but rarely in corn-oil injected group. The representative images were shown

in (A). The fibrosis area was measured by imageJ and shown in (B). There was significant larger

fibrosis area (%) in TAM injected KMDAKT group compared with corn oil injected KMDAKT

group on day 7 after IRI AKI ($p<0.001$) (n=12-14).
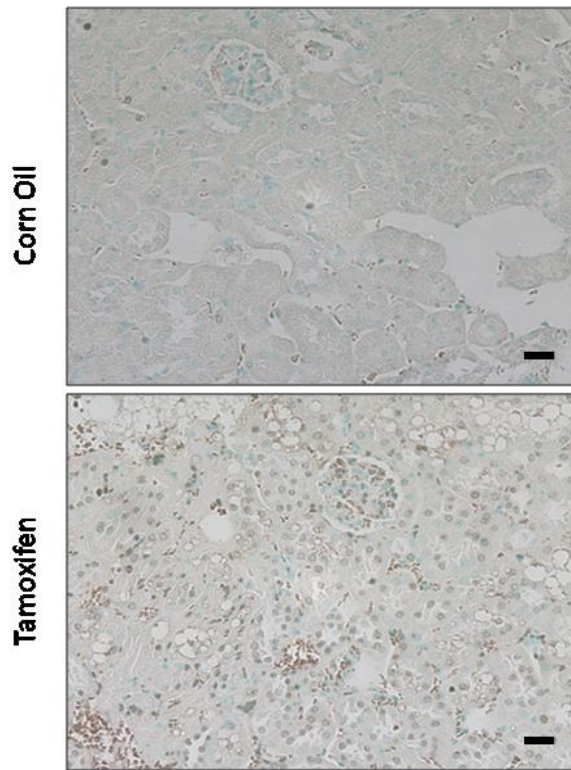
Figure 3.14
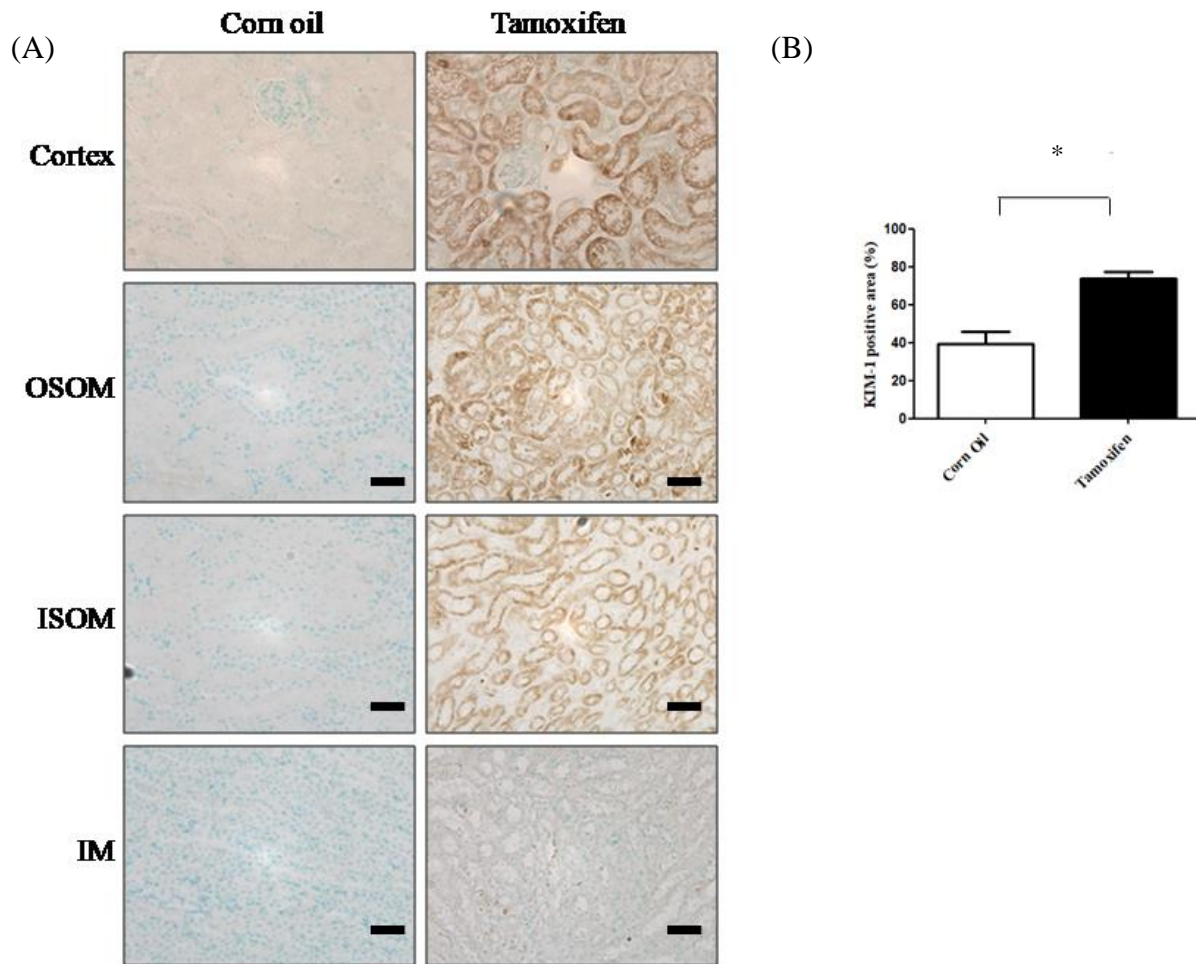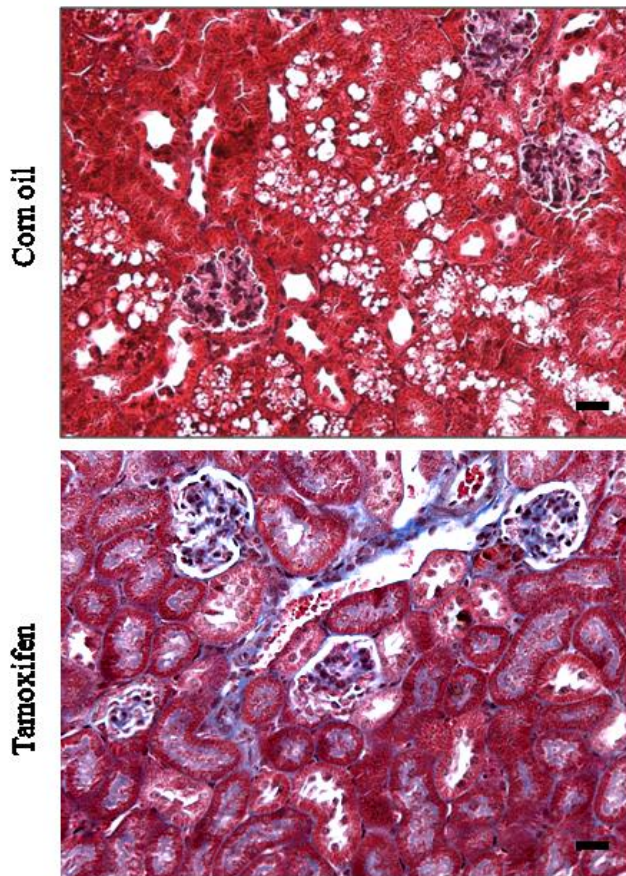(A)   (B)
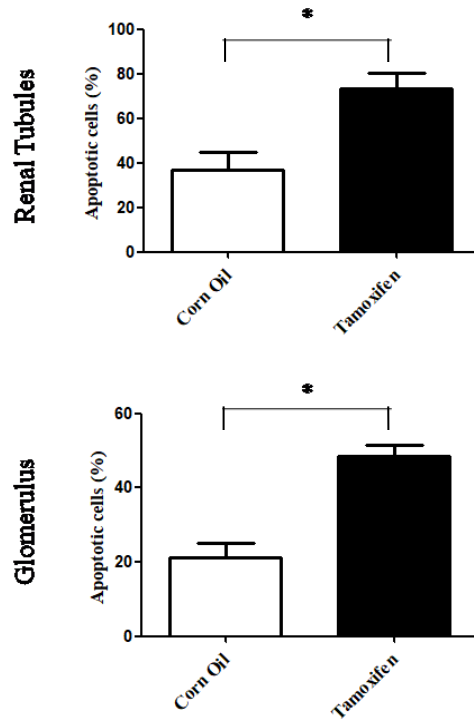
Figure 3.14 **Increased Kidney Apoptosis in the KMDAKT Mice after IRI.** One month after

TAM or corn oil injection, unilateral IRI was performed in the mice. Kidney was harvested and

fixed for histopathology analysis 7 days after IRI. Tunnel assay was performed to examine the

cellular apoptosis. The apoptotic cells (brown staining) were found in both renal tubular cells and

glomeruli. The representative images were shown in (A). The apoptotic area was measured by

imageJ and shown in (B). There was larger apoptotic area (%) in both renal tubules (p=0.0054)

and glomeruli (p<0.001) in TAM injected KMDAKT group when compared with corn oil

injected KMDAKT group on day 7 after IRI (n=12-14).

Figure 3.15

(A)

(B)
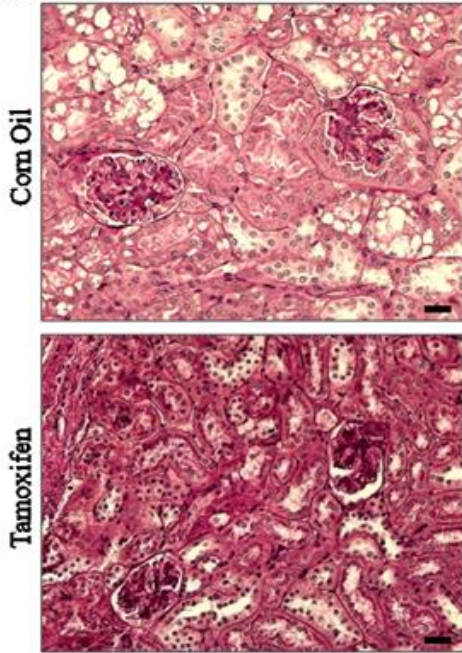
	Corn Oil (7days)	Tamoxifen (7days)
Grade 0	0	0
Grade 1	66	54
Grade 2	546	516
Grade 3	483	597

(C)

10 mice (50 glomeruli per animal)

(D)

(E)
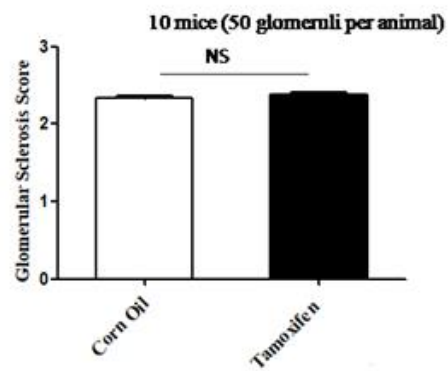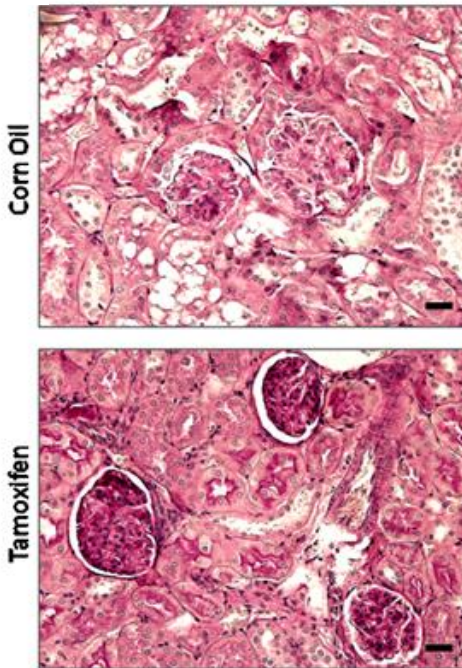
	Corn Oil (45 days)	Tamoxifen (45 days)
Grade 0	0	0
Grade 1	97	48
Grade 2	732	686
Grade 3	111	327

(F)

10 mice (50 glomeruli per animal)
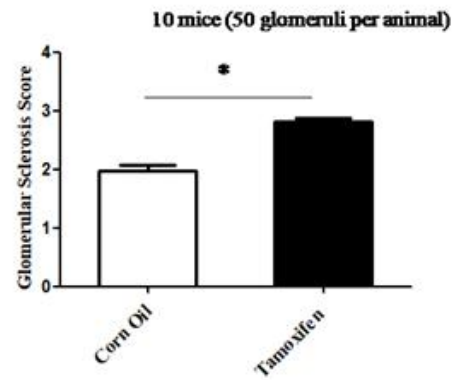
Figure 3.15 **Increased Glomerulosclerosis in the KMDAKT Mice on Day 45 after IRI.** One

month after TAM or corn oil injection, unilateral IRI was induced in the mice. Kidney was

harvested and fixed for histopathology analysis 7 or 45 days after IRI. Glomerulosclerosis was

examined by Periodic acid–Schiff (PAS) staining. The PAS result is graded as follows: 0 (no

lesions), 1 (lesions in up to 25% of glomeruli), 2 (lesions in 25 to 50% of glomeruli) or 3 (lesions

in > 50% of glomeruli). The representative images were shown in (A) for Day 7 results and (D)

for Day 45 results. The glomerulosclerosis was scored accordingly and shown in (B) and (E) and

plotted as histograghic in (C) and (F). At least 50 glumeri were scored for each mouse and at

least 10 mice were scored for each group. Glomerular sclerosis score was higher in Day 45 after

IRI in TAM injected KMDAKT group as compared with corn oil injected KMDAKT group

(*p<0.001*). However, there is no difference in glomerulosclerosis 7 days after IRI AKI

(*p=0.2634*).

Figure 3.16

(A)   (B)
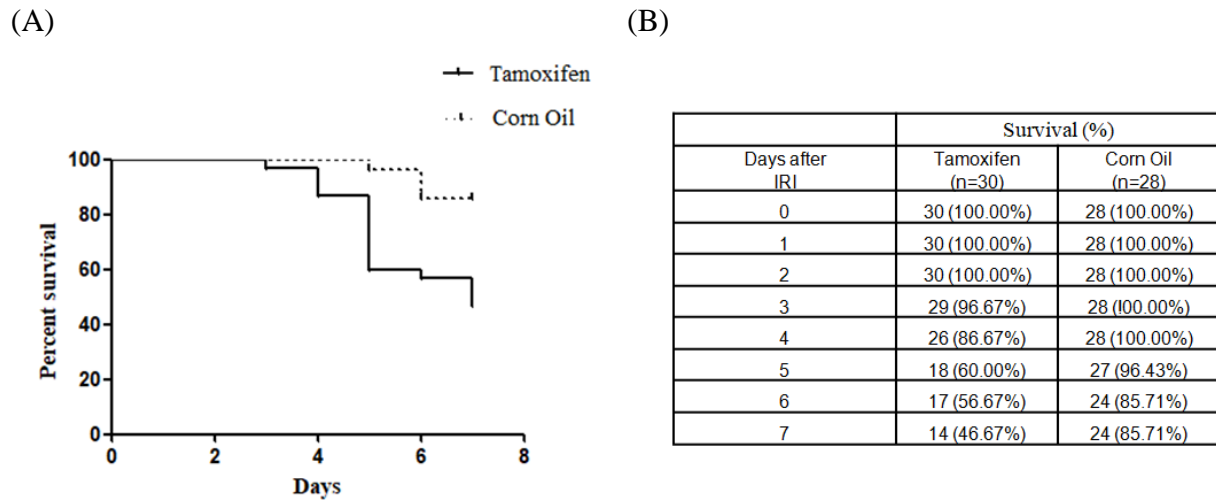
Figure 3.16 **Decreased Survival after Unilateral IRI AKI in TAM treated KMDAKT Group**.

One month after injection with TAM or corn oil, KMDAKT mice were subjected to unilateral

IRI AKI injury. Survival rate was recorded after surgery (A&B). The 7 day survival rate after

unilateral IRI was significantly lower in group with TAM injected KMDAKT (46.67%) as

compared to groups with corn oil injected KMDAKT (85.71%) (*p=0.0013*).

Figure 3.17

(A)
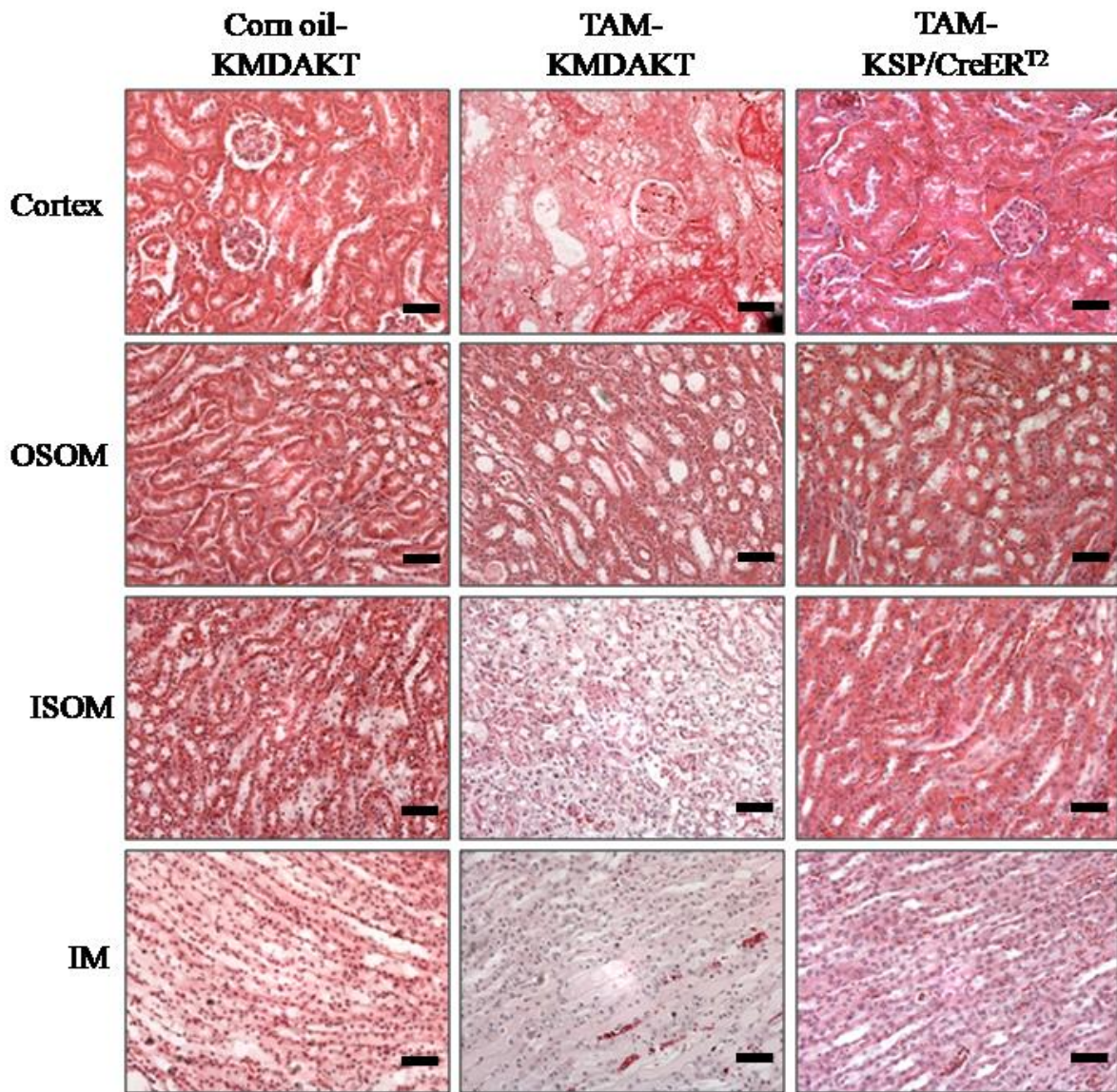
(B)
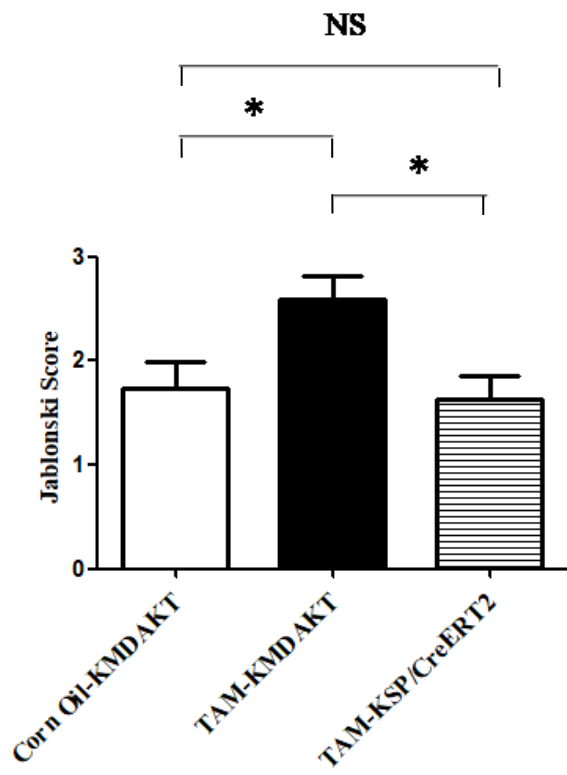
Figure 3.17 **No Cre Recombinase-associated Toxicity or Tamoxifen-associated Toxicity in AKI.** One month after TAM or corn oil injection, unilateral IRI was induced in the mice. Kidney was harvested and fixed for histopathology analysis 7 days after IRI. Tubular necrosis, tubular lysis, tubular dilation, and cast were found in cortex, OSOM, ISOM, IM in KMDAKT mice injected with TAM, but not in corn-oil injected group or tamoxifen-injected KSP/Cre ERT2 group. The representative images were shown in (A). The tubular injury was scored by Jablonski score and shown in (B). There was significant higher Jablonski scores between TAM injected KMDAKT group compared with TAM injected KSP/Cre ERT2 group on day 7 after IRI AKI (p=0.0072). But there was no significant differences of Jablonski scores between corn oil injected KMDAKT group compared with TAM injected KSP/Cre ERT2 group on day 7 after IRI AKI (p=0.7613).

CHAPTER 4

Activation of Tubule Mitochondrial AKT1 Improved the Outcomes of AKI

I. **Introduction**

Our laboratory has been investigating the role mitochondrialAKT1 signaling and the development of cardiomyopathy. Our data suggested that activation mitochondrial AKT1 could protect cardiomyocytes from IRI by reducing oxidative stress, preventing cross-membrane electrochemical gradient loss and inhibiting cardiomyocyte deaths [12]. In the last chapter, my data showed that inhibition of tubular mitochondrial AKT1 signaling aggravating renal injuries upon IRI and increased progression from AKI to CKD. This raised the possibility that we may be able to improve the outcomes of AKI by enhancing mitochondrial AKT1 signaling in the renal tubules. The following experiments are designed to test a new hypothesis that enhancing tubular mitochondrial AKT1 signaling can protect kidney against AKI and subsequent development of CKD after IRI. To test this hypothesis, we have developed a novel transgenic mouse harboring an inducible tubular cell-specific, mitochondria-targeting constitutively active AKT1 with Cre-lox strategy (KMCAKT mice).

II. **Materials and Methods**

1. **Bi-transgenic Mice for Renal Tubule-specific Mitochondria-targeting Constitutively Active AKT1**

The murine AKT1 was mutated T308 to D308 and S473 to E473 to construct a constitutively active AKT1 [71]. To target AKT1 to mitochondria, we fused a mitochondrial targeting sequence (MSVLTPLLLRGLTGSARRLPVPRAKIHSL) at the amino terminus of constitutively active AKT1 (Figure 4.1). In addition, we attached a His-tag at the carboxyl

terminus of constitutively active AKT1.We have generated a transgenic mouse line by knocking in a TAM-inducible mitochondria-targeting constitutively active AKT (mcaAKT) with CAG promoter into the Rosa26 locus. We crossed the TAM-inducible mcaAKT mice with the KSP/CreER[T2] mice (courtesy of Dr. Peter Igarashi from UT Southwestern Medical School) driven by renal tubular cell specific cadherin promoter to produce a new bi-transgenic mouse line, KMCAKT, for renal tubule-specific expression of mcaAKT [73]. The renal tubule-specificity was achieved with Cre-Lox strategy (Figure 4.2).

a. TAM Treatment

KMCAKT were administered TAM to induce Cre/loxP recombination. TAM (Sigma), was dissolved in corn oil to a final concentration of 25 mg/ml. Mice were administered TAM (100 mg/Kg body weight) daily by intraperitoneal injection for five consecutive days. Control animals received an equal volume of vehicle alone (corn oil). The transgene expression was confirmed 4 weeks after the first day of injection. Animal were arranged IRI AKI 4 weeks after the first day of injection.

b. Experimental Animals

KMCAKT mice were kept in humidity-controlled environment within a thermoneutral zone. Mice were fed with standard laboratory chow (2020X, EnvigoTeklad, UK) and water until the start of the experiment. All mice were kept under identical condition. The experimental protocol was approved by the Institutional Animal Care and Use Committee at the University of California at Irvine and complied with the National Institutes of Health guidelines.

c. **Mice Model of IRI AKI**

Mice were anesthetized with 2.5% tribromoethanol (avertin). Unilateral renal ischemia was induced by ligating the left renal pedicles for 30 minutes under anesthesia with concurrent contralateral total Nx. During the surgery, the core body temperature was maintained at 34°C–36°C. Reperfusion was induced by releasing the ligation. Mice were kept at ambient temperature (30°C–32°C) after ischemia and reperfusion at indicated time intervals. Control mice were subjected to the same procedure (sham), but the renal pedicles were not ligated and no Nx was performed.

d. **Mitochondrial AKT1 Activity in TAM treated KMCAKT**

To analyze the mcaAKT effect on mitochondrial AKT activity, IP-kinase assay was performed using GSK3alpha, downstream target of AKT, as substrate and mitochondrial lysate as kinase source. Renal mitochondrial AKT1 activity decreased in TAM injected KMCAKT compared to corn oil injected KMCAKT. As control, mitochondrial lysate from KMCAKT mice without AKT specific antibody incubation was used for IP-kinase assay (lane 3). P-GSK-3α: phosphorylated GSK-3-α. GSK-3α is the downstream substrate of AKT.

e. **Serum BUN and Cr.**

At the end of experiment, blood was collected from the retro-orbital plexus under anesthesia with avertin. Serum was obtained by centrifugation at 10,000 RCF for 30 min at room temperature. Serum BUN and Cr. was determined with a colorimetric assay kit (BioAssay Systems, Hayward, CA), and analyzed with a Biotek Synergy HT plate reader.

f. Renal Histology

i. HE Staining

Kidney samples were fixed in 10% formalin for 24 hours, dehydrated, and embedded in paraffin. Paraffin-embedded kidney blocks were sectioned at 4μm thick.

HE staining was performed to evaluate renal structure injury. After deparaffinization, the tissue sections were stained in Mayer's hematoxylin solution (Sigma-Aldrich, MO) for 15 minutes, rinsed with running tap water for 2 minutes, and stained with bluing solution (0.1% sodium bicarbonate) for 5 minutes. The slides were counterstained with eosin-phloxine solution for 20 seconds, mounted and dehydrated with ethanol (70, 90, and 100%). Images were captured with Keyence BZ-X810 Inverted Microscope (Keyence, Osaka, Japan) and analyzed with Keyence BZ-X800 Analyzer software. Cross-sectional glomerular area (in μm) were determined from at least 20 randomly images from each sample. The investigators who analyzed the histology were blinded to the samples. Renal damage in proximal tubules from cortex area, OSOM, ISOM, and IM of the kidney were evaluated with a semi-quantitative analysis of histological damage areas as previously described [59]. The Jablonski grading scale (0–4) was used for the assessment of IRI induced necrosis of the overall proximal tubules[60]. In both analysis, about one hundred tubules were scored in each section and the total scores divided by the number of tubules analyzed, and according to the following criteria: 0, normal; 1, areas of tubular epithelial cell swelling, vacuolar degeneration, necrosis and desquamation involving< 25% of the tubular profile; 2, similar changes involving> 25% but< 50% of the tubular profile; 3, similar changes involving> 50% but< 75% of the tubular profile; 4, similar changes involving> 75% of the tubular profile [59].

ii. Masson's Trichrome Staining

Paraffin-embedded tissues were de-paraffinized in xylene (2 washes for 3 min each) and hydrated in graded ethanol to distilled water. Masson's trichrome staining was performed to evaluate collagen fibrils in renal tissues by using the reagents from Sigma-Aldrich (MO, USA) [61]. The slides were mordant in Bouin's solution (picric acid, formaldehyde, and glacial acetic acid) overnight. After washing with water, and the slides were stained with Weigert's Iron Hematoxyline Solution for 30 minutes, Biebrich Scarlet-Acid Fucshin for 15 minutes, phosphomolybdic-phosphotungstic acid solution for 10 minutes, and then aniline blue for 20 minutes. After briefly submerged in 0.5% acetic acid solutions, the slides were dehydrated through 95% alcohol, 100% alcohol, and xylene. Blue coloration, indicative of collagen in the extracellular matrix (ECM), was digitally calculated with ImageJ [62], ECM content was quantified as mean blue intensity per tissue area.

iii. IHC Staining of KIM-1

Paraffin-embedded kidney sections were deparaffinized and incubated with 0.05% saponin at room temperature for 30 minutes for antigen unmasking. Then the slides were sequentially incubated with 4% BSA for background blocking, anti-KIM-1 antibody at 4 °C overnight, and biotinylated α-rabbit secondary antibody (Vector Lab) for 45 minutes at room temperature. After several rinses in PBS, they were incubated with VECTASTAIN ABC kit (Vector Lab) to recognize biotinylated secondary antibody and conjugate with horseradish HRP. After several rinses in PBS, the bound peroxidase was visualized by incubating the sections with a solution containing DAB (Sigma-Aldrich, MO) following the manufacturer's instructions. Finally, the slides were counterstained with1% Methyl Green. 20 microscopic fields were randomly selected

from each tissue section and the percentage of positive staining tubules was evaluated by ImageJ.

iv. TUNEL Staining

To detect the apoptosis of renal tissues, I used the In Situ Cell Death Detection Kit (Roche, Basel, Switzerland). Paraffin-embedded kidney sections were deparaffinized and incubated with 0.05% saponin at room temperature for antigen unmasking. It was performed to evaluate apoptosis following the protocol provided by the manufacturer [75]. Then the slides were counterstained in 1% Methyl Green. For quantification, 20 fields were randomly selected from each tissue section and the positive staining nuclei were evaluated by the manual in ImageJ. And positive cells were compared between TAM injected mice and control with two-tailed Student's t-test.

v. IF Staining

Paraffin-embedded kidney sections were deparaffinized and immersed with 0.1M Tris (pH 10) antigen retrieval buffer and they were heated in an 1100 W GE microwave oven for three sequential 5-min cycles at power levels 5, 4 and then 3 in microwave oven. After washing with PBS, slides were incubated with specific primary antibodies overnight at 4°C, washed with PBS, conjugated secondary antibodies with 3 minutes heating cycle and 2 minutes incubation, counterstained with4',6-diamidino-2-phenylindole (DAPI, 1ug/ml) and mitotracker (10nM), and analyzed with Keyence BZ-X810 Inverted Microscope (Keyence, Osaka, Japan).

2. Mitochondria Preparation

Renal cortical and outer medulla tissues were isolated from the kidney, minced, washed with ice-cold PBS 3 times, and suspended in mitochondria isolation buffer (20 mM HEPES-KOH, pH 7.2, 10 mM KCl, 1.5 mM $MgCl_2$, 1.0 mM sodium EDTA, 1.0 mM sodium EGTA, 1.0 mM dithiothreitol, 2 mM phenylmethylsulfonyl fluoride, 20 mM NaF, 2 mM Na3VO4, and 250 mM sucrose). After centrifugation at 2500 RPM for 10 min at 4°C, the samples were incubated on ice for 30 min and homogenized with 20 strokes of loose pestle and 50 strokes of tight pestle in a Dounce homogenizer. The nuclei and cell debris were removed by centrifugation at 1,000g for 15 min at 4°C. The supernatants were centrifuged at 10,000g for 30 min at 4°C, and the resulting mitochondrial fractions were re-suspended with mitochondria isolation buffer. The supernatants were further centrifuged at 100,000g for 1 hour at 4°C. The supernatants and mitochondrial fractions were stored at -80°C if not immediately used for biochemical analysis.

3. **Western Blots**

The mitochondrial fractions were dissolved in 2% lauryl maltoside solution supplemented with 10% Sigma FAST[TM]protease inhibitor (Sigma-Aldrich, S8820). Protein contents were determined with an EppendorfBioPhotometer by BCA method [63]. Equal amounts of proteins from each sample were resolved with 10% SDS-polyacrylamide gel and then transferred onto polyvinylidene difluoride membranes. The membranes were blocked with 5% fat-free milk or 5% BSA for one hour before incubation with primary antibodies overnight at 4℃, washed three times with TBS-T (20mM Tris–HCl, pH7.5, 0.5 mM NaCl, and 0.1% Tween 20), incubated with anti-rabbit IgG, horseradish peroxidase -linked antibody (#7074) (1:2000 dilution in 5% fat-free milk or 5% BSA), washed three times with TBS-T, and then incubated with West Pico

Chemiluminescent Substrate (Thermo Scientific, Pittsburgh, PA) to visualize the proteins. The images were acquired with a Syngene G:BOX and analyzed with ImageJ.

4. Materials

Primary antibody: His-Tag(D3I1O) XP® (♯12698) antibodies were purchased from Cell Signaling Technology (Danvers, MA). KIM-1 (♯AF1817) antibodies were purchased from R&D Systems (Minneapolis, MN).VDAC was purchased from MiliporeSigma (Burlington, MA). MitoTracker®Green FM (M7514) were purchased from Invitrogen (Carlsbad, CA, USA).Secondary antibody Alexa Fluor® 555 (A31572) was purchased from Thermo Fisher Scientific (Waltham, MA). The QuantiChrom^{TM} Urea Assay Kit and QuantiChrom^{TM} Creatinine Assay Kit were purchased from BioAssay Systems (Hayward, CA).

5. Statistical Analysis

Data are presented as mean ± SD, unless noted otherwise. Statistical data were analyzed with GraphPd Prism 5 software, with Student's t test or ANOVA when indicated. The ROI of western blot was quantified by ImageJ, normalized with the ROI value of loading control and analyzed with Student's t test. The statistical significance level was set at $p < 0.05$.

V. Results

1. Renal Tubule-Specific Expression of mcaAKT after Tamoxifen Injection

The first goal of this chapter was to establish a transgenic mice model with renal tubular specific mitochondria-targeting constitutive active AKT1. To this end, I crossed the TAM-inducible mcaAKT mouse with the KSP/CreER^{T2} mice to produce a bi-transgenic KMCAKT

mouse (Figure 4.1). The transgene was induced by TAM injections. To confirm transgene

expression, mitochondria prep was isolated by gradient centrifugation and mitochondrial

proteins were resolved with SDS-PAGE (Figure 4.3). Western blot showed that TAM

successfully induced the expression of mutant AKT1 in renal mitochondria. The mutant protein

could not be detected in the vehicle injected KMCAKT mice, KSP/CreER^{T2} mice, or wild type

(WT) mice (Figure 4.3A). Therefore, the transgene was successfully induced as expected. To

verify organ specific expression, mitochondrial proteins were extracted from various organs of

KMCAKT after TAM injection. The His-tagged mutant AKT could only be found in the kidney

(Figure 4.3B). To verify the mutant AKT was localized to the mitochondria in renal tubule,

renal sections were used to visualize co-localization of mutant AKT and mitochondria with IF

staining (Figure 4.3C). The results showed all mutant AKT stained with His-tag localized to

mitochondria. No mutant AKT was seen in other parts of kidney. To evaluate the activity of

mcaAKT, we compared the enzymatic activities of AKT in the mitochondria isolated from the

TAM-treated and corn-oil-treated mice, the results showed renal mitochondrial AKT activities

were significantly increased in the TAM-treated KMCAKT mice (Figure 4.4). These results are

similar to the results of KMDAKT mice, further verified the specificity of mitochondria-

targeting strategy. This transgenic model provides a good in vivo model to study the role of

renal tubular mitochondria AKT.

2. **Improvement of Renal Failure and Renal Fibrosis in KMCAKT Mice after IRI**

The effect of mcaAKT in AKI was investigated with KMCAKT mice, by unilateral IRI

protocol with concurrent contralateral Nx as described earlier in this thesis. To study whether

activation of tubular mitochondria AKT played a role in the outcome of IRI AKT, I compared

the changes of serum renal function of TAM-KMCAKT and control post IRI AKI (Figure 4.5). There was significantly higher serum Cr. on day 2 and day 7 after AKI in corn oil injected KMCAKT ($p=0.0003$, $p=0.0092$, respectively). There was significantly higher serum BUN on day 7 after AKI in corn oil injected KMCAKT ($p=0.03$) in BUN or Cr. Both Cr. and BUN were significantly higher 45 days after AKI ($p=0.0055$, $p=0.0313$, respectively) in corn oil injected KMCAKT mice. These results indicated that activation of mitochondrial AKT in renal tubules during IRI led to improvement of consequent CKD. To gain insight into the changes of renal structure, kidney histology was analyzed. HE staining of renal sections from these mice showed severe renal injuries in the corn oil-injected mice. Jablonski scores of renal tubular injury were higher with more tubular brush border loss, tubular lysis, and debris in tubular lumen space in the controls ($p=0.038$) (Figure 4.6A and B). Marker for renal tubule injury KIM-1 was also significantly lower in the TAM-KMCAKT mice ($p<0.001$) (Figure 4.7). Masson's trichrome stain showed smaller fibrosis area (%) in the TAM-KMCAKT mice after IRI ($p=0.002$) (Figure 4.8). TUNEL staining showed more apoptotic cells in the corn oil-KMCAKT after IRI. Renal tubule apoptosis and glomerular apoptosis were significantly less in the TAM-KMCAKT mice ($p=0.0064$ and $p=0.0021$) (Figure 4.9A and B). Glomerulosclerosis was accordingly reduced 7 days and 45 days after IRI in the TAM-KMCAKT mice ($p=0.001$) (Figure 4.10). Therefore, activating tubular mitochondrial AKT1 during IRI protected against tubular cell injuries, prevented debris accumulation in the renal tubules, and attenuated the glomerular damages that followed tubular injury.

3. **Activation of Renal Tubule Mitochondrial AKT1 Improved Long-term Survival after AKI**

To examine the long-term outcome post AKI, I analyzed the survival rate of TAM-KMCAKT mice and control mice after induction of IRI. The survival rate on day 7 after IRI AKI of TAM-injected KMCAKT mice was significantly higher when compared to the corn-oil injected KMCAKT mice ($p<0.001$) (Figure 4.11).

VI. Discussion

The data presented in this chapter provide strong evidence to support our hypothesis that enhancing tubular mitochondrial AKT1 activation can protect kidney against AKI and subsequent development of CKD after IRI, and confirmed the critical role of mitochondrial AKT signaling in modulating the outcome of kidney injury and AKI transition to CKD. Survival after AKI was significantly increased in the TAM-KMCAKT mice, accompanied by lesser renal tubular damage, glomerulosclerosis, renal fibrosis, and better overall renal function.

It is well known that AKI may precipitate development of CKD. Although the exact mechanisms underlying the transition of AKI to CKD are not fully understood, recent studies suggest proximal tubule injury might trigger transition to CKD [87, 90, 91]. Administration of diphtheria to a transgenic model expressing proximal tubule-specific expression of diphtheria toxin receptor led to renal fibrosis and glomerulosclerosis, and the severity and frequency of proximal tubule injury determined the progression to CKD [91]. Identification of tubulointerstitial histopathology in the pathogenesis of chronic kidney disease has shifted the glomerulocentric paradigm of kidney injury to new attention on the pathophysiological role of proximal tubule in kidney injury and transition to CKD [92, 93]. It has been proposed that proximal tubular injury could lead to loss of tubular cell polarity, loss of cell-cell junction, cell

shedding into tubule, obstruction of tubule, loss of tubule function, and retrograde damage to glomerulus and glomerular filtration [94, 95].

Currently there is no effective therapy that can be used to reduce the risk of CKD in human AKI. The results of experiments presented in this chapter suggest that proximal tubule mitochondria AKT1 could be a novel therapeutic target for the prevention of AKI progression into CKD. New strategies to enhance proximal tubule mitochondrial AKT1 activities should be further explored for better prevention and treatment of AKI and CKD.

Figures

Figure 4.1

MSVLTPLLLRGLTGSARRLPVPRAKIHSL
Mitochondrial targeting sequence

$T^{308} \rightarrow E^{308}$ $S^{473} \rightarrow E^{473}$

NH2 — [PH Domain] [Kinase Domain] — COOH

6XHis
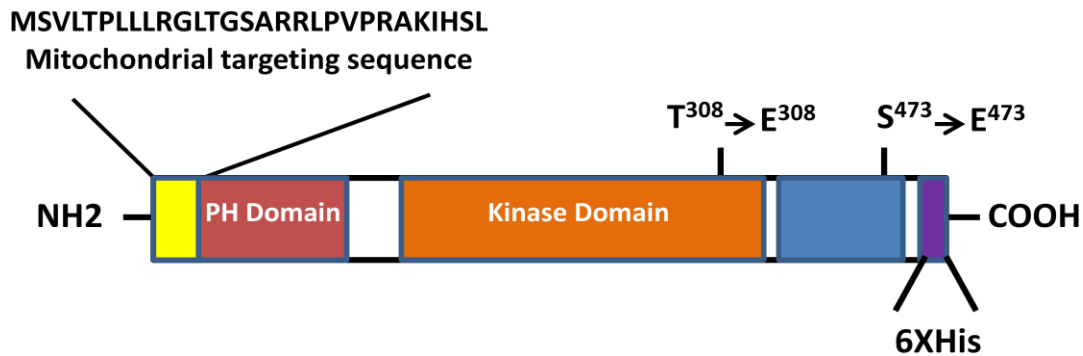
Figure 4.1 **The Mitochondria-targeting Constitutive Active AKT1 Construct.** Mitochondria targeting sequence was in frame fused to AKT1 cDNA at the N terminus. A 6X His was in frame fused to the C terminus of AKT1 cDNA. To generate the constitutive active AKT1, the AKT1 phosphorylation sites, threonine (T) 308 and serine (S) 473 were mutated to glutamic acid (E) to mimick phosphorylation.

Figure 4.2
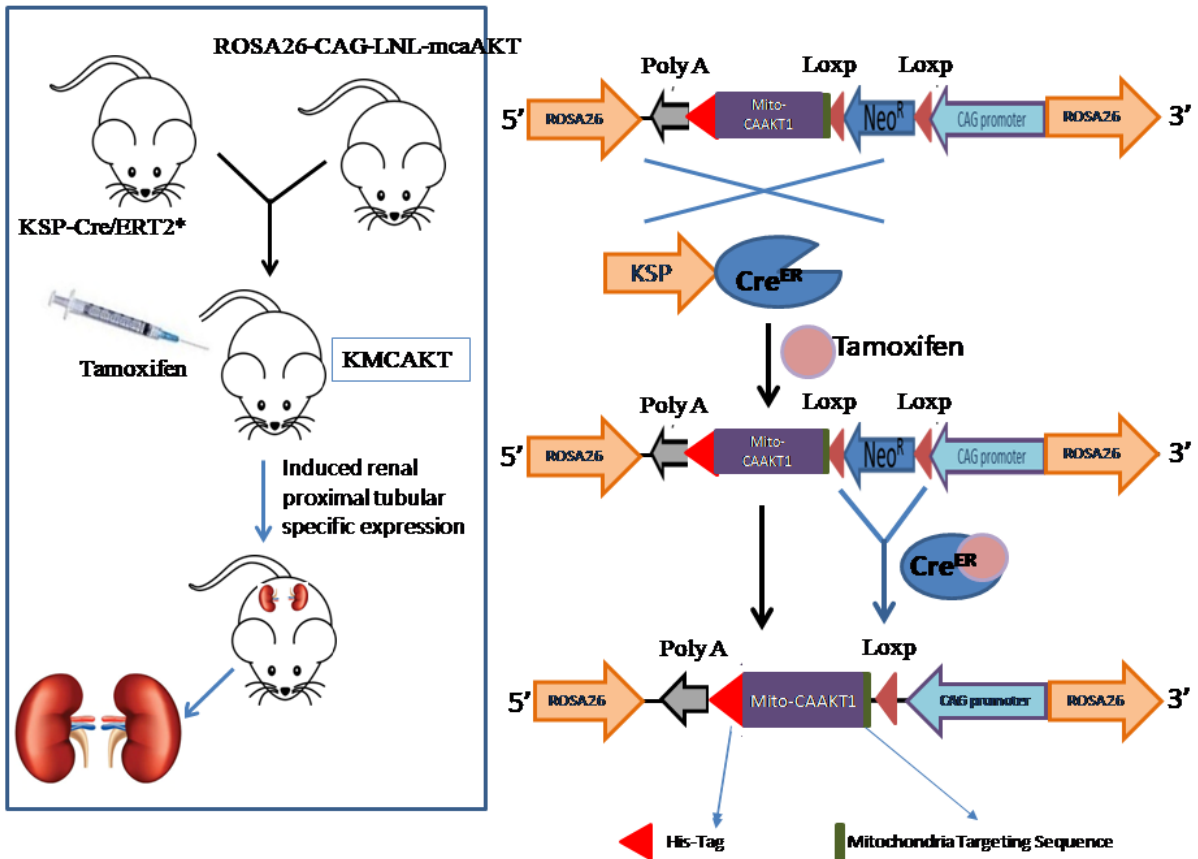
Figure 4.2 **Design of Bi-transgenic Mice (KMCAKT) for Renal Tubule Specific Mitochondria-targeting Constitutive Active AKT1 (mcaAKT1) Expression.** This scheme outlines the strategy for renal-specific overexpression of mitochondria-targeting constitutive active AKT1. A mitochondria-targeting sequence was inserted at the 5' end of the AKT1 cDNA with T308 and S473 mutated into Glutamic acid. A mouse with Cre recombinase driven by renal tubular epithelial cell promoter (KSP/CreER[T2]) was used to cross with mcaAKT1 mice, TAM injection induces mcaAKT in the tubules [73].

Figure 4.3

(A)

(B)

(C)

Figure 4.3.**Renal Tubule-specific Expression of mcaAKT.** KMCAKT mice with inducible mitochondrial-targeting constitutive active AKT1 in renal tubular cells. KMCAKT mice were used for this study. Eight weeks old KMCAKT mice were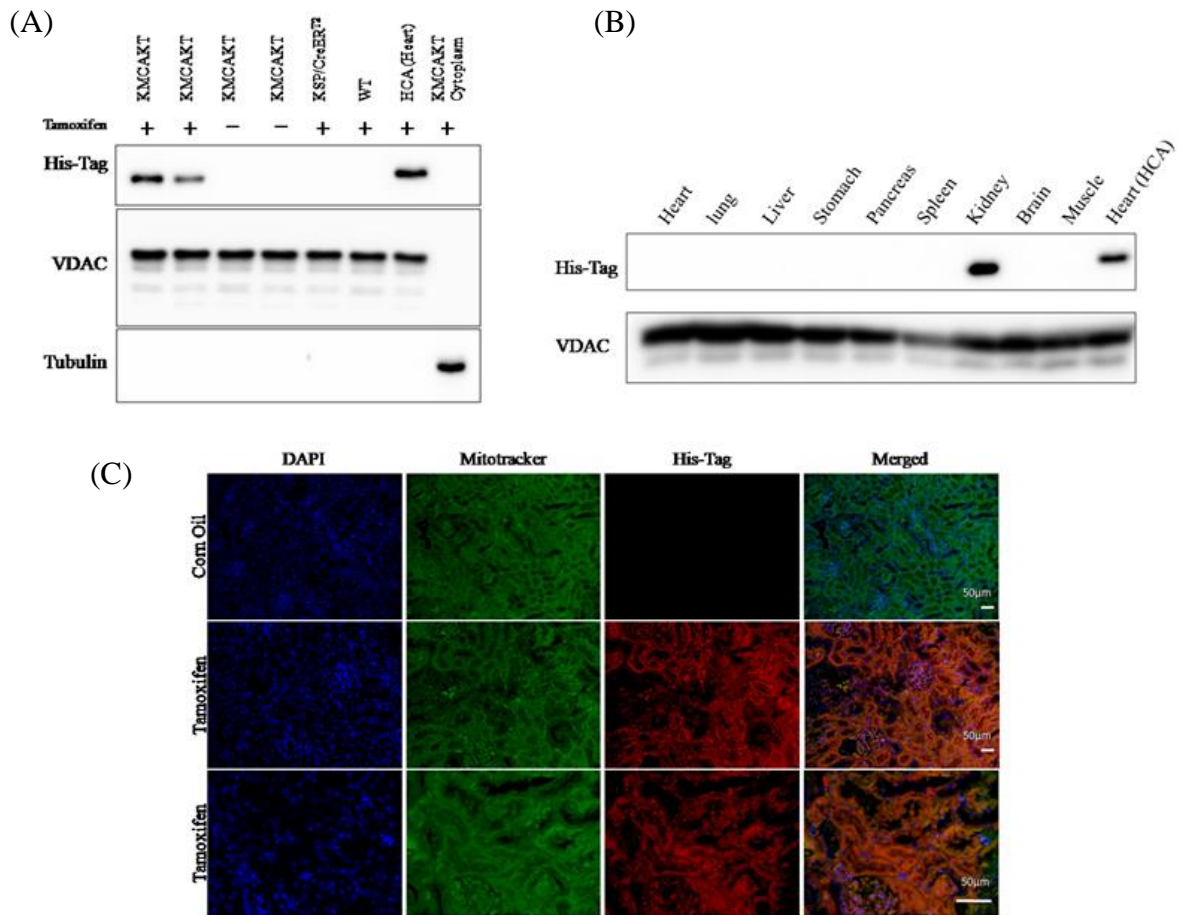 injected with tamoxifen (TAM) or corn oil. The mitochondria fraction was isolated and expression of mcaAKT was examined by Western Blotting analysis using antibodies against His-tag. (A)Western blot with mitochondria proteins showed mcaAKT only expressed in the renal mitochondria isolated from KMCAKT after TAM injection but not in KMCAKT with corn oil injection. mcaAKT was not detected in renal mitochondria of TAM-injected KSP/CreER^{T2} mice or TAM-injected WT mice. mcaAKT expression from the cardiac mitochondria of TAM-injected HCA mice seemed as positive control. (B) Renal specific expression of mcaAKT in TAM-injected KMCAKT mice. After TAM injection, mitochondria fraction was isolated from various organs. mcaAKT expression was detected by antibodies against His-tag. VDAC was used as loading control and mitochondria marker. The expression of mcaAKT was only detected in mitochondria isolated from kidney. (C) Mitochondrial localization of mcaAKT. Co-localization of mcaAKT and mitochondria in the renal tubules was studied by IF staining with anti-His-Tag antibody (His-Tag (D3I1O)XP® and MitoTracker® Green FM (ThermoFisher Scientific) WT: wild type mice, HCA: bi-transgenic heart-specific mcaAKT mice.

Figure 4.4
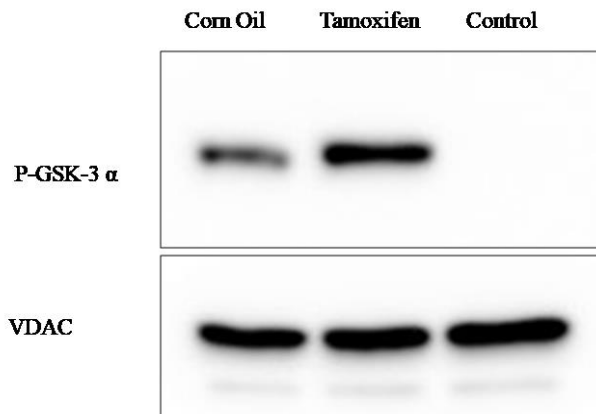
Figure 4.4 Mitochondrial AKT1 Activity in TAM-injected KMCAKT after IRI. To analyze

the mcaAKT effect on mitochondrial AKT activity, IP-kinase assay was performed using

GSK3alpha, a downstream target of AKT, as substrate and mitochondrial lysate as kinase source.

Renal mitochondrial AKT1 activity decreased in TAM-injected KMCAKT as compared to corn

oil-injected KMCAKT one hour after IRI AKI. Mitochondrial lysate from KMCAKT mice

without AKT pull-down was used as negative control. P-GSK-3α: phosphorylated GSK-3-α.

GSK-3α.
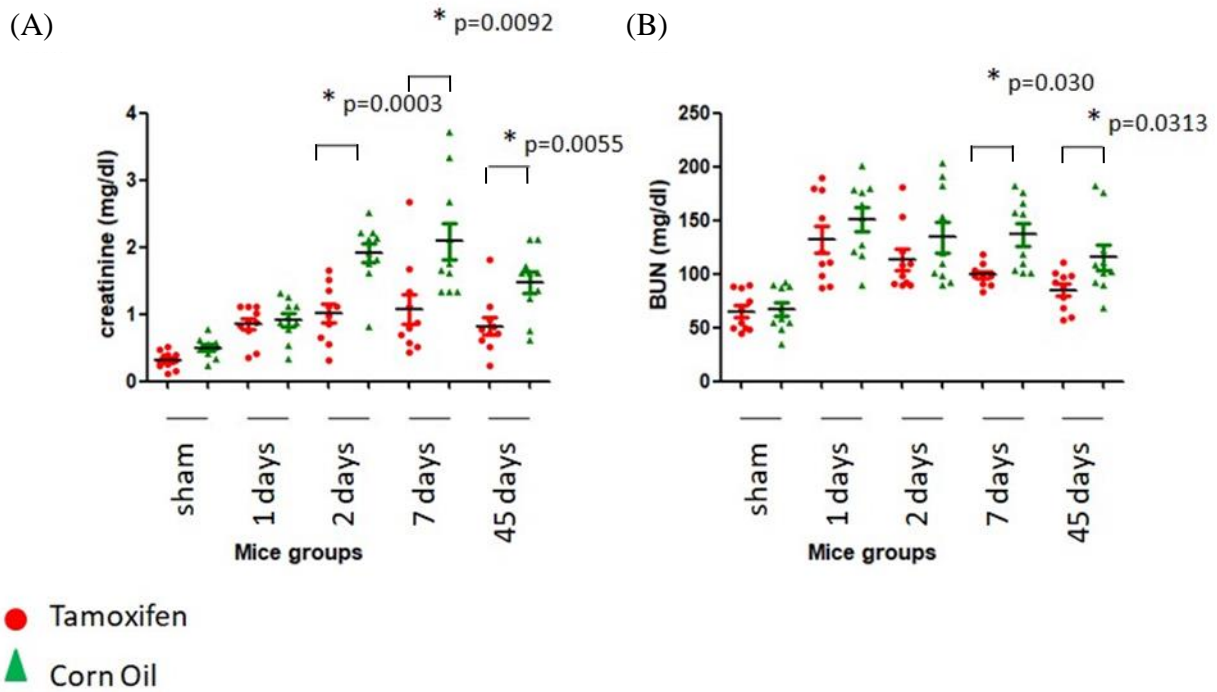
Figure 4.5

Figure 4.5. **Renal Function of KMCAKT Mice after IRI.** One month after TAM or corn oil injection, KMCAKT mice were subjected to IRI AKI. Serum Cr. (A) and BUN (B) were measured. On day 2 after IRI, serum Cr. (*p=0.003*) were significantly lower in TAM-injected KMCAKT mice as compared to the control (corn oil injected) KMCAKT mice. On day 7 after IRI, both serum BUN (*p=0.03*) and Cr. (*p=0.092*) were significantly lower in TAM-injected KMCAKT mice when compared to the control (corn oil injected) KMCAKT mice. 45 days after IRI, both serum BUN (*p=0.0313*) and Cr. (*p=0.055*) were significantly lower in TAM-injected KMCAKT mice when compared to the control (corn oil injected) KMCAKT mice (n=10-11).

Figure 4.6

(A)

(B)
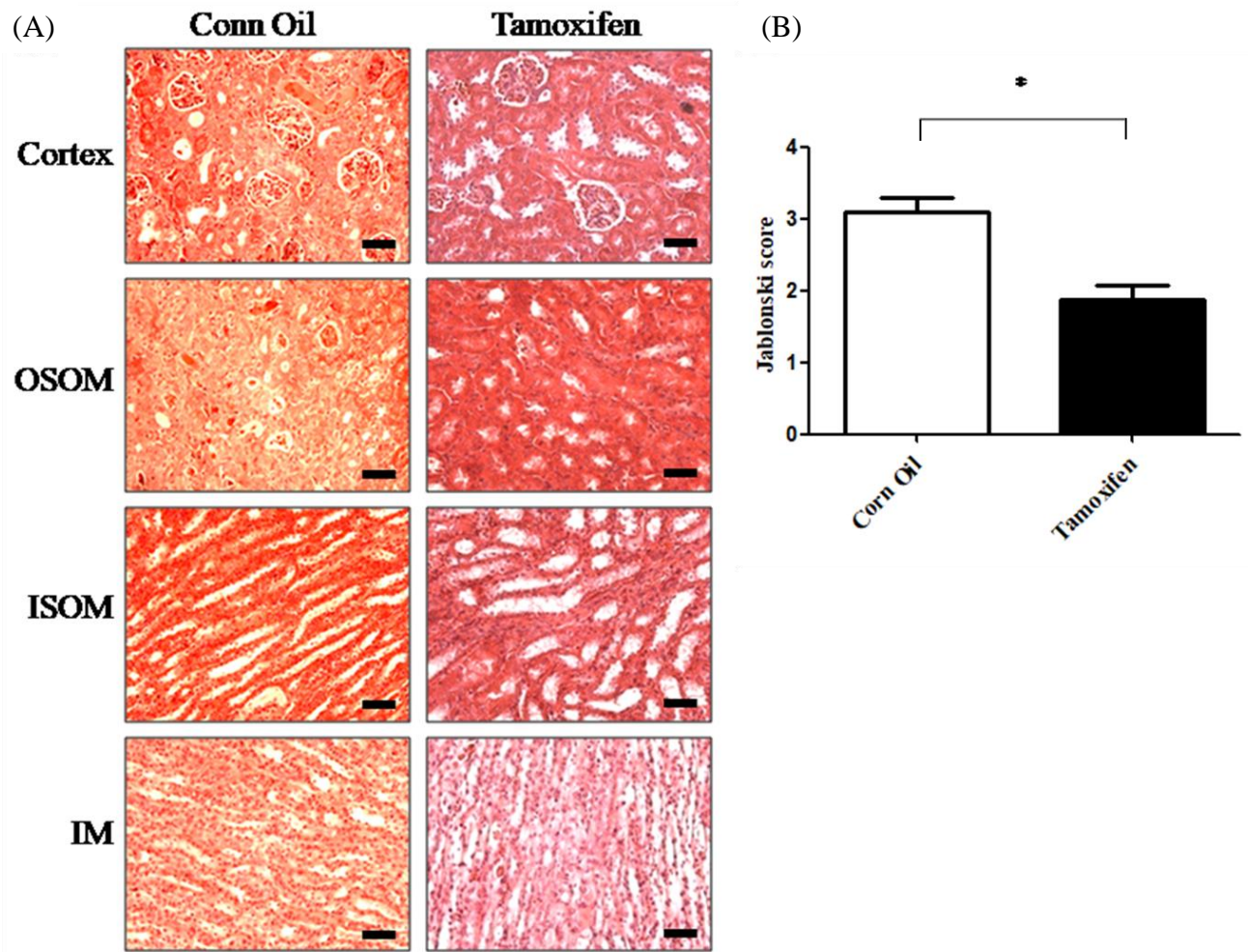
Figure 4.6. **Renal Mitochondrial Constitutive Active AKTAttenuated Kidney Injury after IRI.** One month after TAM or corn oil injection, unilateral IRI was induced with contrlateral Nx in the KMCAKT mice. Kidney was harvested and fixed for histopathology analysis 7 days after IRI. Tubular necrosis, tubular lysis, tubular dilation, and cast were found in cortex, OSOM, ISOM, and IM in KMCAKT mice injected with corn oil, but not in TAM-injected group. The representative images were shown in (A). The tubular injury was scored by Jablonski score and shown in (B). Higher Jablonski score was found in corn oil-injected KMCAKT group when compared with TAM-injected KMCAKT mice (p=0.038) (n=10-11).

Figure 4.7

(A)

Corn Oil   Tamoxifen

Cortex

OSOM

ISOM

IM

(B)
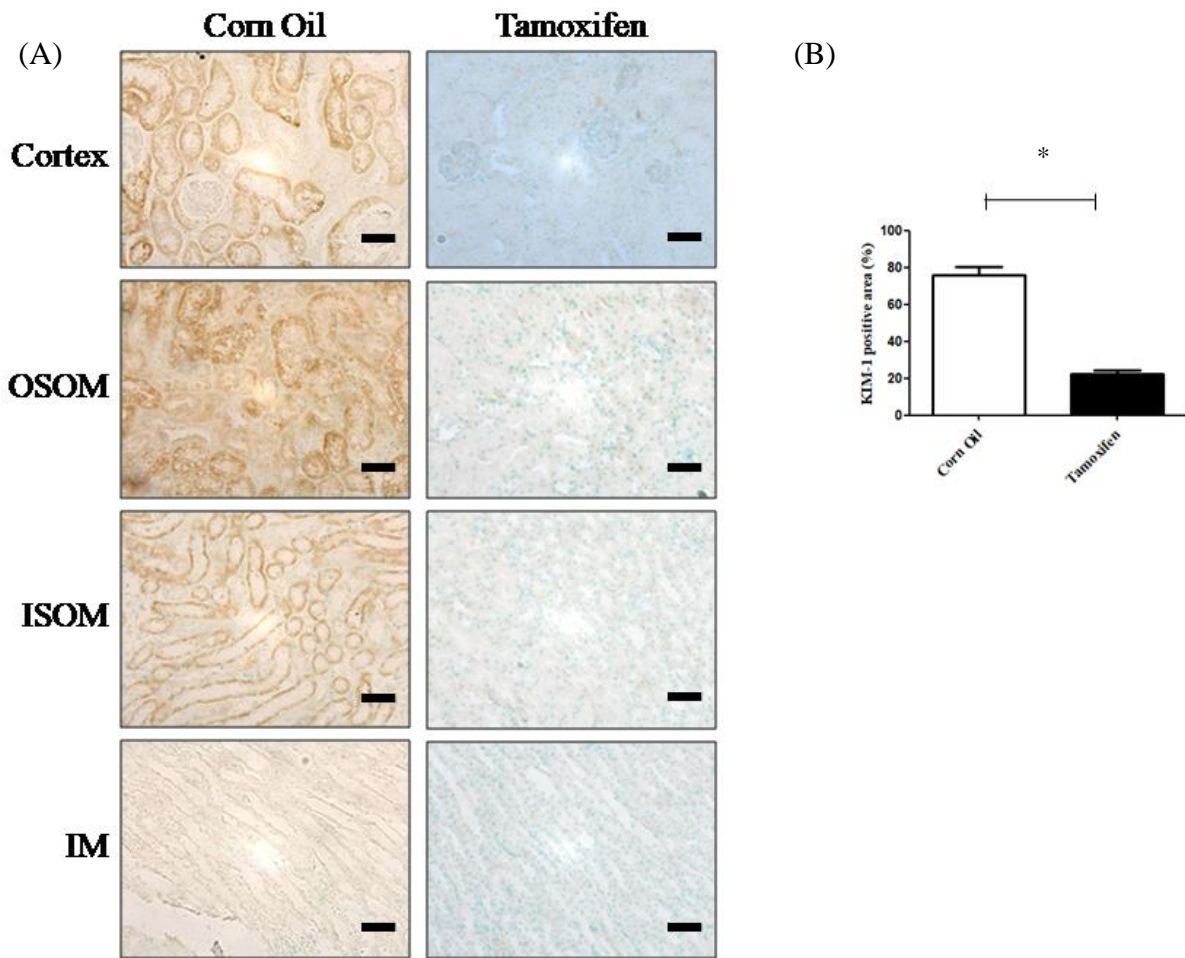
Figure 4.7 **Decreased KIM-1 expression in the TAM-injected KMCAKT Mice after IRI.**

One month after TAM or corn oil injection, IRI was induced in the KMCAKT mice. Kidney was

harvested and fixed for histopathology analysis 7 days after IRI. KIM-1 was analyzed by

immunohistochemistry. KIM-1 protein (brown staining) was found in cortex, OSOM, ISOM, and

IM in KMCAKT mice injected with corn-oil, but rarely seen in TAM injected group. The

representative images were shown in (A). KIM-1 positive area was measured by imageJ and

shown in (B). There was significantly less KIM-1 positive area (%) in TAM injected KMCAKT

mice as compared to the corn oil injected mice after IRI ($p<0.001$)(n=10-11).

Figure 4.8

(A)
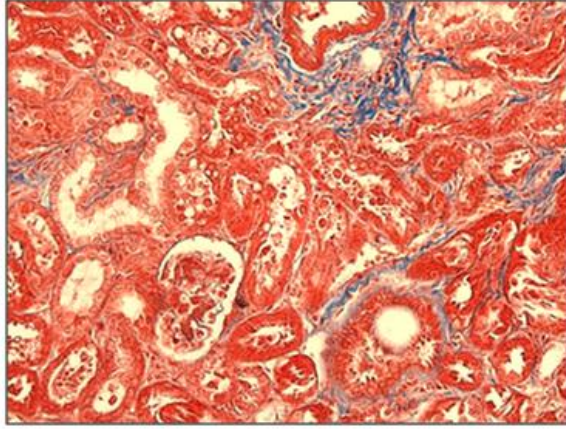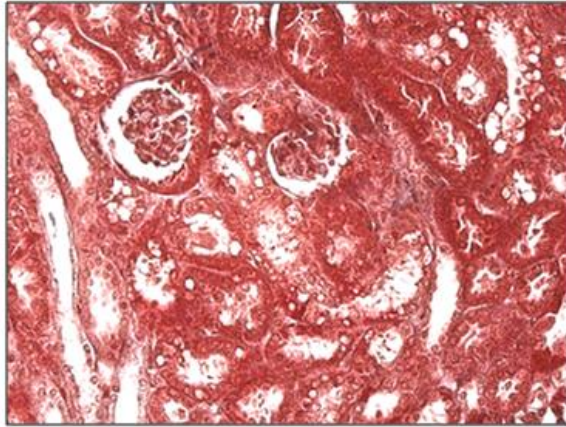
(B)
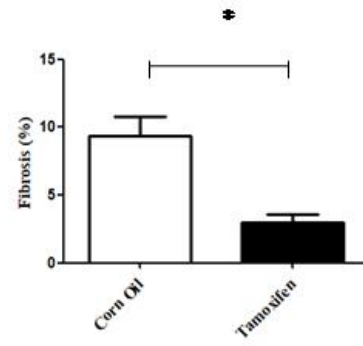
Figure 4.8 **Decreased Renal Fibrosis Areas in Mitochondrial Constitutively Active AKT induced KMCAKT Mice after IRI.** One month after TAM or corn oil injection, IRI was induced in the KMCAKT mice. Kidney was harvested and fixed for histopathology analysis 7 days after IRI. Masson's trichrome staining was performed to define fibrosis. Fibrosis (blue staining) was found in cortex, OSOM, ISOM, and IM in the KMCAKT mice injected with corn-oil, but rare in the TAM-injected group. Representative images were shown in (A). The fibrosis area was measured by imageJ and shown in (B) (p=0.002) (n=10-11).

Figure 4.9

(A)
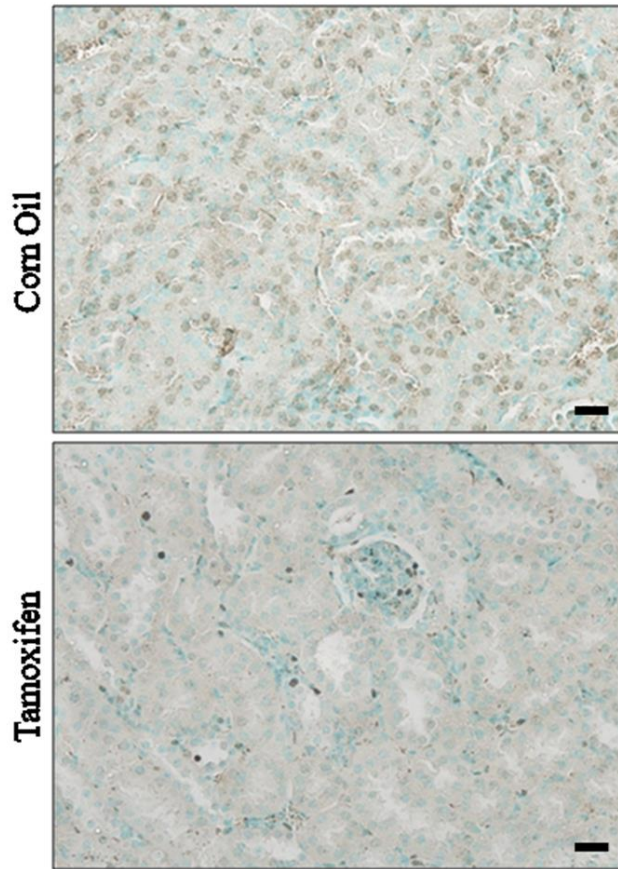
(B)
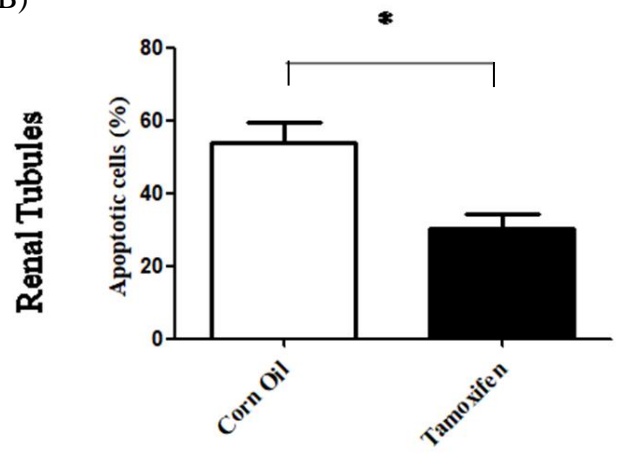
(C)
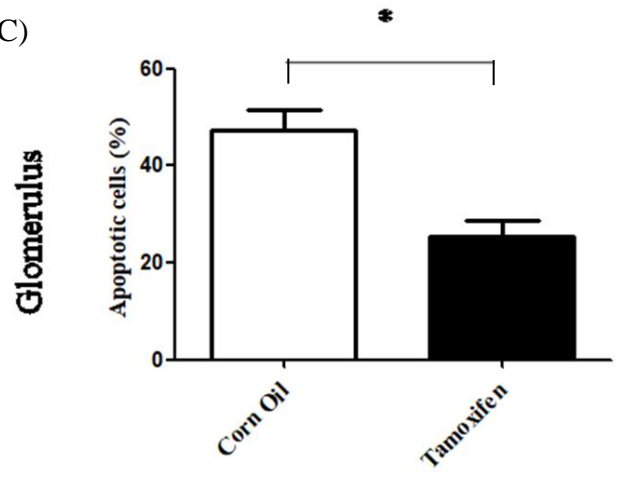
Figure 4.9 **Decreased Apoptosis in the KMCAKT Mice after IRI.** One month after TAM or corn oil injection, IRI was induced. Kidney was harvested and fixed for histopathology analysis 7 days after IRI. TUNEL assay was performed to study apoptosis. Apoptotic cells (brown staining) were found in both renal tubular cells and glomeruli in the corn-oil group. The representative images were shown in (A). Area for apoptosis was measured by imageJ and shown in (B). There was less apoptotic area (%) in renal tubules (p=0.0064) and glomeruli (p=0.0021) in TAM-injected KMCAKT group as compared to corn oil-injected KMCAKT group on day 7 after IRI (n=10-11).

Figure 4.10

(A)

(B)
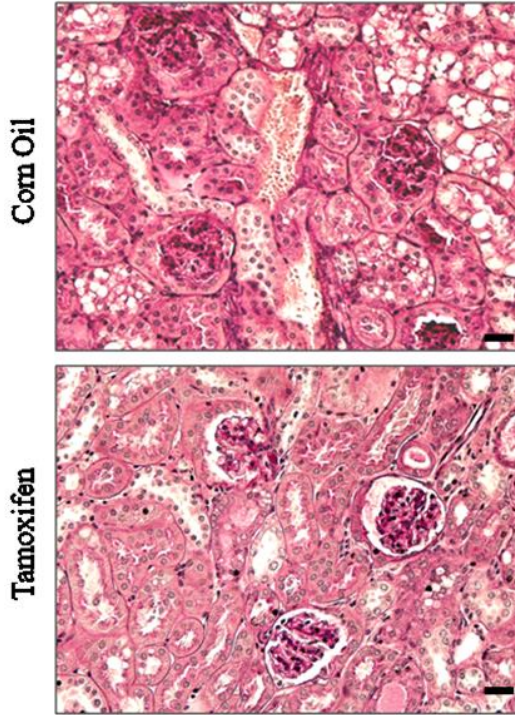
	Corn Oil (7days)	Tamoxifen (7days)
Grade 0	0	0
Grade 1	23	89
Grade 2	584	484
Grade 3	555	507

(C)

10 mice (50 glomeruli per animal)

(D)

(E)
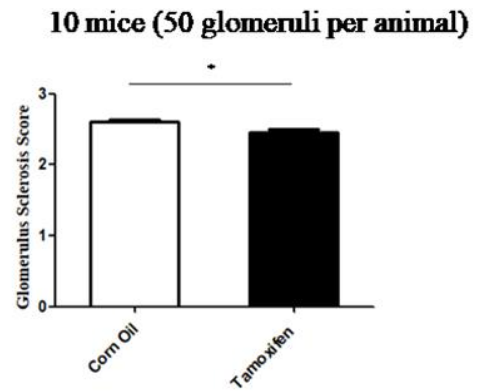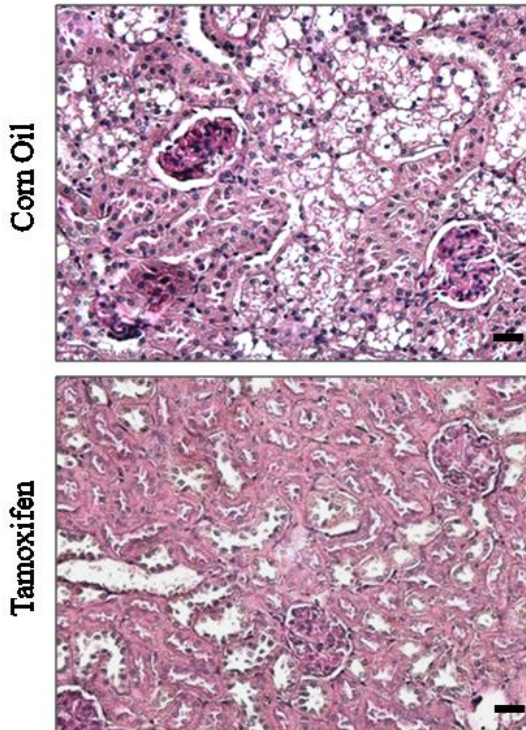
	Corn Oil (45 days)	Tamoxifen (45 days)
Grade 0	0	5
Grade 1	82	113
Grade 2	484	548
Grade 3	528	324

(F)

10 mice (50 glomeruli per animal)
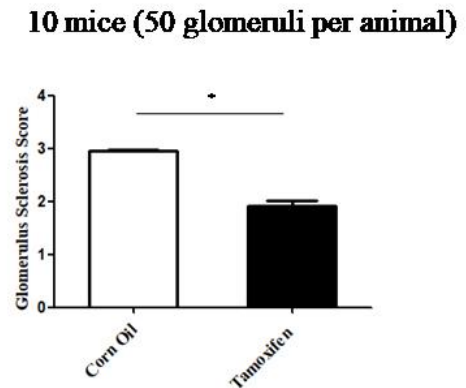
Figure 4.10 **Decreased Glomerulosclerosis in TAM-induced KMCAKT Mice 45 Days after IRI.** One month after TAM or corn oil injection, IRI with contralateral Nx was performed in the mice. Kidney was harvested and fixed for histopathology analysis 7 or 45 days after IRI. Glomerulosclerosis was analyzed by Periodic acid–Schiff (PAS) staining. The severity of PAS staining is graded as follows: 0 (no lesions), 1 (lesions in up to 25% of glomeruli), 2 (lesions in 25 to 50% of glomeruli) or 3 (lesions in > 50% of glomeruli). Representative images were shown in (A) Day 7 and (D) Day 45. Glomerulosclerosis was scored and summarized (B, C, E, and F). At least 50 glumeri were scored from each mouse and at least 10 mice were scored in each group. Less glomerulosclerosis was found in Day 7 ($p=0.001$) and Day 45 ($p<0.001$) after IRI in the TAM-injected KMCAKT group.

Figure 4.11

(A)

(B)

| | Survival (%) | |
Days	Tamoxifen (n=26)	Corn Oil (n=24)
0	26 (100.00%)	24 (100.00%)
1	26 (100.00%)	20 (83.33%)
2	26 (100.00%)	14 (58.33%)
3	26 (100.00%)	10 (41.67%)
4	26 (100.00%)	8 (33.33%)
5	23 (88.46%)	6 (25.00%)
6	20 (76.92%)	5 (20.83%)
7	20 (76.92%)	5 (20.83%)
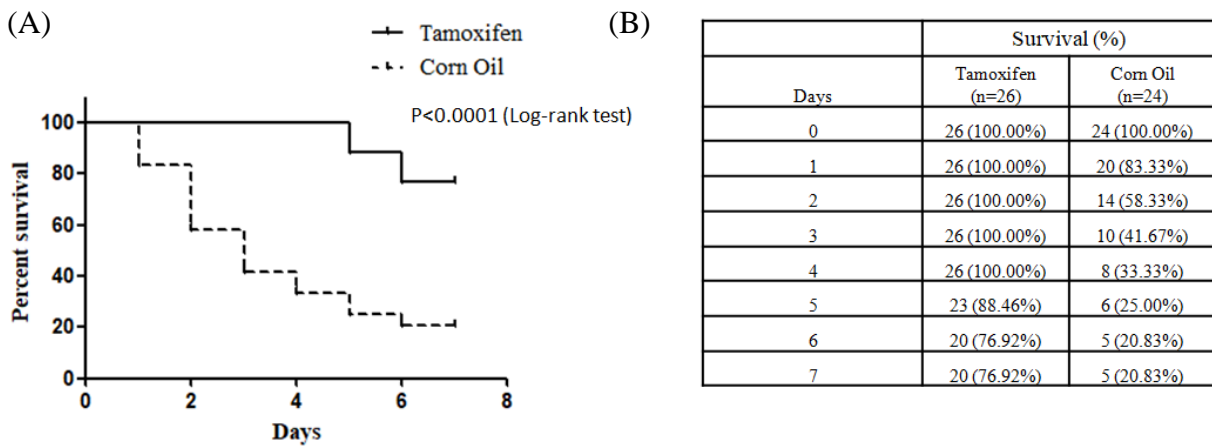
Figure 4.11 **Survival Analysis of KMCAKT Mice after IRI**. One month after TAM or corn oil induction, KMCAKT mice were subjected to IRI to induce AKI. Survival rates were recorded after surgery. The survival rate was significant higher in the TAM-injected group (76.92%) with when compared to the corn oil group (20.83%) (*p<0.001*).

CHAPTER 5

CONCLUSION

In the last four chapters, we demonstrated that 1] IRI induced acute translocation of activated AKT1 to mitochondria in proximal tubules, 2] inhibition of tubule mitochondria AKT aggravated AKI and subsequent development of CKD after IRI, and 3] enhancing tubule mitochondria AKT signaling protected kidney against IRI and attenuated development of CKD. AKI and enhancing mitochondrial AKT1could protect kidney from renal IRI and subsequent renal failure.

Mitochondria is not just the powerhouse of cells, it may regulate cell metabolism, oxidative stress, and cell death. The studies in this dissertation highlight a novel role for mitochondrial AKT1 in the proximal tubules in IRI-induced AKI and subsequent development of CKD. These findings verified my hypothesis that activation of mitochondrial AKT1 during ischemia-reperfusion in renal tubules protects kidney against AKI and subsequent development of CKD.

Acute translocation and activation of AKT1 in proximal renal tubule in response to IRI appears to be a self-protective mechanism to reduce kidney injury. Inhibition of tubular mitochondrial AKT1 signaling aggravated tubule injuries and precipitated glomerular apoptosis and development of glomerulosclerosis, the combination of glomerular and tubular dysfunction ultimately led chronic renal failure (Figure 5.1).

I.   The Role of Mitochondria in Renal Tubule AKI

AKI is characterized by renal tubular damage, inflammation, and vascular dysfunction.

Injury and death of tubular cells had been recognized as key factors in the development of AKI. Furthermore, tubule repair and regeneration has been proposed as a major event in the recovery from AKI[96-99].Although sub-lethal injury may be reversible, the death of tubular cells Leads to inevitable loss of tubular function [100].Renal IRI leads to induction of apoptosis genes and activation of caspases and endonucleases, which contribute to induction of apoptosis [101]. Although renal tubular apoptosis is a common finding in various models of AKI, the signaling pathways upstream from mitochondria are not entirely clear [101].

Activation of the intrinsic pathways of apoptosis in AKI has been characterized in both in vitro and in vivo models, including Bcl-2 protein family and mitochondrial apoptosis machinery [102].The critical roles of Bax and Bak in AKI have been shown recently using global and proximal tubule–specific knock out models [103]. In human, kidney mitochondrial damage associated with Bax and Bak had been observed in ischemia injury [104]. Upregulation of Bcl-2 could preserve mitochondrial integrity and renal tubule cell viability in AKI [105].Mitochondria dysfunction underpinned initiation of apoptosis triggered by ER stress and caspases [106, 107]. Loss of mitochondrial cross-membrane electrochemical gradient is considered a pivotal control point that triggers apoptosis [108].Mitochondrial leakage probably represents a point of no return in the life and death decision during apoptosis [109, 110].

II.   The Crosstalk between Renal Tubules and Glomerulus

Anatomically, tubulointerstitial injury could cause stenosis of the glomerulotubular junction and finally result in atubular glomerus, glomeruli without patent connection to the renal tubule. Tubular epithelial cell dysfunction, compression and obstruction of adjacent tubules by interstitial matrix, and transition of parietal epithelial cells to fibroblast-like cells are potential

mechanisms of ATG. Proximal RTE, especially at S1 region, are sensitive to ischemic injury[111]. In response to injury, RTE may undergo incomplete repair, resulting in tubular atrophy and interstitial fibrosis[112].

Tubular injury may affect glomerular filtration function through tubuloglomerular feedback. Tubuloglomerular feedback is a well-known physiologic cross talk mechanism between tubules and glomeruli, inversely regulating GFR according to intratubular salt concentration and flow [113]. Proximal tubular injury with impaired absorptive capacity is a common feature in various forms of intrarenal AKI [113]. In septic AKI, pro-inflammatory cytokines downregulated tubular transport proteins such as CLCK-1, CLCK-2, Barttin, NHE3, Na/K-ATPase, ROMK, NKCC2, and NCC, thus increased distal tubular delivery of sodium and chloride and reduced GFR through tubuloglomerular feedback [114]. Tubuloglomerular feedback can also activate local paracrine mediators of glomerular disease. In a model of hypertension, upregulation of nNOS and COX-2 in macula densa cells and rennin in juxtaglomerular cells contributed to the development of glomerulosclerosis [115].

III.   Transition of AKI to CKD

The exact mechanisms underlying transition of AKI to CKD remain to be defined. Histologically, both AKI and CKD are associated with renal tubule injuries [116]. It has been known for years that tubulointerstitial pathology is a cardinal feature of all types of CKD [117]. Perturbation of intracellular signaling in renal tubular cells are believed to play a key role during the initiation and progression of CKD and may contribute to the susceptibility of AKI to CKD.

In CKD, the transforming growth factor (TGF)-β signaling pathway is activated and may induce fibrotic extracellular matrix proteins and contribute to glomerulosclerosis and

tubulointerstitial fibrosis [118].However, the role of TGF-β signaling in AKI is inconsistent in different experimental models of AKI [90].Hypoxia activates hypoxia-inducible factors(HIF) to modulate gene transcription [119]. In AKI, HIF activation in renal proximal tubules does not have a major protective role as global renal expression of HIF exhibited renal protective effects in various experimental systems [120]. Nethertheless, other studies failed to confirm the renal protective actions of HIF-1 [121].

Current evidence suggests mitochondrion is a key modulator during the transition of AKI to CKD. Ablation of the proapoptotic Bax and Bak resulted in the amelioration of ischemic and cisplatin-induced AKI [122].In ischemic and nephrotoxic models of AKI, inhibition of mitochondrial fragmentation attenuated kidney injuries [123].The severity of ischemic AKI in diabetic mice was associated with heightened activation of the mitochondrial apoptosis [124]. CKD-associated suppression of mitochondrial function and biogenesis could sensitize kidney cells and tissues to AKI and prevent recovery from AKI [125-127].In CKD, renal mitochondrial dysfunction also occurred during the development and progression of CKD [128].High glucose and albumin overload can induce mitochondria apoptosis signaling in kidney cells in CKD [129]. Mitochondrial fragmentation, as a result of pathologic alterations in mitochondrial fusion and fission, was detected in experimental diabetic kidney disease [130].

The data presented in thesis fill a critical knowledge gap on the role of proximal renal tubule mitochondria in AKI and subsequent transition from AKI to CKD, by activation of AKT1 in mitochondria and by translocation of activated AKT1 from cytosol to mitochondria. This new mechanism of renal protection may represent a novel target to develop new strategies for better prevention and treatment for acute and chronic kidney injury.
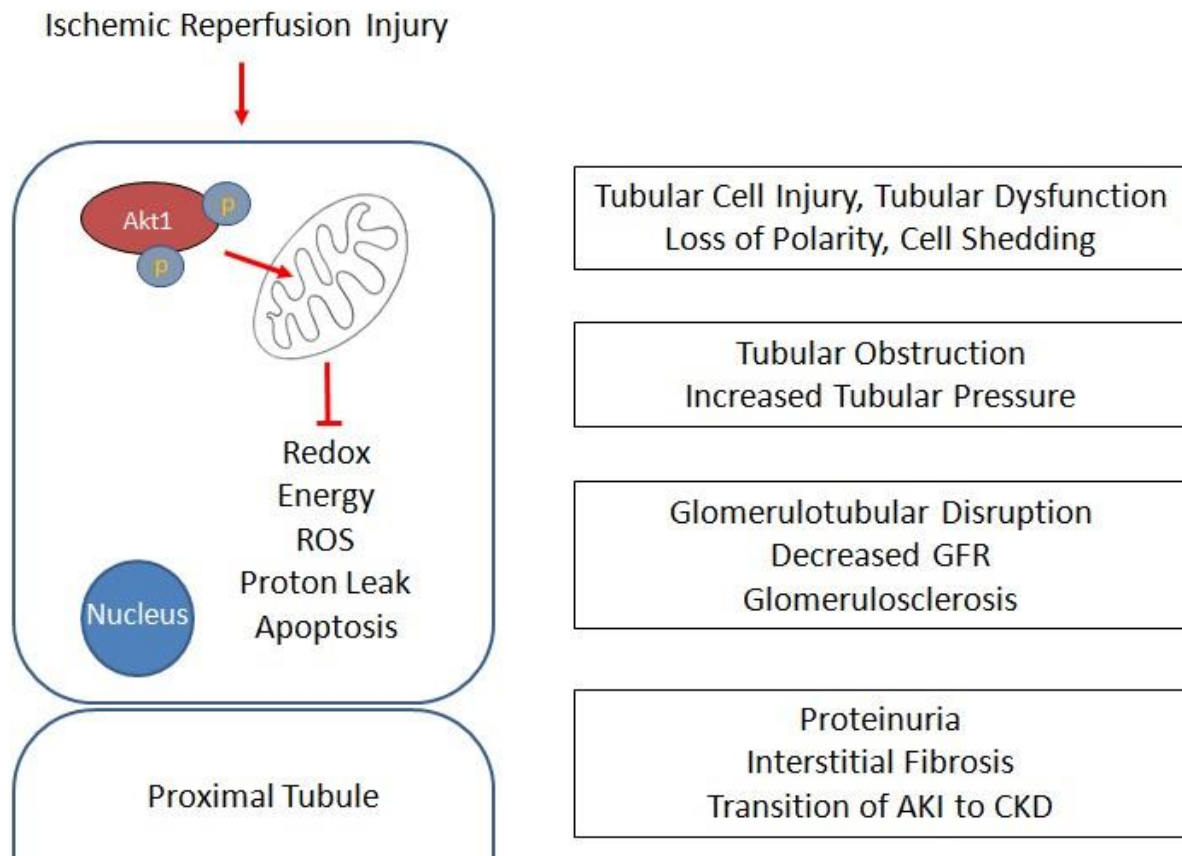
Figure 5.1

Figure 5.1 **How Mitochondrial AKT1 in Renal Proximal Tubules Protected the Kidney**

from IRI

Reference

1.   Wang, L.P. and S.A. Summers, *Measuring insulin-stimulated phosphatidyl-inositol 3-kinase activity.* Methods Mol Med, 2003. **83**: p. 127-36.

2.   Alessi, D.R., et al., *Characterization of a 3-phosphoinositide-dependent protein kinase which phosphorylates and activates protein kinase Balpha.* Curr Biol, 1997. **7**(4): p. 261-9.

3.   Sarbassov, D.D., et al., *Phosphorylation and regulation of Akt/PKB by the rictor-mTOR complex.* Science, 2005. **307**(5712): p. 1098-101.

4.   Feng, J., et al., *Identification of a PKB/Akt hydrophobic motif Ser-473 kinase as DNA-dependent protein kinase.* J Biol Chem, 2004. **279**(39): p. 41189-96.

5.   Canaud, G., et al., *AKT2 is essential to maintain podocyte viability and function during chronic kidney disease.* Nature Medicine, 2013. **19**(10): p. 1288-+.

6.   Cho, H., et al., *Akt1/PKBalpha is required for normal growth but dispensable for maintenance of glucose homeostasis in mice.* J Biol Chem, 2001. **276**(42): p. 38349-52.

7.   Cho, H., et al., *Insulin resistance and a diabetes mellitus-like syndrome in mice lacking the protein kinase Akt2 (PKB beta).* Science, 2001. **292**(5522): p. 1728-31.

8.   Easton, R.M., et al., *Role for Akt3/protein kinase Bgamma in attainment of normal brain size.* Mol Cell Biol, 2005. **25**(5): p. 1869-78.

9.   Hemmings, B.A. and D.F. Restuccia, *PI3K-PKB/Akt pathway.* Cold Spring Harb Perspect Biol, 2012. **4**(9): p. a011189.

10.   Coa, L.L., et al., *AKT/protein kinase B associates with beta-actin in the nucleus of melanoma cells.* Biosci Rep, 2019. **39**(1).

11.   Yang, J.Y., et al., *Impaired translocation and activation of mitochondrial Akt1 mitigated mitochondrial oxidative phosphorylation Complex V activity in diabetic myocardium.* J Mol Cell Cardiol, 2013. **59**: p. 167-75.

12.   Deng, W., et al., *Protein kinase B (PKB/AKT1) formed signaling complexes with mitochondrial proteins and prevented glycolytic energy dysfunction in cultured cardiomyocytes during ischemia-reperfusion injury.* Endocrinology, 2014. **155**(5): p. 1618-28.

13.   Schapira, A.H., *Mitochondrial disease.* Lancet, 2006. **368**(9529): p. 70-82.

14.   Nunnari, J. and A. Suomalainen, *Mitochondria: in sickness and in health.* Cell, 2012. **148**(6): p. 1145-59.

15.   Nicholls, D.G., Fergusson, S.J.,, *Bioenergetics*, in *4 ed. Academic Press.* 2013.

16.   Yang, M., T. Soga, and P.J. Pollard, *Oncometabolites: linking altered metabolism with cancer.* J Clin Invest, 2013. **123**(9): p. 3652-8.

17.   Tannahill, G.M., et al., *Succinate is an inflammatory signal that induces IL-1beta through HIF-1alpha.* Nature, 2013. **496**(7444): p. 238-42.

18.   Koehler, C.M., *Protein translocation pathways of the mitochondrion.* FEBS Lett, 2000. **476**(1-2): p. 27-31.

19.   Fujio, Y., et al., *Akt promotes survival of cardiomyocytes in vitro and protects against ischemia-reperfusion injury in mouse heart.* Circulation, 2000. **101**(6): p. 660-7.

20.   Datta, S.R., et al., *Akt phosphorylation of BAD couples survival signals to the cell-intrinsic death machinery.* Cell, 1997. **91**(2): p. 231-41.

21.   Bullock, A.N., et al., *Structure and substrate specificity of the Pim-1 kinase.* J Biol Chem, 2005. **280**(50): p. 41675-82.

22.   Pastukh, V., et al., *Contribution of the PI 3-kinase/Akt survival pathway toward osmotic preconditioning.* Mol Cell Biochem, 2005. **269**(1-2): p. 59-67.

23.   Kato, K., et al., *Adrenomedullin gene delivery attenuates myocardial infarction and apoptosis after ischemia and reperfusion.* Am J Physiol Heart Circ Physiol, 2003. **285**(4): p. H1506-14.

24.   Chae, Y.C., et al., *Mitochondrial Akt Regulation of Hypoxic Tumor Reprogramming.* Cancer Cell, 2016. **30**(2): p. 257-272.

25.   Stewart, B.E. and R.H. Rice, *Differentiation-associated expression of the proto-oncogene pim-1 in cultured human keratinocytes.* J Invest Dermatol, 1995. **105**(5): p. 699-703.

26.   Liang, H., W. Hittelman, and L. Nagarajan, *Ubiquitous expression and cell cycle regulation of the protein kinase PIM-1.* Arch Biochem Biophys, 1996. **330**(2): p. 259-65.

27.   Leduc, I., et al., *The Pim-1 kinase stimulates maturation of TCRbeta-deficient T cell progenitors: implications for the mechanism of Pim-1 action.* Int Immunol, 2000. **12**(10): p. 1389-96.

28.   Ellwood-Yen, K., et al., *Myc-driven murine prostate cancer shares molecular features with human prostate tumors.* Cancer Cell, 2003. **4**(3): p. 223-38.

29.	Katakami, N., et al., *Role of pim-1 in smooth muscle cell proliferation.* J Biol Chem, 2004. **279**(52): p. 54742-9.

30.	Wang, Z., et al., *Specific metabolic rates of major organs and tissues across adulthood: evaluation by mechanistic model of resting energy expenditure.* Am J Clin Nutr, 2010. **92**(6): p. 1369-77.

31.	Fantus, D., et al., *Roles of mTOR complexes in the kidney: implications for renal disease and transplantation.* Nat Rev Nephrol, 2016. **12**(10): p. 587-609.

32.	Kim, Y. and C.W. Park, *Adenosine monophosphate-activated protein kinase in diabetic nephropathy.* Kidney Res Clin Pract, 2016. **35**(2): p. 69-77.

33.	Abe, Y., et al., *Bioenergetic characterization of mouse podocytes.* Am J Physiol Cell Physiol, 2010. **299**(2): p. C464-76.

34.	Kim, E.Y., M. Anderson, and S.E. Dryer, *Sustained activation of N-methyl-D-aspartate receptors in podoctyes leads to oxidative stress, mobilization of transient receptor potential canonical 6 channels, nuclear factor of activated T cells activation, and apoptotic cell death.* Mol Pharmacol, 2012. **82**(4): p. 728-37.

35.	Schoolwerth, A.C., B.C. Smith, and R.M. Culpepper, *Renal gluconeogenesis.* Miner Electrolyte Metab, 1988. **14**(6): p. 347-61.

36.	Li, S.Y. and K. Susztak, *The Role of Peroxisome Proliferator-Activated Receptor gamma Coactivator 1alpha (PGC-1alpha) in Kidney Disease.* Semin Nephrol, 2018. **38**(2): p. 121-126.

37.	Portilla, D., et al., *Alterations of PPARalpha and its coactivator PGC-1 in cisplatin-induced acute renal failure.* Kidney Int, 2002. **62**(4): p. 1208-18.

38.	Dugan, L.L., et al., *AMPK dysregulation promotes diabetes-related reduction of superoxide and mitochondrial function.* J Clin Invest, 2013. **123**(11): p. 4888-99.

39.	Lin, Y.W., et al., *Melatonin protects brain against ischemia/reperfusion injury by attenuating endoplasmic reticulum stress.* Int J Mol Med, 2018. **42**(1): p. 182-192.

40.	Zhou, H., et al., *The Dichotomy of Endoplasmic Reticulum Stress Response in Liver Ischemia-Reperfusion Injury.* Transplantation, 2016. **100**(2): p. 365-72.

41.	Nakka, V.P., A. Gusain, and R. Raghubir, *Endoplasmic reticulum stress plays critical role in brain damage after cerebral ischemia/reperfusion in rats.* Neurotox Res, 2010. **17**(2): p. 189-202.

42.	de Almeida, T.N., et al., *Effect of Hepatic Preconditioning with the Use of Methylene Blue on the Liver of Wistar Rats Submitted to Ischemia and Reperfusion.* Transplant Proc, 2018. **50**(3): p. 841-847.

43.	Gracia-Sancho, J., A. Casillas-Ramirez, and C. Peralta, *Molecular pathways in protecting the liver from ischaemia/reperfusion injury: a 2015 update.* Clin Sci (Lond), 2015. **129**(4): p. 345-62.

44.	Zoratti, M. and I. Szabo, *The mitochondrial permeability transition.* Biochim Biophys Acta, 1995. **1241**(2): p. 139-76.

45.	Teoh, N.C. and G.C. Farrell, *Hepatic ischemia reperfusion injury: pathogenic mechanisms and basis for hepatoprotection.* J Gastroenterol Hepatol, 2003. **18**(8): p. 891-902.

46.	Lin, X.L., et al., *Molecular mechanisms of autophagy in cardiac ischemia/reperfusion injury (Review).* Mol Med Rep, 2018. **18**(1): p. 675-683.

47.	Kellum, J.A., R. Bellomo, and C. Ronco, *Kidney attack.* JAMA, 2012. **307**(21): p. 2265-6.

48.	Ali, T., et al., *Incidence and outcomes in acute kidney injury: a comprehensive population-based study.* J Am Soc Nephrol, 2007. **18**(4): p. 1292-8.

49.	Liangos, O., et al., *Epidemiology and outcomes of acute renal failure in hospitalized patients: a national survey.* Clin J Am Soc Nephrol, 2006. **1**(1): p. 43-51.

50.	Sawhney, S., et al., *Long-term prognosis after acute kidney injury (AKI): what is the role of baseline kidney function and recovery? A systematic review.* BMJ Open, 2015. **5**(1): p. e006497.

51.	Xue, J.L., et al., *Incidence and mortality of acute renal failure in Medicare beneficiaries, 1992 to 2001.* J Am Soc Nephrol, 2006. **17**(4): p. 1135-42.

52.	Wu, V.C., et al., *Long-term risk of coronary events after AKI.* J Am Soc Nephrol, 2014. **25**(3): p. 595-605.

53.	Wonnacott, A., et al., *Epidemiology and outcomes in community-acquired versus hospital-acquired AKI.* Clin J Am Soc Nephrol, 2014. **9**(6): p. 1007-14.

54.	Ftouh, S., et al., *Prevention, detection and management of acute kidney injury: concise guideline.* Clin Med (Lond), 2014. **14**(1): p. 61-5.

55.	Zuk, A. and J.V. Bonventre, *Acute Kidney Injury.* Annu Rev Med, 2016. **67**: p. 293-307.

56.   Wang, H.L., N.M. Liu, and R. Li, *Role of adult resident renal progenitor cells in tubular repair after acute kidney injury.* J Integr Med, 2014. **12**(6): p. 469-75.

57.   Aksu, U., C. Demirci, and C. Ince, *The pathogenesis of acute kidney injury and the toxic triangle of oxygen, reactive oxygen species and nitric oxide.* Contrib Nephrol, 2011. **174**: p. 119-28.

58.   Ferenbach, D.A. and J.V. Bonventre, *Mechanisms of maladaptive repair after AKI leading to accelerated kidney ageing and CKD.* Nat Rev Nephrol, 2015. **11**(5): p. 264-76.

59.   Miyaji, T., et al., *Role of the increase in p21 in cisplatin-induced acute renal failure in rats.* J Am Soc Nephrol, 2001. **12**(5): p. 900-8.

60.   Jablonski, P., et al., *An experimental model for assessment of renal recovery from warm ischemia.* Transplantation, 1983. **35**(3): p. 198-204.

61.   Masson, P., *Some histological methods: trichrome stainings and theirpreliminary technique.* J Tech Methods, 1929. **12**: p. 75.

62.   Schneider, C.A., W.S. Rasband, and K.W. Eliceiri, *NIH Image to ImageJ: 25 years of image analysis.* Nat Methods, 2012. **9**(7): p. 671-5.

63.   *BioPhotometer Operating Manual*. Available from: https://arboretum.harvard.edu/wp-content/uploads/Biophotometer-manual.pdf.

64.   Bijur, G.N. and R.S. Jope, *Rapid accumulation of Akt in mitochondria following phosphatidylinositol 3-kinase activation.* J Neurochem, 2003. **87**(6): p. 1427-35.

65.   Santi, S.A. and H. Lee, *The Akt isoforms are present at distinct subcellular locations.* Am J Physiol Cell Physiol, 2010. **298**(3): p. C580-91.

66.   Barksdale, K.A. and G.N. Bijur, *The basal flux of Akt in the mitochondria is mediated by heat shock protein 90.* J Neurochem, 2009. **108**(5): p. 1289-99.

67.   Miyamoto, S., A.N. Murphy, and J.H. Brown, *Akt mediates mitochondrial protection in cardiomyocytes through phosphorylation of mitochondrial hexokinase-II.* Cell Death Differ, 2008. **15**(3): p. 521-9.

68.   Yang, J.Y., et al., *Insulin stimulates Akt translocation to mitochondria: implications on dysregulation of mitochondrial oxidative phosphorylation in diabetic myocardium.* J Mol Cell Cardiol, 2009. **46**(6): p. 919-26.

69.   Su, C.C., et al., *Mitochondrial Akt-regulated mitochondrial apoptosis signaling in cardiac muscle cells.* Am J Physiol Heart Circ Physiol, 2012. **302**(3): p. H716-23.

70.   Jablonski, P., et al., *An Experimental-Model for Assessment of Renal Recovery from Warm Ischemia.* Transplantation, 1983. **35**(3): p. 198-204.

71.   Zhou, B.P., et al., *HER-2/neu blocks tumor necrosis factor-induced apoptosis via the Akt/NF-kappaB pathway.* J Biol Chem, 2000. **275**(11): p. 8027-31.

72.   Chen, Y.H., et al., *Mitochondrial Akt Signaling Modulated Reprogramming of Somatic Cells.* Sci Rep, 2019. **9**(1): p. 9919.

73.   Patel, V., et al., *Acute kidney injury and aberrant planar cell polarity induce cyst formation in mice lacking renal cilia.* Human Molecular Genetics, 2008. **17**(11): p. 1578-1590.

74.   *Akt Activity Assay Kit Instructions for Use*. Available from: https://www.abcam.com/ps/products/65/ab65786/documents/ab65786%20Akt%20Activity%20Assay%20Kit%20v2%20(website).pdf.

75.   *In Situ Cell Death Detection Kit, Fluorescein*. 2012; Available from: http://sjweb.herokuapp.com/downloads/tunel.pdf.

76.   *Seahorse Bioscience XF24 Extracellular Flux Analyzer Manual*. Available from: http://hpst.cz/sites/default/files/attachments/102609-400-xfe24-operators-manual-ra.pdf.

77.   *ATP Detection Assay Kit-Luminescence*. Available from: https://www.caymanchem.com/pdfs/700410.pdf.

78.   Soltoff, S.P., *ATP and the regulation of renal cell function.* Annu Rev Physiol, 1986. **48**: p. 9-31.

79.   Zhang, S., et al., *The pivotal role of pyruvate dehydrogenase kinases in metabolic flexibility.* Nutr Metab (Lond), 2014. **11**(1): p. 10.

80.   Molitoris, B.A., *Therapeutic translation in acute kidney injury: the epithelial/endothelial axis.* J Clin Invest, 2014. **124**(6): p. 2355-63.

81.   Gobe, G.C. and D.W. Johnson, *Distal tubular epithelial cells of the kidney: Potential support for proximal tubular cell survival after renal injury.* Int J Biochem Cell Biol, 2007. **39**(9): p. 1551-61.

82.   Kiyama, S., et al., *Strategic locus for the activation of the superoxide dismutase gene in the nephron.* Kidney Int, 1995. **47**(2): p. 536-46.

83.   Hall, A.M., et al., *Multiphoton imaging reveals differences in mitochondrial function between nephron segments.* J Am Soc Nephrol, 2009. **20**(6): p. 1293-302.

84.   Blondin, J., et al., *Renal function and metabolism after relief of unilateral ureteral obstruction.* Proc Soc Exp Biol Med, 1975. **150**(1): p. 71-6.

85.   Gomez, H., et al., *A unified theory of sepsis-induced acute kidney injury: inflammation, microcirculatory dysfunction, bioenergetics, and the tubular cell adaptation to injury.* Shock, 2014. **41**(1): p. 3-11.

86.   Marcussen, N., *Atubular glomeruli in renal artery stenosis.* Lab Invest, 1991. **65**(5): p. 558-65.

87.   Chevalier, R.L., *The proximal tubule is the primary target of injury and progression of kidney disease: role of the glomerulotubular junction.* Am J Physiol Renal Physiol, 2016. **311**(1): p. F145-61.

88.   Forbes, M.S., B.A. Thornhill, and R.L. Chevalier, *Proximal tubular injury and rapid formation of atubular glomeruli in mice with unilateral ureteral obstruction: a new look at an old model.* Am J Physiol Renal Physiol, 2011. **301**(1): p. F110-7.

89.   Galarreta, C.I., et al., *Tubular obstruction leads to progressive proximal tubular injury and atubular glomeruli in polycystic kidney disease.* Am J Pathol, 2014. **184**(7): p. 1957-66.

90.   Gewin, L., et al., *Deleting the TGF-beta receptor attenuates acute proximal tubule injury.* J Am Soc Nephrol, 2012. **23**(12): p. 2001-11.

91.   Takaori, K., et al., *Severity and Frequency of Proximal Tubule Injury Determines Renal Prognosis.* J Am Soc Nephrol, 2016. **27**(8): p. 2393-406.

92.   Lim, B.J., et al., *Tubulointerstitial fibrosis can sensitize the kidney to subsequent glomerular injury.* Kidney Int, 2017. **92**(6): p. 1395-1403.

93.   Gilbert, R.E., *Proximal Tubulopathy: Prime Mover and Key Therapeutic Target in Diabetic Kidney Disease.* Diabetes, 2017. **66**(4): p. 791-800.

94.   Basile, D.P., M.D. Anderson, and T.A. Sutton, *Pathophysiology of acute kidney injury.* Compr Physiol, 2012. **2**(2): p. 1303-53.

95.   Kellum, J.A. and J.R. Prowle, *Paradigms of acute kidney injury in the intensive care setting.* Nat Rev Nephrol, 2018. **14**(4): p. 217-230.

96.   Bonventre, J.V. and L. Yang, *Cellular pathophysiology of ischemic acute kidney injury.* J Clin Invest, 2011. **121**(11): p. 4210-21.

97. Kinsey, G.R., R. Sharma, and M.D. Okusa, *Regulatory T cells in AKI.* J Am Soc Nephrol, 2013. **24**(11): p. 1720-6.

98. Sharfuddin, A.A. and B.A. Molitoris, *Pathophysiology of ischemic acute kidney injury.* Nat Rev Nephrol, 2011. **7**(4): p. 189-200.

99. Zarjou, A. and A. Agarwal, *Sepsis and acute kidney injury.* J Am Soc Nephrol, 2011. **22**(6): p. 999-1006.

100. Ratliff, B.B., et al., *Messengers without borders: mediators of systemic inflammatory response in AKI.* J Am Soc Nephrol, 2013. **24**(4): p. 529-36.

101. Basnakian, A.G., et al., *DNase I-like endonuclease in rat kidney cortex that is activated during ischemia/reperfusion injury.* J Am Soc Nephrol, 2002. **13**(4): p. 1000-7.

102. Saikumar, P., et al., *Role of hypoxia-induced Bax translocation and cytochrome c release in reoxygenation injury.* Oncogene, 1998. **17**(26): p. 3401-15.

103. Wei, Q., et al., *Bax and Bak have critical roles in ischemic acute kidney injury in global and proximal tubule-specific knockout mouse models.* Kidney Int, 2013. **84**(1): p. 138-48.

104. Wolfs, T.G., et al., *Apoptotic cell death is initiated during normothermic ischemia in human kidneys.* Am J Transplant, 2005. **5**(1): p. 68-75.

105. Wang, J., et al., *Minocycline up-regulates Bcl-2 and protects against cell death in mitochondria.* J Biol Chem, 2004. **279**(19): p. 19948-54.

106. Ruiz-Vela, A., et al., *Proapoptotic BAX and BAK control multiple initiator caspases.* EMBO Rep, 2005. **6**(4): p. 379-85.

107. Gao, Z., Y. Shao, and X. Jiang, *Essential roles of the Bcl-2 family of proteins in caspase-2-induced apoptosis.* J Biol Chem, 2005. **280**(46): p. 38271-5.

108. Martinou, J.C. and D.R. Green, *Breaking the mitochondrial barrier.* Nat Rev Mol Cell Biol, 2001. **2**(1): p. 63-7.

109. Green, D.R., et al., *Immunogenic and tolerogenic cell death.* Nat Rev Immunol, 2009. **9**(5): p. 353-63.

110. Kroemer, G., L. Galluzzi, and C. Brenner, *Mitochondrial membrane permeabilization in cell death.* Physiol Rev, 2007. **87**(1): p. 99-163.

111. Lan, R., et al., *Mitochondrial Pathology and Glycolytic Shift during Proximal Tubule Atrophy after Ischemic AKI.* J Am Soc Nephrol, 2016. **27**(11): p. 3356-3367.

112.   Yang, L., et al., *Epithelial cell cycle arrest in G2/M mediates kidney fibrosis after injury.* Nat Med, 2010. **16**(5): p. 535-43, 1p following 143.

113.   Singh, P. and M.D. Okusa, *The role of tubuloglomerular feedback in the pathogenesis of acute kidney injury.* Contrib Nephrol, 2011. **174**: p. 12-21.

114.   Morrell, E.D., et al., *Epithelial transport during septic acute kidney injury.* Nephrol Dial Transplant, 2014. **29**(7): p. 1312-9.

115.   Weichert, W., et al., *Upregulation of juxtaglomerular NOS1 and COX-2 precedes glomerulosclerosis in fawn-hooded hypertensive rats.* Am J Physiol Renal Physiol, 2001. **280**(4): p. F706-14.

116.   Linkermann, A., et al., *Regulated cell death in AKI.* J Am Soc Nephrol, 2014. **25**(12): p. 2689-701.

117.   Nath, K.A., *Tubulointerstitial changes as a major determinant in the progression of renal damage.* Am J Kidney Dis, 1992. **20**(1): p. 1-17.

118.   Loeffler, I. and G. Wolf, *Transforming growth factor-beta and the progression of renal disease.* Nephrol Dial Transplant, 2014. **29 Suppl 1**: p. i37-i45.

119.   Eckardt, K.U., et al., *Role of hypoxia in the pathogenesis of renal disease.* Blood Purif, 2003. **21**(3): p. 253-7.

120.   Schley, G., et al., *Selective stabilization of HIF-1alpha in renal tubular cells by 2-oxoglutarate analogues.* Am J Pathol, 2012. **181**(5): p. 1595-606.

121.   Higgins, D.F., et al., *Hypoxia promotes fibrogenesis in vivo via HIF-1 stimulation of epithelial-to-mesenchymal transition.* J Clin Invest, 2007. **117**(12): p. 3810-20.

122.   Jiang, M., et al., *Nutlin-3 protects kidney cells during cisplatin therapy by suppressing Bax/Bak activation.* J Biol Chem, 2007. **282**(4): p. 2636-45.

123.   Brooks, C., et al., *Regulation of mitochondrial dynamics in acute kidney injury in cell culture and rodent models.* J Clin Invest, 2009. **119**(5): p. 1275-85.

124.   Brooks, C., et al., *Fragmented mitochondria are sensitized to Bax insertion and activation during apoptosis.* Am J Physiol Cell Physiol, 2011. **300**(3): p. C447-55.

125.   Smith, J.A., et al., *Suppression of mitochondrial biogenesis through toll-like receptor 4-dependent mitogen-activated protein kinase kinase/extracellular signal-regulated kinase signaling in endotoxin-induced acute kidney injury.* J Pharmacol Exp Ther, 2015. **352**(2): p. 346-57.

126. Garrett, S.M., et al., *Agonism of the 5-hydroxytryptamine 1F receptor promotes mitochondrial biogenesis and recovery from acute kidney injury.* J Pharmacol Exp Ther, 2014. **350**(2): p. 257-64.

127. Whitaker, R.M., et al., *cGMP-selective phosphodiesterase inhibitors stimulate mitochondrial biogenesis and promote recovery from acute kidney injury.* J Pharmacol Exp Ther, 2013. **347**(3): p. 626-34.

128. Granata, S., et al., *Mitochondrial dysregulation and oxidative stress in patients with chronic kidney disease.* BMC Genomics, 2009. **10**: p. 388.

129. Li, X., et al., *PKC-delta promotes renal tubular cell apoptosis associated with proteinuria.* J Am Soc Nephrol, 2010. **21**(7): p. 1115-24.

130. Wang, W., et al., *Mitochondrial fission triggered by hyperglycemia is mediated by ROCK1 activation in podocytes and endothelial cells.* Cell Metab, 2012. **15**(2): p. 186-200.